

Department of Precision and Microsystems Engineering

Predictable Opto-Mechanical Design for a Critical Reflective Surface

R. Kleer

Report no : 2020.001
Coach : dr. ir. L. Cacace
Professor : ir. J.W. Spronck
Specialisation : Optomechatronics
Type of report : Master of Science Thesis
Date : January 23, 2020

Predictable Opto-Mechanical Design for a Critical Reflective Surface

by

R. Kleer

to obtain the degree of Master of Science
at the Delft University of Technology,
to be defended publicly on Thursday January 23, 2020 at 15:00 AM.

Student number:	4494474	
Project duration:	November 12, 2018 – January 23, 2020	
Thesis committee:	ir. J.W. Spronck,	TU Delft, chair
	Dr. R.A. Norte,	TU Delft, external member
	Dr.ir. L. Cacace,	TU Delft, supervisor
	ir. R.A.C.M. Beerens,	ASML, supervisor
	ing. F. Verhouden,	ASML, supervisor

An electronic version of this thesis is available at <http://repository.tudelft.nl/>.



Abstract

As the world becomes more connected, smarter, and more eco-friendly, computer microchips represent both the limitation and the heart of the process. To keep up with this growth, ASML creates machines that are able to produce computer-chips that are increasingly powerful & energy efficient. State of the art machines are converting CO₂ laser light into Extreme Ultra Violet (EUV) light that is crucial for the process. However, the conversion efficiency depends a lot on the beam quality of the CO₂ laser light. This beam quality depends, among other things, on the optics (mirrors) and their associated surface deformations.

Many examples exist in Opto-Mechanical oriented literature about mounting mirrors. However, many of them are tailored to the specific circumstances. In order to present and use existing knowledge, a literature study is conducted that summarises and elaborates on current technology.

The purpose of this thesis is to present an existing Opto-Mechanical error in current design of a subsystem of the EUV machine, and thereby propose a new design, tailored to the requirements. The research follows the well known V-model, beginning with derivation of clear requirements leading to a verification table that analyse those specifications. This conceptual design has shown to have up to a 4X improvement in terms of astigmatism which mainly occurred due to the temperature variations during transport.

For reasons of confidentiality, some values mentioned in the thesis at hand are merely indicative / for illustrative purposes only.

Preface

This thesis is written for the completion of the Master's degree in Mechanical engineering with a focus in Opto-Mechatronics at the TU Delft. This graduation thesis is written at ASML, the company where I worked at during the last year. During this time, I was introduced to a company that defines the state of the art in the lithography industry and where I was able to learn everyday more and more. In addition to technical lessons, I learned a number of things about my personal situation which were not only useful during the thesis period but will also benefit me for years to come.

Acknowledgements

I want to thank Ruud Beerens first, for all the weekly meetings which were really helpful. Second, for listening to my stories and for taking the time to discuss all things that I saw as difficult, both in and outside ASML.

I want to thank Frank Verhouden for all the weekly meetings and for the help with whatever I needed during my time at ASML.

I want to thank Martin van Mierlo, who has become a really close friend, for being my student colleague. I loved the discussions on a day to day basis about both of our theses.

I want to thank Lennino Cacace for the first Opto-Mechatronics courses offered at TU Delft, for being my supervisor, and for arranging all the biweekly meetings with the other OM students.

I want to thank Pieter Kappelhof for his time that he made free to meet and discuss some of the problems I faced.

I want to thank my parents, brother, and sister for supporting me during this period. I felt always very welcome to come home after a busy week in Eindhoven.

*R. Kleer
Delft, January 2020*

Nomenclature

Abbreviation	Full term
λ	wavelength
99%EE	99 percent Encircled Energy
AOI	Angle Of Incidence
AST	ASTigmatism
BDS	Beam Delivery System
CD	Critical Dimension
CE	Conversion Efficiency
CTE	Coefficient of Thermal Expansion
D4 σ	Diameter across 4 standard deviations
DL	CO ₂ Drive Laser
DUV	Deep UltraViolet
EUV	Extreme UltraViolet
FEM	Finite Element Model
FF	Final Focus
FFA	Final Focus Assembly
FFA-FU	Final Focus Assembly-Focus Unit
FFA-OP	Final Focus Assembly-Optical Platform
k	thermal conductivity
LIDT	Laser Induced Damage Threshold
M1	Mirror 1
M2	Mirror 2
M3	Mirror 3
MP	Main Pulse
NA	Numerical Aperture
PP	PrePulse
RMS	Root Mean Square
RSA	Rapid Solidification Alloys
RSP	Rapid Solidification Proces
Z#	numbered Zernike polynomial
Z1	piston
Z2	tip
Z3	tilt
Z4	defocus
Z5	vertical astigmatism
Z6	oblique astigmatism
Z7	horizontal coma
Z8	vertical coma
Z9	primary spherical
Z12	vertical secondary astigmatism
Z16	secondary spherical
ZrN	Zirconium Nitride

Contents

Abstract	i
Preface	iii
Nomenclature	v
1 Introduction	1
1.1 Technical background	1
1.2 Research objective	2
1.3 Thesis structure	2
I State Of The Art Current design	4
2 State Of The Art Current design	5
2.1 Analysis of existing design	5
2.2 Optical definitions	7
2.3 Conclusion State of the Art	8
3 Requirements	9
3.1 Operation State	9
3.1.1 Sensitivity table	9
3.1.2 Optical aberrations	13
3.2 Transportation	17
3.2.1 Temperature variations	17
3.2.2 Shock load	17
3.3 Mechanical constraints	17
3.4 Summary requirements	17
4 Problem of current design	19
4.1 Design evaluation	19
4.2 Optical surface deformation	19
4.3 COMSOL model to compare	23
4.3.1 Model transport	23
4.3.2 Model Operation state	29
4.4 Conclusion	30
II Literature Survey Mounting concepts	31
5 Literature survey	32
5.1 Mirrormounts	32
5.1.1 Whiffle tree	33

5.1.2	Hoop strap	33
5.1.3	Topology optimization	33
5.1.4	Nest of springs	34
5.1.5	Hexapod	34
5.1.6	Blade flexure design	34
5.1.7	Summary mirror mounts	35
5.2	A-thermal design	38
5.2.1	Insensitive for deformations & scaling effects	38
5.2.2	Materials to compensate	38
5.2.3	Material properties	39
III	Design	40
6	High-level Design	41
6.1	Material comparison	41
6.1.1	Thermal stability	41
6.1.2	Thermal stability Vs Absorption	42
6.1.3	Specific stiffness Vs (Thermal stability/Watt absorbed)	43
6.2	Cooling channels	44
6.3	Mirror size	46
6.4	Manufacturing	47
6.5	Model	48
6.6	Conclusion mirror	49
7	Mirror mount	50
7.1	Expansion freedom	50
7.2	Boundaries of a flexure	51
7.3	Combined Flexures	52
7.3.1	Design options	53
7.3.2	Hexapod	53
7.3.3	Six folded flexures	54
7.3.4	Three folded flexures and three rods	54
7.3.5	Conclusion design choice	55
7.4	Concept detailed design	55
7.4.1	Backplate & location flexures	55
7.4.2	Folded leafspring design	56
7.4.3	Flexure fixation	58
7.4.4	Conclusion Conceptual design	59
8	Evaluation of Detailed Design	61
8.1	Eigenfrequency & Stiffness	61
8.2	Stress	61
8.3	Shock Load	62
8.4	Cooling forces	62
8.5	Tooling and placing	63
8.6	Manufacturing	64
8.7	Sensitivity	65
8.7.1	Astigmatism	66

IV Comparison Proposed design	67
9 Discussion	68
9.1 Mechanical performance	68
9.2 Optical validation	69
10 Conclusion & Recommendations	71
10.1 Recommendations	71
V Appendices	73
A Material deformation	74
A.1 Fake material 1	74
A.2 Fake material 2	74
A.3 Fake material 3	75
A.4 Fake material 4 / Diamond	75
A.5 Copper	76
A.6 SiSic	76
A.7 Titanium	77
A.8 RSA-443	77
A.9 RSA-462 T6	78
A.10 Aluminium (6061)	78
A.11 Stainless Steel	79
A.12 SiSic 70% absorbed power	79
A.13 Diamond 19% absorbed	80
B Model check	82
B.1 Mirror surface measurement setup	82
B.2 AST vs Angle	83
C Forces of cooling water	85
D Isostatic mounts	87
D.1 Backplate table	90

List of Figures

1.1	Machine History	1
1.2	Beam Delivery System	2
2.1	Schematic view of the FFA-FU	5
2.2	Schematic optical system	6
2.3	Mirror shapes	6
3.1	Sensitivity figures M2	10
3.2	Sensitivity figures M1	11
3.3	Zernike Polynomials	13
3.4	Ideal focal spot Vs astigmatism focal spot	14
3.5	Ideal PSF Vs aberated AST PSF [1]	14
3.6	Astigmatism[2]	15
3.7	Rays from two sides	16
4.1	Frontside of M2	19
4.2	Deformation due to Transport	20
4.3	Zernike Polynomials of measurement	20
4.4	Thermal expansion	21
4.5	Slip conditions	23
4.6	Transportation model M2	24
4.7	Deformation due to thermal expansion	25
4.8	Force per bolt	25
4.9	Temperature VS force per bolt part 1	26
4.10	Temperature VS force per bolt part 2	27
4.11	Surface deformation in x, y and z direction	27
4.12	Y_{max} Vs Diameter	28
4.13	Zernike Polynomials simulation Vs measurement	29
4.14	Operation model M2	29
4.15	Forces at bolts	30
4.16	Mirror surface deformation due to laser power	30
5.1	Kinematic mount	32
5.2	Whiffle tree	33
5.3	Hoop strap	33
5.4	Topology	33
5.5	Nest of springs	34
5.6	Hexapod	34
5.7	Blade flexure	34
5.8	A-thermal design	38
6.1	Thermal stability	42
6.2	Thermal stability Vs Absorption	43

6.3	Specific stiffness Vs (Thermal stability/Watt absorbed)	44
6.4	Minimal thickness with cooling channels	44
6.5	Minimal mirror thickness	46
6.6	Support paramater C_A	47
6.7	Eigenfrequency Vs Thickness	47
6.8	Material model	48
6.9	Effect of varying CTE and Conductivity	48
6.10	Zernike of different materials	49
7.1	Deformation due to change in temperature	50
7.2	Single flexure	51
7.3	Combined flexures	52
7.4	Hexapod	53
7.5	Six folden flexures	54
7.6	Three folded flexures and three rods	54
7.7	Back-plate design	56
7.8	Folded leafspring	56
7.9	Solutions within the allowed stress	57
7.10	Flexure positions	57
7.11	Final folden flexures	58
7.12	Flexure fixation	58
7.13	Shear and bending	59
7.14	Proposed design	60
8.1	Eigenfrequency	61
8.2	Von mises stress	62
8.3	Shock load	62
8.4	Cooling forces	63
8.5	Tooling	64
8.6	Vacuum effect	65
8.7	Zernike Polynomials vacuum deformation	65
8.8	Laser power sensitivity	66
8.9	Zernike Polynomials laser sensitivity	66
10.1	Sensitivity system level	72
A.1	Fake material 1	74
A.2	Fake material 2	75
A.3	Fake material 3	75
A.4	Fake material 4	76
A.5	Copper	76
A.6	SiSic	77
A.7	Titanium	77
A.8	RSA-443	78
A.9	RSA-462 T6	78
A.10	Aluminium (6061)	79
A.11	Stainless Steel	79
A.12	SiSic 70% absorbed power	80
A.13	Diamond 19% absorbed	80
A.14	Zernike Ploynomials of all the tested materials	81
A.15	Zernike Ploynomials of relevant tested materials	81
B.1	Measurement setup	82

B.2	Numbers used to get to Zernike Polynomials	83
B.3	Deformation Vs Laser angle	83
B.4	Check HTC	84
C.1	Forces of flow	85
C.2	Cooling hoses stiffness	86
D.1	Iso-static mounts part 1	87
D.2	Iso-static mounts part 2	88
D.3	Iso-static mounts part 3	88
D.4	Iso-static mounts part 4	89
D.5	Iso-static mounts part 5	90

List of Tables

2.1	Optical specifications[3]	8
3.1	Sensitivity table M2	10
3.2	Tolerance table M2	11
3.3	Sensitivity table M1	11
3.4	Tolerance table M1	12
3.5	Astigmatism given in $m\lambda$ FFA-FU	15
3.6	Astigmatism budget	15
3.7	Sensitivity table Z5 & Z6	16
3.8	Position precision M2 based on astigmatism	17
3.9	Requirements	17
3.10	Environmental conditions	18
3.11	Mechanical constraints	18
4.1	Material properties	21
4.2	Friction coefficient vs Temperature	22
4.3	Compare COMSOL values with hand calculations	24
5.1	Mirror mounts	35
5.2	All mounts	36
5.3	Selected mounts	37
5.4	Material properties	39
6.1	PV and max temperature	49
7.1	Stiffness	51
7.2	Parameters and comparison Hexapod	53
7.3	Parameters and comparison of sixfolded leafsprings	54
7.4	Stiffness three folded leafsprings and three rods	55
7.5	Final dimensions of the folden flexures	58
7.6	Fixation pads	59
9.1	Mechanical validation	68
9.2	Optical validation Z5	69
9.3	Optical validation Z6	69
9.4	Total AST comparison	70

Chapter 1

Introduction

In a world where every new computer chip will increase in computational power, machines to produce those chips will become preciser and more complex at the same time. With more computational power, world problems can be solved by doing more difficult calculations.

This thesis kicks off with a brief introduction of ASML, the company at which the subject at hand is investigated. The start will be very broad by explaining some history and the different machines of the company. Thereafter, focus in the direction of the problem description and a motivation of the research will be given.

1.1 Technical background

ASML is a Dutch company and currently the largest supplier in the world of photolithography systems for the semiconductor industry. The company manufactures machines for the production of Integrated Circuits (IC's) [4].

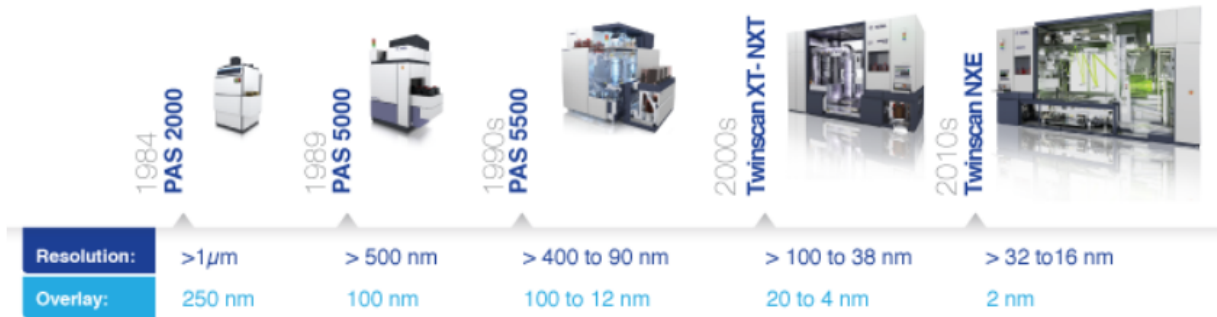


Figure 1.1: Machine History

Figure 1.1 depicts ASML's machine platforms over the past decades, where the resolution of the IC's is getting smaller and smaller. The size of a single transistor should be reduced, in order to keep up with Moore's law, which states that the number of transistors in a dense integrated circuit doubles about every two years [5]. In order to reduce the size of a transistor even further, a well known relationship (1.1) is used.

$$CD \sim \frac{\lambda}{NA} \quad (1.1)$$

This formula describes the Critical Dimension (CD) of features. What easily can be seen is that by enlarging the Numerical Aperture (NA) and/or reducing the wavelength (λ), the critical dimension can be decreased. Therefore, the newest machine, the Twinscan NXE, is using Extreme Ultra Violet (EUV) light with a wavelength of 13.5 nm [6]. To create this EUV light, a tin droplet is hit 50 thousand times a second with a multi kW laser. Because of the large size, the laser is placed outside the machine and thus a system is used

to get the laser beam to the the machine. This system is called the Beam Delivery System (BDS) and is used to deliver the laser beam in a safe way to the machine. A schematic overview of the BDS is given in fig. 1.2.

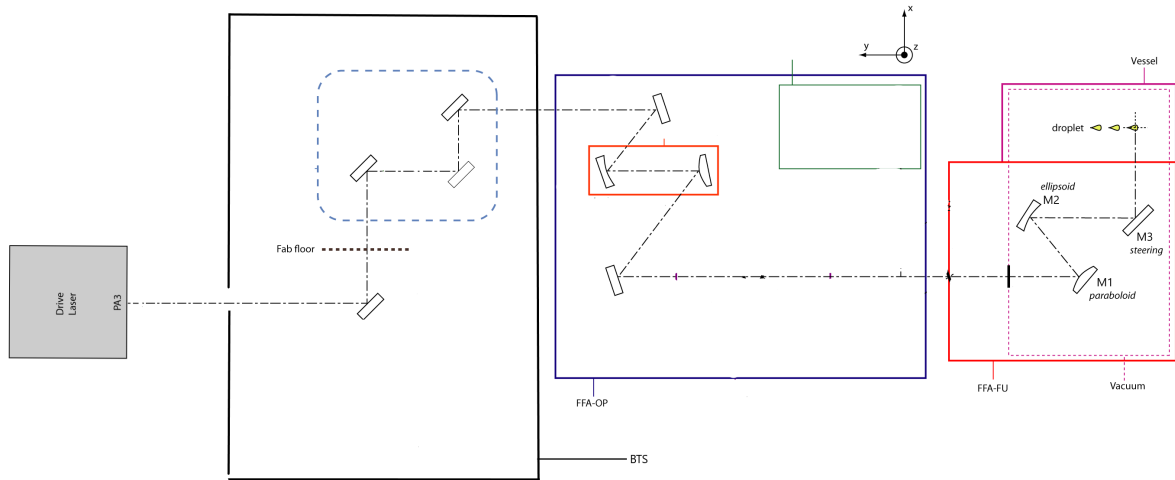


Figure 1.2: Beam Delivery System

The BDS can be split in three parts; those being the Beam Transport System (BTS), Final Focus Assembly Optics Platform (FFA-OP) and the Final Focus Assembly Focus Unit (FFA-FU). The drive laser provides the BDS with a CO₂ laser of a certain spectral density which will later be separated into the pre-pulse and the main-pulse (explanation to follow). The parallel Gaussian beam exits the drive laser and will enter the first part. This is the BTS where the beam is expanded for wavefront control and where it will travel the furthest. From here, the beam will enter the FFA-OP where the beam is compressed and the pre-pulse is separated from the main-pulse. Next, the beam is forwarded to FFA-FU. Finally, inside the FFA-FU the laser beam is focused and aimed on the tin droplet to generate the EUV light.

1.2 Research objective

This thesis will challenge an existing design of the Mirror 2 (M2) versus its specification and, if needed, propose an alternative design.

NXE systems are production/throughput limited by their source despite improvements made in the past years. Typical knobs to increase source power are CO₂ power increase and convergence efficiency; the latter being achievable by improved aberration robustness. Unfortunately, power increase and aberration robustness don't go hand in hand as thermal increase results in opto-mechanical deformation of optics, especially mirrors. Given the apparent contradiction, the thesis will focus on the characteristics of the largest curved mirror of the FFA-FU; this being the M2. The M2 has the largest aspect ratio (thickness versus diameter), is placed in vacuum, and is position sensitive as a result of its curvature. It is believed that the following analysis holds for other mirrors in the BDS due to these additional challenges for the M2.

1.3 Thesis structure

Chapter 2 will dive into the State of the art and describes the function and way of working of the FFA-FU; thereby the two mirrors will be explained and why the M2 has a high aspect ratio. The chapter will conclude with a limited design evaluation of the current design.

Chapter 3 sets out the requirements and will also explain the conditions wherein the FFA-FU has to survive and will make a distinction between transport and operation mode. The chapter concludes with a summary

of the requirements and boundaries within which the system should be operating.

Chapter 4 kicks off with a comparison between two figures where the mirror shapes are measured before and after transportation. This is followed by a hand calculation where it is shown that stick-slip at the bolt interface is possible during transportation. To validate this hand calculation, a 3D model is built in COMSOL. With this model, it is possible to check the stress below each bolt and determine which bolt slips first. This is done for both states, from which the conclusion is that the main issue is during transportation.

Chapter 5 consists of the literature study where different existing mirror mounts are investigated and concludes with a table and an explanation of why a custom made mount should be made. The second part of the literature study describes the concept of making an A-thermal design which can either use the same material for the whole system or use materials to compensate one another.

Chapter 6 will dive into the design of the mirror itself. Calculated is the thickness based on eigenfrequency and validation on the cooling channels is done for the models later on. An investigation in different materials for the mirrors is done for two reasons, namely, to check whether the same material can be used for the structure and the mirrors, and at the same time to verify the deformation of the optical surface due to the laser load. The conclusion is to stick with a copper mirror due to the risk of low bare material reflection.

Chapter 7 is where the actual mirror mount is designed. It kicks off with a basic flexure design and calculates the boundaries the flexures have to meet. A step is made to decide to use flexures that have just one degree of freedom. COMSOL and Excel are intensively used to choose the best concept. The geometry of the flexures are calculated and verified on an individual basis. Additionally, the flexure position and back-plate geometry are also determined. The chapter will close with the final detailed design.

Chapter 8 walks through each requirement and shows that the new design fulfills all the specs. Also, a tooling device in the form of a alignment mechanism is shown to place the design to the exact position.

Chapter 9 will give a comparison where a table will elaborate on every aspect of the new and old design. The pros and cons are discussed and from there a recommendation will be given to further improved the proposed design.

Chapter 10 will end this thesis. This is done with the conclusion and recommendations for future work.

Part I

State Of The Art Current design

Chapter 2

State Of The Art Current design

This chapter will explain the state of the art of the focusing unit. The shapes and sizes of both of the mirrors will be elaborated on and basic calculations are done in order to check the values and understand the design choices.

2.1 Analysis of existing design

This project will focus on the last part of the BDS, the FFA-FU. Figure 2.1 shows a schematic overview and illustrates the current layout of the beam and mirrors. Assumed is a collimated beam of ≈ 40 mm diameter entering the vacuum environment via the diamond window (W). A diamond window is needed because of the high power laser and also to separate the vacuum from the atmospheric environment. The beam will propagate further until it hits the convex mirror M1. This mirror will diverge the beam to the concave mirror M2; from here the beam will converge and reflect at the mirror M3 and hit the target (the tin droplet). The focus is on M1/M2 as these two are mainly responsible for the optical power resulting in the required spot size. The FFA-FU is in vacuum to ensure the EUV light can propagate further since EUV light is absorbed if no special care is taken [7].

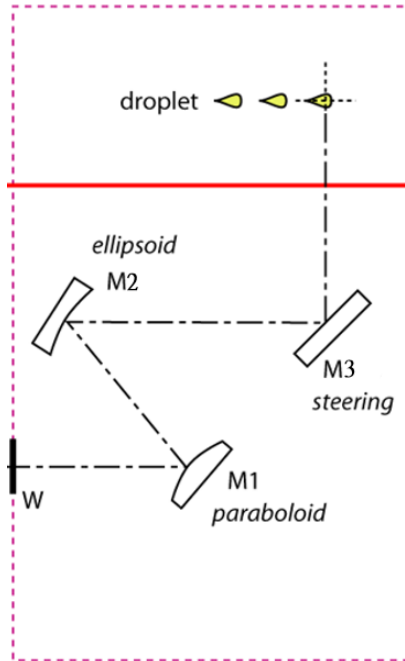


Figure 2.1: Schematic view of the FFA-FU

After the tin droplet is converted into EUV light, this light is captured by a collector-mirror and ensures the transfer further through the machine. Figure 2.2a illustrates the FFA-FU as being lenses. In this picture,

the laser enters from the left and is drawn as dotted lines. Those lines are extended to a virtual focus plane, this plane simulates the same behavior as the real focal plane. But the beam first diverges, after which it is converged again. The reason has to do with two things, namely, the small final spot size and the amount of space needed for the collector. To create more distance for the collector a Schwarzschild optical system is used. A 2D Schwarzschild optical system is shown in fig. 2.2b and consists of a parabolic and an elliptical mirror. Note that the beam enters from the left and that both mirrors are just a tiny part of the ellipse and parabola.

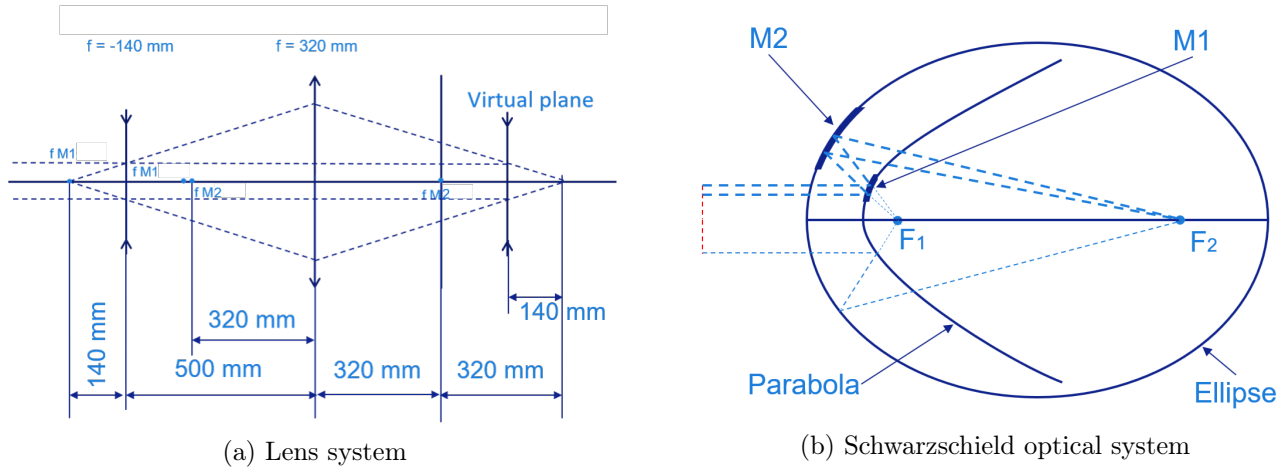


Figure 2.2: Schematic optical system

The M1 has a paraboloid shape which means that a collimated beam propagating parallel to the optical axis will exactly focus on the focal point of this paraboloid. Figure 2.3a shows the schematic shape of the M1 and the virtual focus point and the reflected beam as a result.

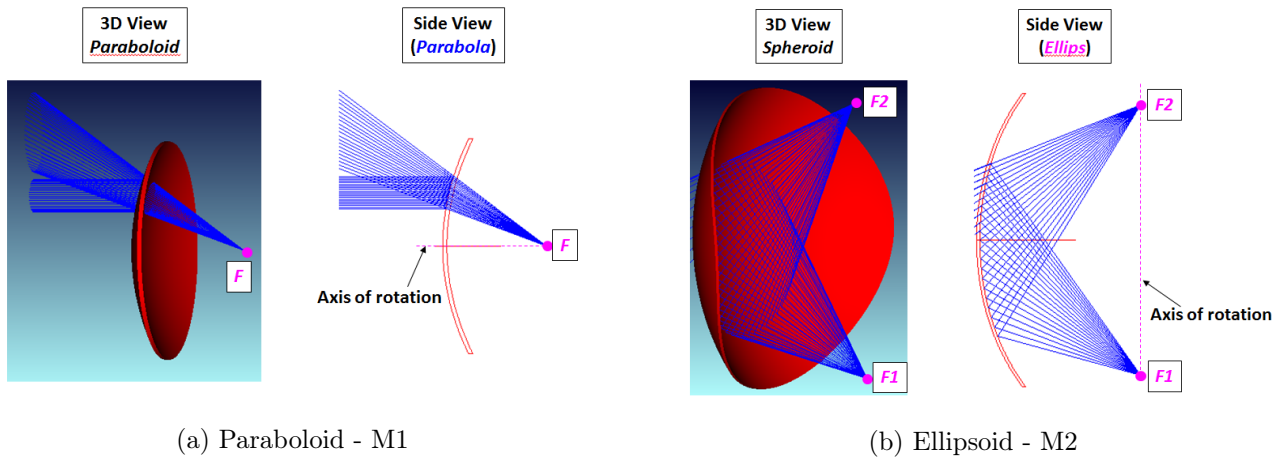


Figure 2.3: Mirror shapes

After the M1, the beam will meet the M2 which is an ellipsoid shaped mirror and can be seen in fig. 2.3b, this shape has an elliptical cross-section along the axis of rotation and a circular cross-section perpendicular to that. A remarkable fact of such a shape is that there are two focus points, given the characteristic that all rays of light crossing the first focal point will also cross the second focal point. The elliptical shape of a mirror ensures a diffraction-limited spot size. This mirror has an oval-shaped aperture but is almost a sphere, the picture is overdone here to illustrate the effect but the oval shape is needed to get this diffraction-limited spot size. The specifications of the mirrors are given in section 2.2.

The NA can be calculated with eq. (2.1) and will be used to explain why the M2 has such a large size. The EE99 diameter of the beam and the focal length of the virtual plane are ≈ 44 mm and 140 mm respectively.

$$NA \sim \frac{D}{2f} \quad (2.1)$$

where

NA = Numerical aperture [-]
 D = Diameter of the beam [m]
 f = focal length [m]

By filling in the assumed EE95 beam diameter of 44 mm and the virtual focal length of 140 mm the NA is calculated as 0.1566. It can be noticed in fig. 2.2a that the M2 has the same NA. Due to the length from the M2 till the droplet, simple geometry can be used to check the size of the beam on the M2 as approximately 200 mm which is comparable with the EE99 specified before. But to calculate the size of the focal point, this assumption is not enough. In the eq. (2.2) is the non-ideal Gaussian laser intensity profile M^2 added as 1.4. $D4\sigma$ is given as ≈ 28 mm.

$$NA \simeq \frac{2\lambda_p}{\pi D_{spot}} \Rightarrow D_{spot} \sim \frac{4M^2\lambda_p f}{\pi D4\sigma} \quad (2.2)$$

where

λ_p = wavelength of pre-pulse [m]
 D_{spot} = Diameter of the final spot size [m]
 M^2 = Beam quality factor [-]
 $D4\sigma$ = Diameter of beam x 4σ

The wavelength λ_p of the drive laser is 10.26 μ m and calculated is a spot diameter of approximately 100 μ m. The conclusion here is that by increasing the focal length the spot size becomes larger, and by enlarging the $D4\sigma$ diameter the spot size decreases. Thus, by varying one of the two it has to be compensated with the other parameter.

2.2 Optical definitions

To do first-order calculations, some definitions need to be made clear. Those values will be used throughout the document and used to determine the design chooses. As said before the drive laser provides CO₂ laser light of two wavelengths, both of which are needed to create EUV light. The pre-pulse is to transform the droplet into a pancake shape and the main-pulse will change the tin droplet into plasma which creates the EUV light. Another definition to discuss is the beam size. For this, there are different ways to specify, but in this thesis, it will be either EE99 or $D4\sigma$. EE99 means the diameter in which 99 percent of the encircled beam energy is located. A beam is often specified with the 13.5% ($1/e^2$) intensity level which is the same diameter as $D4\sigma$ for a perfect Gaussian beam and will be assumed to be true throughout the full document. A factor of 1.52 is used between both the $D4\sigma$ and the EE99 diameters. The final diameter that needs to be specified is the clear aperture, which is the diameter of the optical surface itself. Those values are summarised in table 2.1. In the table the power of the pre- and main-pulse is added, the wavelength range where CO₂ laser light has it's most energy is around 10.6 μ m. Therefore, is this assumed to be the used wavelength in both cases. In reality this can vary a bit.

Optical definitions			
Pre-pulse	$\lambda_p \approx 10.6$	Pre-pulse + Main-pulse	
Main-pulse	$\lambda_m \approx 10.6$	25 - 50 kW	
Mirror	M2		M1
Shape	Ellipsoid		Paraboloid
Focallength	320 mm		-140 mm
Material	-		-
Coating	Yes, 1% absorption		Yes, 1% absorption
Diameter	230 mm - 250 mm		90 mm - 110 mm
D4 σ	$x = 130mm$	$y = 130mm$	$x = 28mm$ $y = 28mm$
EE99	$x = 197.6mm$	$y = 197.6mm$	$x = 42.5mm$ $y = 42.5mm$
Clear aperture	$x = 228mm$	$y = 220mm$	$x = 100mm$ $y = 100mm$

Table 2.1: Optical specifications[3]

What can be seen in table 2.1 is that the diameter is different from the clear aperture, this is because the clear aperture is determined by the aperture in the mirror-block. Also in reality the difference in the coordinates x and y are representing the outer beam profile at the mirror. This is a result of the angle of incidence (AOI) that is given as 15° at the M2 mirror.

2.3 Conclusion State of the Art

Discussed in this section is the state of the art of the focus unit, it has shown how both mirrors interact with each-other and a simplified sketch is given. Both shapes, parabolic and elliptical, are explained and with that there specific optical property is to diverge and converge the beam in the direction of the final focus. Determined is that the size of the large mirror M2 is due to the trade of between the length from mirror to the final focus and the final sport size to hit the droplet. Optical definitions are shown and summarized in table 2.1.

Chapter 3

Requirements

The requirements will be split up into two parts namely the operation state and transport state. During operation, the system should perform within the specifications. The operational requirements will be split up into two sections, a mechanical part and an optical part that are mostly will address aberrations. During transportation, the most important requirement is that it should be robust and withstand corresponding temperatures and forces.

3.1 Operation State

The most important thing in order to create EUV light is that the laser beam hits the tin droplet. Therefore position tolerances will be specified for both mirrors. To keep the mirror at the specified position it should be able to handle disturbances. Both mirrors should operate inside the machine that will provide vibrations. This section will dive into the boundary conditions that will occur during operation mode.

3.1.1 Sensitivity table

In order to set requirements the mechanical tolerances for the M2 mirror position are put in a sensitivity table. In this table, it can be seen what will happen to the focal point due to first-order misalignments and deformation of the surface. This is done by ray tracing and misaligning the M2, where the M2 is given as a lens system. Figure 3.1a shows the ideal system where the mirror is at the exact place where it should be. It should again be noticed that the FFA-FU has an steering mirror to compensate for misalignments in x , y and z . But since the mirrors are not flat, misalignments of the mirrors will also introduce aberrations. To investigate the effect at the position of the droplet, the sensitivity table will be filled with numbers and a tolerance table is created.

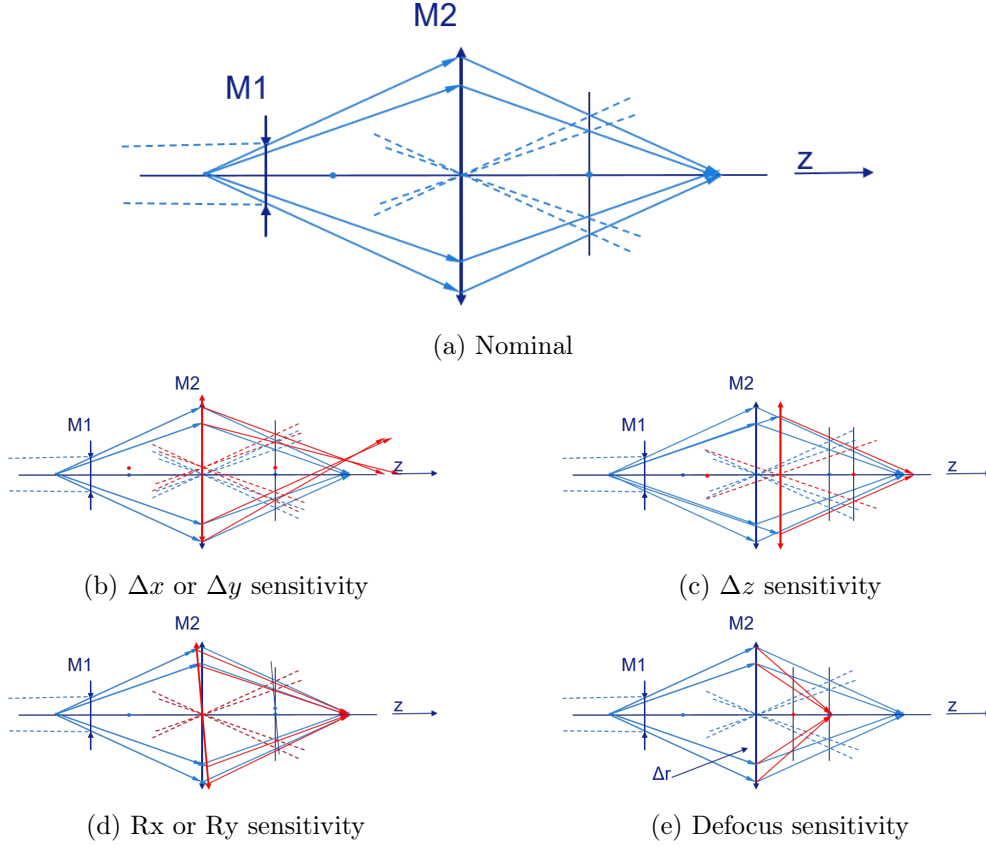


Figure 3.1: Sensitivity figures M2

Figure 3.1 shows the displaced mirror and the effects of it. In table 3.1 the sensitivities are given in formulas where top row specifies the error in position, incoming angle and beam size. The first column specifies the displacements of the M2 mirror. Translations x , y , and z , rotations as R_x , R_y , and R_z . Furthermore is defocus ($Z4$) in the mirror specified. As a result for the final focus position is given as x_f , y_f and z_f . The incoming angle in at the final focus is given as R_{xf} and R_{yf} . Also, the beam size at the original focus place is given.

M2	Δx_f	Δy_f	Δz_f	ΔR_{xf}	ΔR_{yf}	Beamsize@focus
Δx	$2x$	0	0	0	0	0
Δy	0	$2y$	0	0	0	0
Δz	0	0	$0.5z$	0	0	$\Delta z_f/NA$
ΔR_x	$2L\sin(\Delta r_x)$	0	$L - L\cos(\Delta R_x)$	$2\Delta R_x$	0	$\Delta z_f\cos(\Delta R_x)/NA$
ΔR_y	0	$2L\sin(\Delta r_y)$	$L - L\cos(\Delta R_y)$	0	$2\Delta R_y$	$\Delta z_f\cos(\Delta R_y)/NA$
ΔR_z	$h\sin(\Delta r_z)$	$h - h\cos(\Delta r_z)$	0	0	0	0
$\Delta Z4$	0	0	$\Delta r/2$	0	0	$(\Delta r/2)/NA$

Table 3.1: Sensitivity table M2

L is the distance between the mirror and the position of the droplet, the optical NA is already specified as 0.1566. Parameter h is the height between the mirrors center and droplet position and is given as 129.4 mm. Δr specifies the defocus in the mirror as a difference in radius in this mirror. Table 3.2 shows the tolerance table of the mirror, the tolerance is given in μm and the deltas are given in m.

M2	Tolerance	Δx_f	Δy_f	Δz_f	ΔR_{xf}	ΔR_{yf}	<i>Beamsize@focus</i>
Δx	10 μm	2.0E-05	0	0	0	0	0
Δy	10 μm	0	2.0E-05	0	0	0	0
Δz	10 μm	0	0	5E-06	0	0	6.39E-05
ΔR_x	50 μrad	6.4E-05	0	8E-10	1E-04	0	5.1E-09
ΔR_y	50 μrad	0	6.4E-05	8E-10	0	1E-04	5.1E-09
ΔR_z	50 μrad	6.5E-06	1.6E-10	0	0	0	0
$\Delta Z4$	1 μm	0	0	5E-07	0	0	3.19E-06

Table 3.2: Tolerance table M2

The same methodology can be applied for the M1 mirror, the initial condition will be the same and is shown in fig. 3.2a. In fig. 3.2b is the sensitivity given due to the misalignment of the plane of the mirror. Figure 3.2c shows the sensitivity while the mirror is misaligned parallel over the optical axis. The tilt of the mirror is illustrated in fig. 3.2d and rotation over its axis is shown in fig. 3.2e. This is a different sketch since a lens is not sensitive to rotation over its axis but the M1 has its focal point not on the axis as described before. Finally a defocused mirror is illustrated in fig. 3.2f.

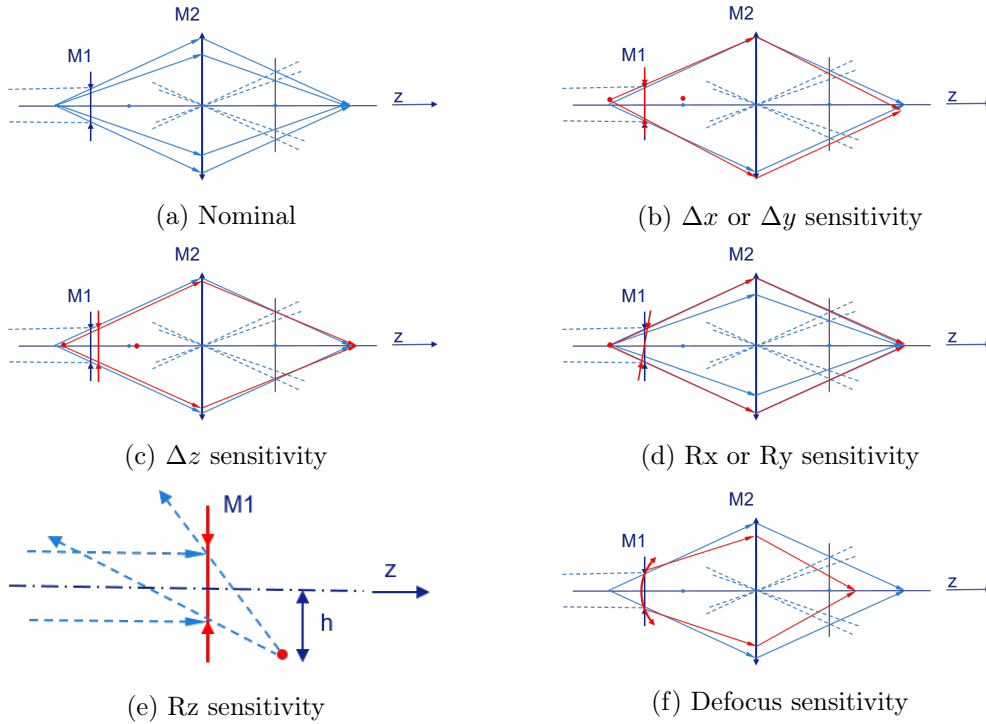


Figure 3.2: Sensitivity figures M1

Associated sensitivity table for the M1 mirror is given in table 3.3.

M1	Δx_f	Δy_f	Δz_f	ΔR_{xf}	ΔR_{yf}	<i>Beamsize@focus</i>
Δx	$-\Delta x$	0	0	0	0	0
Δy	0	$-\Delta y$	0	0	0	0
Δz	0	0	Δz	0	0	$\Delta z_f / NA$
ΔR_x	$f_{130} \sin(\Delta R_x)$	0	$f_{130} - f_{130} \cos(\Delta R_x)$	$2\Delta R_x$	0	$\Delta z_f \cos(\Delta R_x) / NA$
ΔR_y	0	$f_{130} * \sin(\Delta R_y)$	$f_{130} - f_{130} * \cos(\Delta R_y)$	0	$2\Delta R_y$	$\Delta z_f \cos(\Delta R_y) / NA$
ΔR_z	$h \sin(\Delta R_z)$	$h - h \cos(\Delta R_z)$	0	0	0	0
$\Delta Z4$	0	0	$\Delta r / 2$	0	0	$(\Delta r / 2) / NA$

Table 3.3: Sensitivity table M1

Corresponding tolerance table with added tolerance values is given in table 3.4, the tolerance is given in μm and the deltas are given in m. The parameters here are f_{130} which represents the focal length of the M1, h is the distance between the optical axis and the focal point of the M1. The rest of the parameters is the same as in table 3.1.

M1	Tolerance	Δx_f	Δy_f	Δz_f	ΔR_{xf}	ΔR_{yf}	$Beamsize@focus$
Δx	10 μm	-1.0E-05	0	0	0	0	0
Δy	10 μm	0	-1.0E-05	0	0	0	0
Δz	10 μm	0	0	1.0E-05	0	0	6.39E-05
ΔR_x	50 μrad	7.0E-03	0	1.8E-07	1E-04	0	1.1E-06
ΔR_y	50 μrad	0	0.007	1.8E-07	0	1E-04	1.1E-06
ΔR_z	50 μrad	6.5E-06	1.6E-10	0	0	0	0
$\Delta Z4$	1 μm	0	0	5.0E-07	0	0	3.19E-06

Table 3.4: Tolerance table M1

As previously described is it possible to correct for the position of the focal point. However, it is not possible to correct for aberrations which will arise by a misaligned mirror. The precision in which the M2 needs to be mounted in, is unknown at ASML. However, an astigmatism budget is specified. This specification will be shown later, in the optical aberration section. Thus the tolerance in which the mirror should be positioned will be shown in section 3.1.2.

Eigenfrequency

Both mirrors should operate inside the machine that will provide vibrations. A system that operates at its natural frequency will oscillate in the absence of any damping. This makes the amplitude of this vibration increase significantly and thereby irreparable damage can occur. The common oscillations of the machine are at 20 - 30 Hz. By designing the mirrors with a higher first natural frequency than 30 Hz the system should operate within mechanical specifications but to create safety it's decided to design for a higher eigenfrequency as 150 Hz.

Environment

As previously mentioned the FFA-FU is operating in a mostly vacuum environment, its purged with hydrogen to flush away contamination's created as a side product of the EUV light. The design should survive in this environment thus most important is to use the right materials also keep design strategy for vacuum environment in account [7]. Another thing that should be noticed is hydrogen embrittlement. This is the process where materials will become brittle due to the introduction and subsequent diffusion of hydrogen into the material. Just as given in the final design evaluation the mirrors now are protected against the hydrogen embrittlement with a coating of 1 % absorption to the optical surface.

Thermal laser load

The thermal load of the laser on the mirror surface nowadays is specified as 1% of the laser power of 20 - 30 kW. In this thesis a load of 250W on the optical surface will be used to do the calculations. However, in the future, the power can go up and in this thesis is assumed to go double. Thus up to 50kW and consequently a 500W absorption on the optical surface.

Temperature Range

During operation the machine will operate inside a cleanroom, this cleanroom has a specified temperature range from 20 to 24 °C. On top of this the hydrogen can also have a temperature variation. Specified as variation is ± 5 K. This means that worst case the temperature during operation is from 15 till 29 °C, thus a ΔT of 14 °C. It should be noticed that this variation in one machine probably never will occur. But rather

focal point, that can be seen in fig. 3.4b, it can be seen that the D_{spot} is larger. And thus by shooting on a droplet with a larger area then the droplet will not end upon the droplet en thus is a lost of energy.

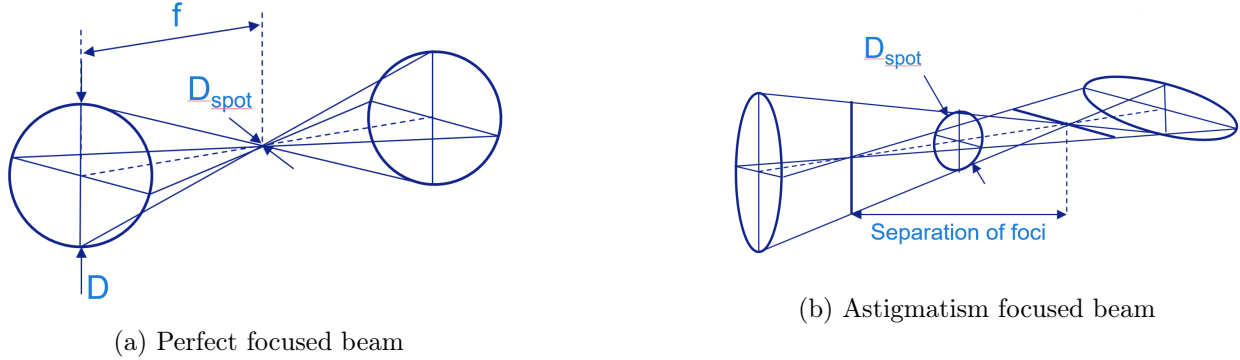


Figure 3.4: Ideal focal spot Vs astigmatism focal spot

By taking a look to the general Point Spread Function (PSF) fig. 3.5a. And comparing this with the general PSF of a non-aberrated wavefront fig. 3.5 it can be seen that at the non-aberrated figure the first dip occurs at -1.22 and 1.22. And lets assume now that this is the diameter of the 100 μm that was calculated in section 2.2. Then it is clear that the majority of the energy will end up in this diameter. On the other hand, in fig. 3.5b the same diameter is drawn and it is clear that the energy is spread out more. This means that the power that will end up at the droplet is less and thereby makes the irradiance go down four times.

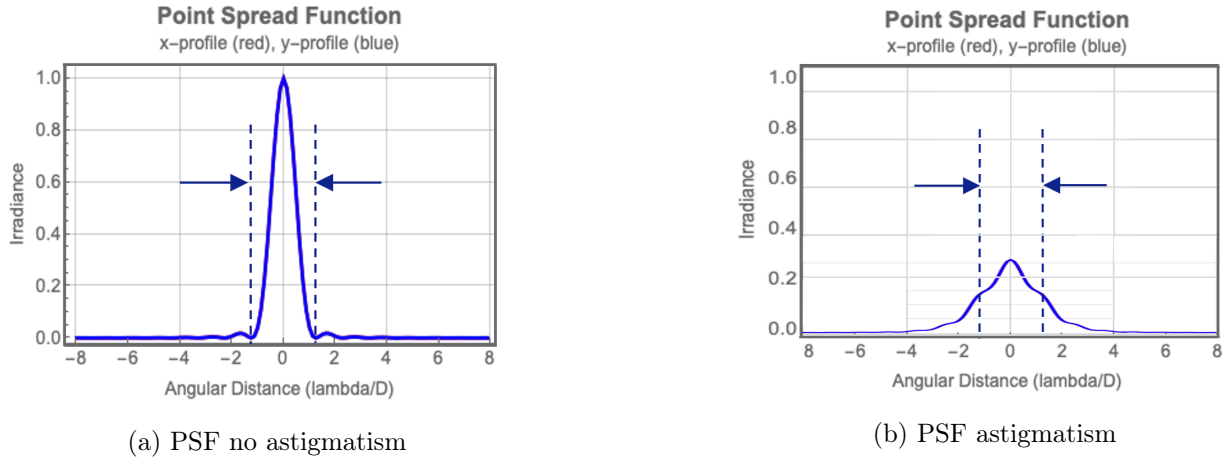


Figure 3.5: Ideal PSF Vs aberrated AST PSF [1]

Astigmatism originates basically from three ways and will all have a negative effect on the energy conversion. As, the first one will occur when the laser is not angle aligned with respect to the optical axis. In this case, the focal points will be separated and this is how astigmatism manifests itself. Figure 3.6 shows astigmatism created due to misalignment and the 2 separated focal points small in the right upper corner what is enlarged in fig. 3.4b.

The second reason can be the mounting of the mirror. For example, fixing the mirror with four bolts, one at each corner can bend the mirror in a saddle shape which can relate to astigmatism.

The third way of occurring astigmatism is by hitting a mirror with a high power laser whereby thermal effect causes the mirror surface to deform. Especially when a hot beam is entering from an angle, this ensures an elliptical beam on the surface where this surface will deform locally. Section 6.1 will dive into the deformation created by the laser and explain this further.

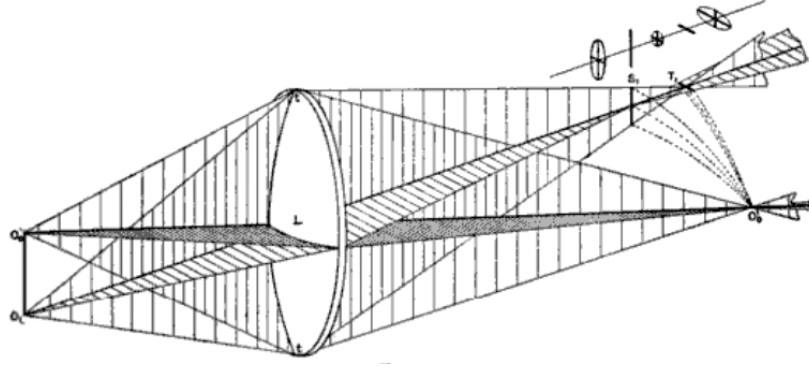


Figure 3.6: Astigmatism[2]

In the best case the droplet will be hit by the circle of least confusion [8], this is the point where the focus point has the least area and thus has the most power to hit the droplet. It can be noticed that even it is hit in this area that is always larger than a non-aberrated system. Second and third astigmatism type will occur when the shape of the optics is deformed, which can occur by a heat load or by an induces stress from the mounting the mirror. The requirements for astigmatism are specified and in FFA-FU mk11 [7] two maximum astigmatism requirements are taken and given in table 3.5. The requirements without the M150 will be given for the pre- and main pulse. The requirements for low power are higher since the size of, the area were to hit the droplet with, is smaller. Because the droplet is just 30 μm and after being hit by the pre-pulse, the main-pulse will hit the bigger pancake. However, since the thermal time constant of the mirror is way larger then the 50000 Hz, the pre-pulse will suffer from the deformation created by the main-pulse.

FFA-FU contribution to AST @ full power, excl. M150	Z5: 0.137 λ	Z6: 0.137 λ
FFA-FU contribution to AST @ low power (Cold AST), excl. M150	Z5: 0.080 λ	Z6: 0.080 λ

Table 3.5: Astigmatism given in $\text{m}\lambda$ FFA-FU

In table 3.6 the individual astigmatism budget per mirror is given. And split up in parts for the mounting and manufacturing describes as mirror cold. And finally the thermal deformation is also specified. This separated the budget is found in μm [9]. A simple calculation is done to check the order of the magnitude of the budget.

$$0.080\lambda * 10.26e - 6 = 0.82\mu\text{m} \quad (3.1)$$

For cold astigmatism, it can be seen that 2 mirrors of 0.3 μm are in the order of the calculated 0.82 μm .

FU M1 Mirror cold	0.3 μm
FU M1 Mounting	0.18 μm
FU M1 Thermal deformation	0.8 μm
FU M2 Mirror cold	0.3 μm
FU M2 Mounting	0.18 μm
FU M2 Thermal deformation	0.8 μm

Table 3.6: Astigmatism budget

Position tolerance based on AST

What could be seen in fig. 3.1b is that by moving the mirror in one direction the focal point was also shifting in the same direction. Because of this effect, no AST was arising. However, was this in 2D and just in one

direction was looked at. If the mirror is shifted in the y axis, and it is being looked only in this plane nothing happens. But, by taking a look at the light rays perpendicular to that something is happening. Shown in fig. 3.7a in red is the moved mirror and in blue the original positing. The rays in the x-plane will end up in the blue focal point and the rays in the y-plane will end up in the new focal point as shown in fig. 3.7b.

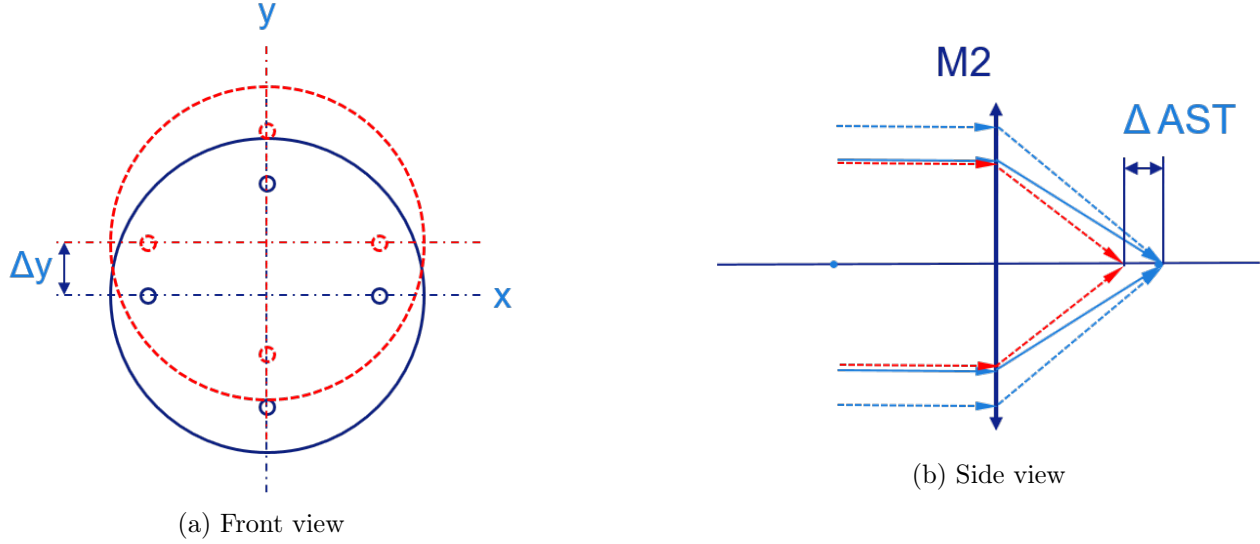


Figure 3.7: Rays from two sides

With some trigonometry the Δ AST can be calculated. By moving the mirror 0.01 mm in the y direction, Δ AST becomes 0.064 mm. Then by using the formula for sag of a circle, the difference in AST distance should be back calculated to AST wave-front. By doing so, $0.4 \mu\text{m}$ AST is found. The optical modeling program Zemax is used to obtain the amount of AST by misalign the mirror in multiple directions. This is done in all six DOF, so three translations and 3 rotations. Corresponding Z5 and Z6 is given in column next to the amount of misalignment.

M2 Position sensitivity Z5 & Z6							
	mm	Z5[λ]	Z6[λ]		deg	Z5[λ]	Z6[λ]
x	0.001	-0.00015	-0.00015	Rx	0.001	0.001676	-0.00165
x	0.01	-0.00148	-0.0015	Rx	0.01	0.016758	-0.01649
x	0.1	-0.01476	-0.01501	Rx	0.1	0.167139	-0.1654
y	0.001	-0.00015	0.000148	Ry	0.001	-0.00165	-0.00168
y	0.01	-0.0015	0.001476	Ry	0.01	-0.01648	-0.01676
y	0.1	-0.01501	0.01476	Ry	0.1	-0.16433	-0.16706
z	0.001	-3E-07	-2.7E-07	Rz	0.001	0	0
z	0.01	-3E-06	-2.7E-06	Rz	0.01	0	0
z	0.1	-3E-05	-2.7E-05	Rz	0.1	0	0

Table 3.7: Sensitivity table Z5 & Z6

As can be seen table 3.7 is the sensitivity linear with respect tot the position. With this a position specification can be made representative for the mounting budget. Shown in table 3.8 are the chosen precisions in all six DOF with related amount of astigmatism. Finally, in the last column total RMS astigmatism in waves is shown and the wavelength used is $10.6 \mu\text{m}$.

M2 Position sensitivity Z5 & Z6							
M2	x [mm]	y [mm]	z [mm]	Rx [deg]	Ry [deg]	Rz [deg]	RMS [λ]
\pm	0.05	0.05	0.05	0.005	0.005	0.01	
Z5 [λ]	-0.0073821	-0.00751	-0.0000152	0.008381	-0.00824	0	0.015781
Z6 [λ]	-0.0075046	0.007382	-0.0000137	-0.00824	-0.00838	0	0.015781

Table 3.8: Position precision M2 based on astigmatism

To summarize the position tolerance, the translations can be misaligned $\pm 50 \mu\text{m}$ and the rotations are converted from $\pm 0.005 \text{ deg}$ to $\pm 87.26 \mu\text{rad}$.

3.2 Transportation

To get parts from one place to another place the parts need to be transported. During this process, the parts should be able to withstand force as thermal expansion and vibrations. Because of this, transportation requirements are found and described in this section.

3.2.1 Temperature variations

During transport the max temperature change is specified as KN2 which means a variation between 0 to 45 °C with a start temp of 22 °C [7].

3.2.2 Shock load

Shock load is defined due to transport and is found as 7g, so the design should survive those shocks in all directions [7].

3.3 Mechanical constraints

The mechanical constraints will not exactly be specified, the mechanical volume allowed will be in the order of current design. As a result of a growing mirror, this spec could also be enlarged. Because of this reason, a roughly range is specified where the design should fit in. Since the mirror is broadly round, the length and width are specified as 250 - 350 mm. The range in height is specified as 75 - 150 mm.

3.4 Summary requirements

This section summarizes the specifications in terms of requirements table 3.9, Environmental conditions table 3.10 and the mechanical constraints table 3.11 respectively.

Requirements	
Eigenfrequency	>150 Hz
Position precision	50 μm
Angular precision	87 μrad
Astigmatism	0.18 μm

Table 3.9: Requirements

Environment conditions	
Shock Load	7 g
Environment	Vacuum compatible
Thermal laser load	25 - 50 kW
Temperature variations	0 - 45 °C
Cooling water	0.1 - 1 °C

Table 3.10: Environmental conditions

Mechanical constraints	
Length	250 - 350 mm
width	250 - 350 mm
Height	75 - 150 mm

Table 3.11: Mechanical constraints

Chapter 4

Problem of current design

This chapter will investigate the current subsystem and dive into possible problems that are found and will give thereby insight for a new design. This chapter will start with some hand calculations followed by a comparison that is done in COMSOL.

4.1 Design evaluation

Both mirrors are made of copper brazed on a stainless steel slab and the optical surface is coated with a coating to protect the mirror for hydrogen embrittlement. The absorption of this coating is 1% which implies that with a laser of 25 kW, 250 W will be absorbed by the mirror. Cooling channels are integrated beneath the mirror surface to conduct the absorbed laser heat. Water is flowing through those channels to keep the mirror at a certain temperature. The mirrors are fixed in a precisely machined Aluminium mirror housing where the M1 is fixed by 4 bolts and the M2 with 16 bolts. During operation will the Aluminium mirror housing be cooled using integrated cooling channels. The bolt holes of the M2 mirror can be seen in fig. 4.1 specified as ABCD. During the mounting of the mirror, the force on the bolts is adjusted in such a way that the wavefront is being optimized. The bolts that aren't used are left out, so in the fig. 4.1 it can be seen that in both C and B a bolt is missing of the 16 bolts in total.

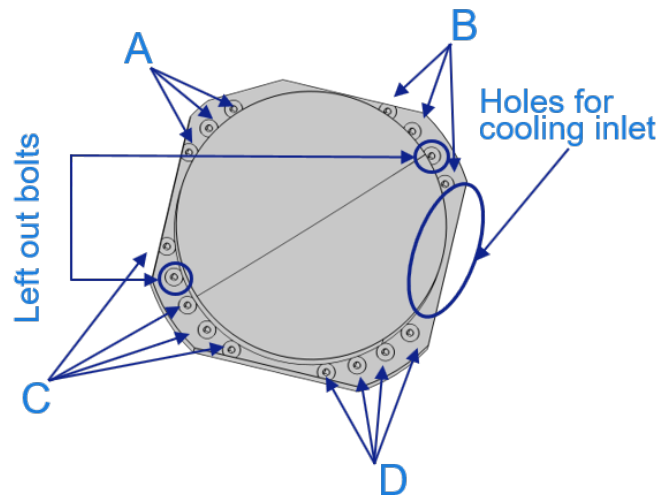
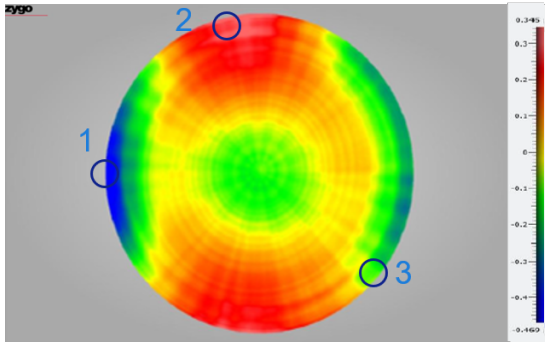


Figure 4.1: Frontside of M2

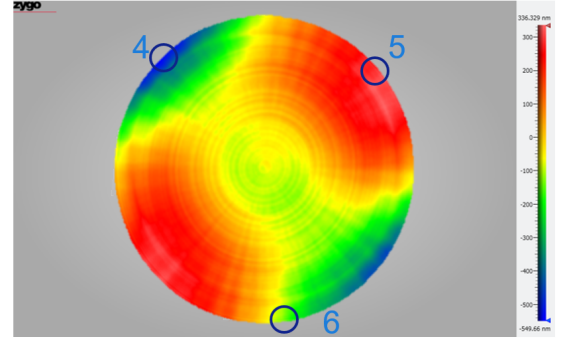
4.2 Optical surface deformation

A possible problem noticed by ASML is the fact that, even without being used, due to transportation a deformation of the mirror is observed. And as described in the requirements this kind of deformations

should either be come from the temperature change or the shock load. Figure 4.2a shows the shape before transport and fig. 4.2b shows the shape after transport. What can be seen is a shift of the highest peak which seems to be rotated of 45 degrees. Rotation should not be possible because the measurement is done in the same setup, therefor a real optical surface deformation should have taken place.



(a) Before shipment PV: 814nm RMS: 139nm



(b) After shipment PV: 886nm RMS: 174nm

Figure 4.2: Deformation due to Transport

The measurement is done with a spherical reference mirror and measures the M1 and M2 at the same time. A picture of the measurement setup can be found in appendix B.1. Yellow in the figure is assumed to be zero deformation, point 1 and 4 are the valley's point and point 2 and 5 are the highest peaks. In fig. 4.2a the difference between point 1 and 2 is $0.814 \mu\text{m}$. Added to this are 25 points, 1 in the center and 16 at the outer ring and in the middle ring another 8. Two figures were those points are shown are given in appendix B.1. Through these points are Zernike polynomials fitted and those can be seen in fig. 4.3. Both before as after shipment is given in the graph and also a delta is added to show the actual deformation due to transportation.

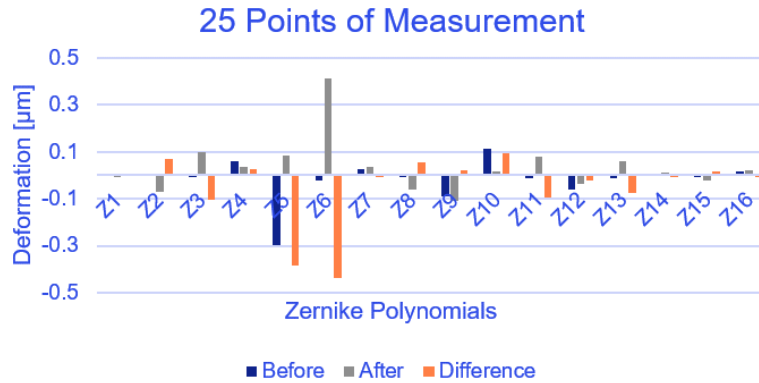


Figure 4.3: Zernike Polynomials of measurement

What also can be seen in fig. 4.3 is that before the shipment the astigmatism Z5 is present and after shipment, this is changed in astigmatism Z6. This can explain the 45-degree rotation as said before. To compare this with the requirements of both cold mirror plus mounting and it can be observed that this mirror does stay within the specification. Also after shipment, the requirement of $2 \times 0.48 \mu\text{m}$ is met. It should be noticed that this is without the laser's thermal deformation and that an unpredictable deformation has taken place.

A possible reason for the mirror deformation can be the stick-slip at the bolts which are used to bold the mirror down. This can either come from the heat load or the shock load. To exclude the shock load during transportation following simple calculation can be done and is presented in eq. (4.1).

$$F_{shock} = m * 7g < F_{friction} = \mu * n * F_N \quad (4.1)$$

where

- F_{shock} = Shock load [N]
- $F_{friction}$ = Friction force created by bolts and friction coefficient [N]
- μ = friction coefficient [-]
- n = number of bolts [-]
- g = gravitational force [m/s²]

The values used will be specified in this heat section below but used are 16 bolts and a F_n of 18100 and a friction coefficient of 0.3. Thereby a maximal mass for the mirror is determined as 379 kg which is around 10x higher than it is now and thus can be the pure shock-load excluded for creating stick-slip.

To show what will happen by temperature changes a simple calculation is done. By showing a model in fig. 4.4 with just two bolts it can be shown that the thermal force will be larger than the friction force created by the bolts. It is assumed to have a common M6 bolt force of 18100 N [10]. The worst case is created by assuming that at the left bolt no stick-slip will occur.

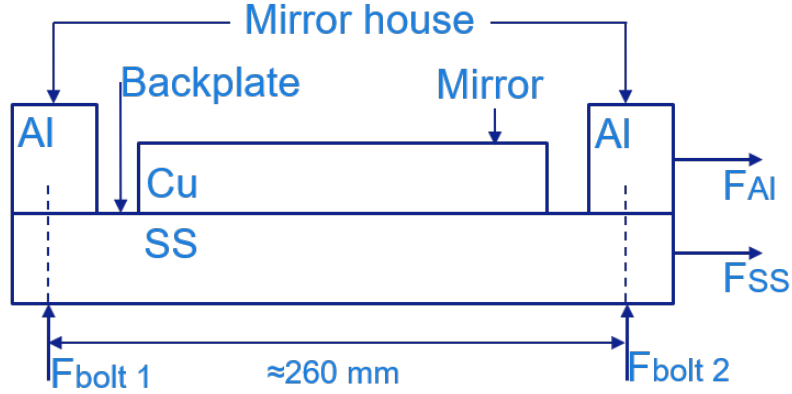


Figure 4.4: Thermal expansion

	E [Pa]	α [1/k]	k [$\frac{w}{m \cdot k}$]
Copper	1.17e11	1.6e-5	400
Stainless steel	2.00e11	1.65e-5	16
Aluminum	6.89e10	2.32e-5	180

Table 4.1: Material properties

Table 4.1 shows the material properties of the materials used in the system, Copper for the mirror, stainless steel for the backside and aluminium for the mirror housing. These properties are used in calculations below. To calculate the force by means of the thermal expansion eq. (4.2) is used and will be used in next equations.

$$\left. \begin{aligned} F &= k * \Delta l \\ \Delta l &= \alpha * l * \Delta T \end{aligned} \right\} F = \frac{EA}{l} * \Delta l = EA\alpha\Delta T \quad (4.2)$$

Since there are two different materials with a different CTE the expansion length will be different. Both eq. (4.3) as eq. (4.4) are used to specify the difference in expansion length.

$$\left. \begin{aligned} \Delta l_{SS} &= \alpha_{SS} * l * \Delta T \\ \Delta l_{AL} &= \alpha_{AL} * l * \Delta T \end{aligned} \right\} \Delta l = \Delta l_{AL} - \Delta l_{SS} = (\alpha_{AL} - \alpha_{SS}) * l * \Delta T \quad (4.3)$$

$$\left. \begin{aligned} F_{AL} &= \frac{E_{AL} A_{AL}}{l} * (\Delta l_{AL} - \Delta l) \\ F_{SS} &= \frac{E_{SS} A_{SS}}{l} * (\Delta l - \Delta l_{SS}) \\ F_{AL} &= F_{SS} \end{aligned} \right\} \Delta l = \frac{(E_{AL} A_{AL} \alpha_{AL} + E_{SS} A_{SS} \alpha_{SS}) * l * \Delta T}{E_{SS} A_{AL} + E_{AL} A_{AL}} \quad (4.4)$$

The area used to calculate the force normal to the surface is assumed to be 50 x 50 mm, this assumption is based on the perimeter divided by the 16 bolts and is comparable with the height of the Stainless Steel plus copper. Also the area of the Aluminium is taken the same.

$$F_{res} = E_{AL} * A_{AL} (\alpha_{AL} * l * \Delta T - \Delta l) \quad (4.5a)$$

$$\mu = \frac{F_{res}}{F_{bolt}} \quad (4.5b)$$

where

F_{SS} or F_{AL}	= Force Stainless steel or Force Aluminium [N]
E_{SS} or E_{AL}	= Young's modulus Stainless steel or Young's modulus Aluminium [N]
α_{SS} or α_{AL}	= Coefficient of thermal expansion Stainless steel or Aluminium [1/k]
ΔT	= Change in temperature [k]
μ	= Friction coefficient [-]
F_{bolt}	= Normal force per bolt [N]

From the website Tribonet [11] it can be seen that the friction coefficient between stainless steel and Aluminium in a vacuum is 0.3. It should be noticed that in a vacuum the friction coefficient can differ and thereby introduce extra uncertainty. The friction coefficient is the ratio between the thermal force and the perpendicular normal force within this case, is given by the bolt force. By comparing the friction force calculated and by a specified value of 0.3 it can be seen that already at a temperature variation of 7 °C a higher friction coefficient is needed to stick, thus stick-slip will occur.

This means that during transportation where the temperature variation can be 7x higher, so it's very likely is that stick-slip will take place but this will be further explained in section 4.3. Stick-slip will ensure an unpredictable movement, this is because due to the heat the material will expand and due to that shall bend. Then at the moment that the slip occurs the material will relax and change shape. By cooling down this stick-slip will have the opposite effect. Because it depends on a lot of variables such as the bolt force, contact shape and thermal fluctuation it's unpredictable to exactly describe this movement. Table 4.2 set outs the forces, corresponding friction coefficients and shows what happens with temperature change. A cycle is shown where it will heat 7 °C and here in red it's indicated were it slips due to passing the 0.3 μ .

$\Delta T[k]$	$F_{SS}[N]$	$F_{AL}[N]$	$F_{res}[N]$	$F_{bolt}[N]$	$\mu[-] \downarrow$
0	0	0	0	18100	0
1	8250	3996	858	18100	0.047
2	16500	7992	1717	18100	0.095
3	24750	11989	2575	18100	0.142
4	33000	15985	3434	18100	0.190
5	41250	19981	4291	18100	0.237
6	49500	23977	5150	18100	0.285
7	57750	27977	6009	18100	0.332

Table 4.2: Friction coefficient vs Temperature

In fig. 4.5 the four stages are shown which are equivalent with the last column of table 4.2. The initial condition where the bolts are fixed is given in fig. 4.5a, the dark blue suggests the stainless steel mirror and the light blue the Aluminium. Then in fig. 4.5b the temperature rises but the friction coefficient has not reached the 0.3μ yet, which gives just a stretch as given in table 4.2. In fig. 4.5c and the last column of table 4.2 the friction coefficient has crossed the boundary of 0.3μ and thus means that the mirror slips. Finally, if hysteresis is ignored for now and the Aluminum contracts again because of the temperature drop a deformation can be seen in fig. 4.5d.

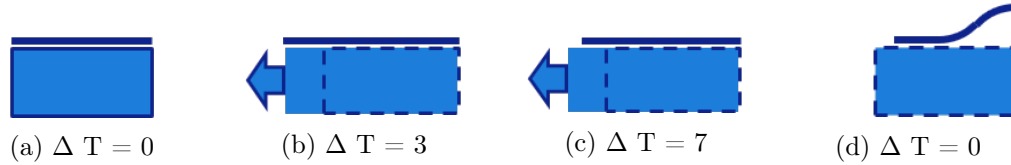


Figure 4.5: Slip conditions

The copper mirror is brazed on a slab of stainless steel but this is excluded in the formula because it can be imagined that if the mirror shape is optimized by the bolt forces and those are varying during expansion the copper mirror shape will change. Another problem of the art is the fact that in the future the laser power will go from 25 kW to 44 kW. Here the thermal gradient will probably grow and therefore the force created will increase. The takeaway message here should be that the forces created by the thermal expansion should be handled by the design of the mirror mount. But a hand calculation which takes into account, the laser heat, cooling channels, and the bolt forces will be difficult. Therefore in the next section, a simulation will be done to explore the forces during operation.

4.3 COMSOL model to compare

This section will simulate the behavior of the mirror in 3D and will explore this in detail. This is done for both operation mode and transportation. The last section has already shown a hand calculation of the forces that arise during transport. The first part of this section will continue with this and the second part will show the simulations during operation.

4.3.1 Model transport

A model is built to investigate the forces and stresses in the mirror as the M2 is nowadays and can be seen in fig. 4.6. The optical surface is facing upwards in the positive y-direction. The blue surface pads illustrate the area where the bolt stress is minimal 50 MPa and thus also is the area where the assumption of the amount of friction force in the connection with the mirror house (not shown) is valid. The radius of the pad is calculated as 8 mm. Also in the model are the materials copper as a mirror with Stainless Steel back.

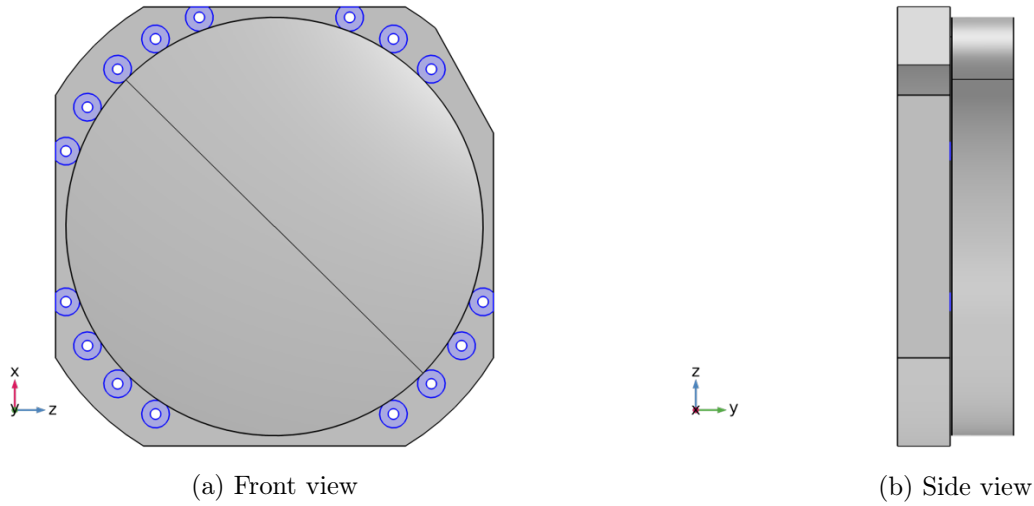


Figure 4.6: Transportation model M2

As specified in the requirements will the temperature vary during transportation between 0 and 45°C. In the COMSOL model will be worked with Kelvins and 293.15 K is used as start value. First, a check is done to verify the hand calculations in the section above. Here, the blue pads are given to be connected with Aluminium, thus the pads feel a CTE at the surface of Aluminium like it's expanding from the center of the mirror. The surrounding is heated and boundary probes are used to measure the shear stress of the pads. The force calculated on the pads is done by taking the integral over each pad. Assumed is that the direction of this force will be in the radial direction of the mirror by homogeneous heating. Table 4.3 shows the forces for the corresponding temperatures and difference between the hand calculations and the COMSOL model in Newton's and percent.

Temperature	Force in COMSOL (N)	Handcalculation (N)	Difference (N)	Difference (%)
293.15	0	0	0	0%
294	912.19	858	-54.19	-6%
295	1983.2	1717	-266.2	-13%
296	3051.7	2575	-476.7	-16%
297	4118.2	3434	-684.2	-17%
298	5182.5	4291	-891.5	-17%
299	6244.6	5150	-1094.6	-18%
300	7304.4	6009	-1295.4	-18%

Table 4.3: Compare COMSOL values with hand calculations

It can be seen in fig. 4.7a that the mirror has deformed and stresses are build up in the pads. No conclusions are made now but just validating the model. By comparing the hand calculations it is shown that the assumption of getting slip after a few degrees is valid. The hand calculations and COMSOL values are plotted in a graph it can be seen that they are both linear but have a slightly different slope. The reason for this can be the stiffness of the structure that is neglected in the hand calculation or the assumed areas are not correct. However, the results are in the same order of magnitude and therefore an indication that the model is valid.

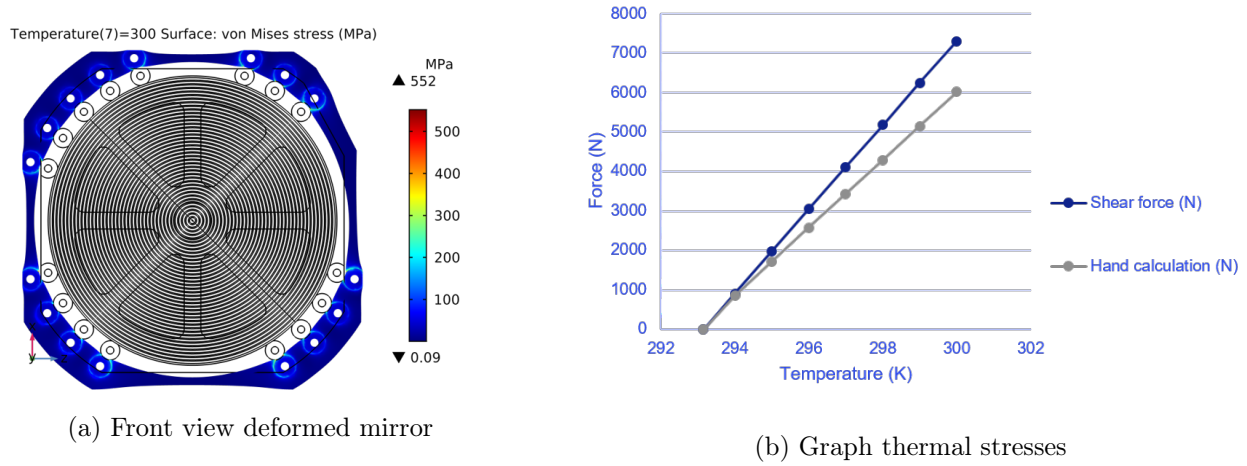


Figure 4.7: Deformation due to thermal expansion

To check which bolt will slip first all forces per bolt need to be known the values of bolt 8 were already investigated and are shown in table 4.3. This is done for each bolt and a plot is made that can be seen in fig. 4.8b. The bolts are numbered clockwise as shown in fig. 4.8a, started left with number one. Interesting to see is the fact that the force differs per bolt and that it gets worse with increasing temperature. For example, bolt 8 takes the most force here, this is also very likely by looking at the position of this bolt. Bolt 8 is in a series of 3 bolts and between bolt 8 and bolt 9 is the largest amount of material without bolts.

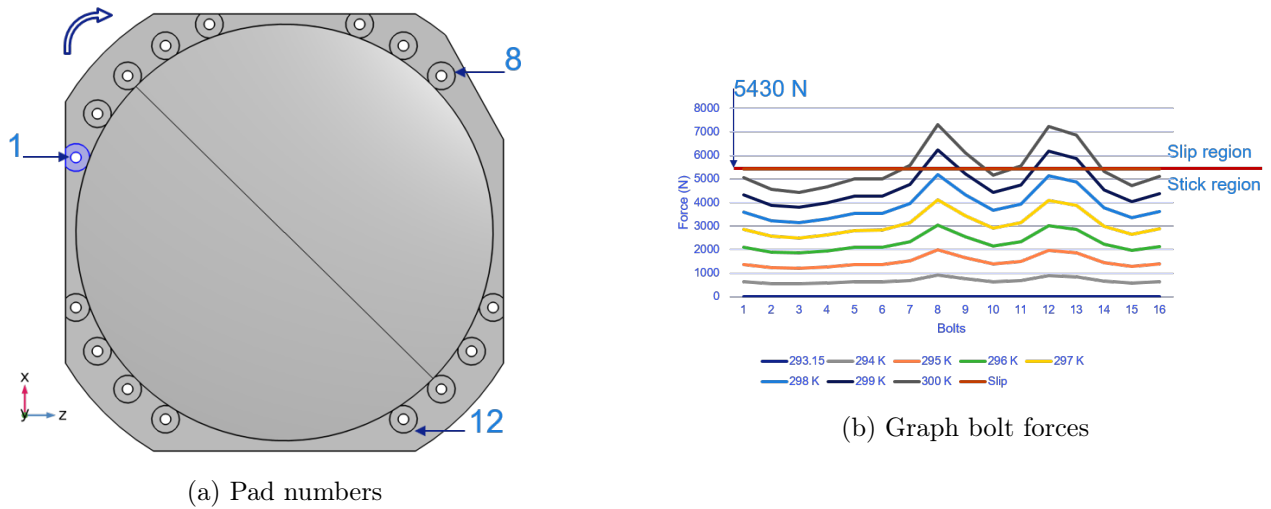


Figure 4.8: Force per bolt

It is known which bolt slips first, namely bolt 8. But it can be seen that bolt 12 is also really close at the friction boundary. The slip condition here is calculated as the bolt force*friction coefficient as 5430 N. To determine what exactly will happen a sequence is used and shown in a list here.

1. Fix all 16 bolts.
2. Heat up.
3. Check at what temperature the first bolt slips.
4. Remember that temperature.
5. Loose that bolt and put a roller constraint on it.
6. Heat up to the remembered temperature.

7. Check if there is another bolt that slips. if yes go to step 5 again. if no go to the next step.
8. Check the positions of the holes of which the bolt has slipped.
9. Move the holes to the opposite position as if they are pushed back in.
10. Check optical surface

Step 1 to 4 can relate to fig. 4.9a and it can be concluded that at 298 K bolt 8 will slip first. The moment that bolt 8 slips, bolt 7 gets more force which gives the feeling that this one will slip earlier than for example bolt 12. To simulate this, bolt 8 is not fixed anymore and the model is heated up again as described in points 5 and 6.

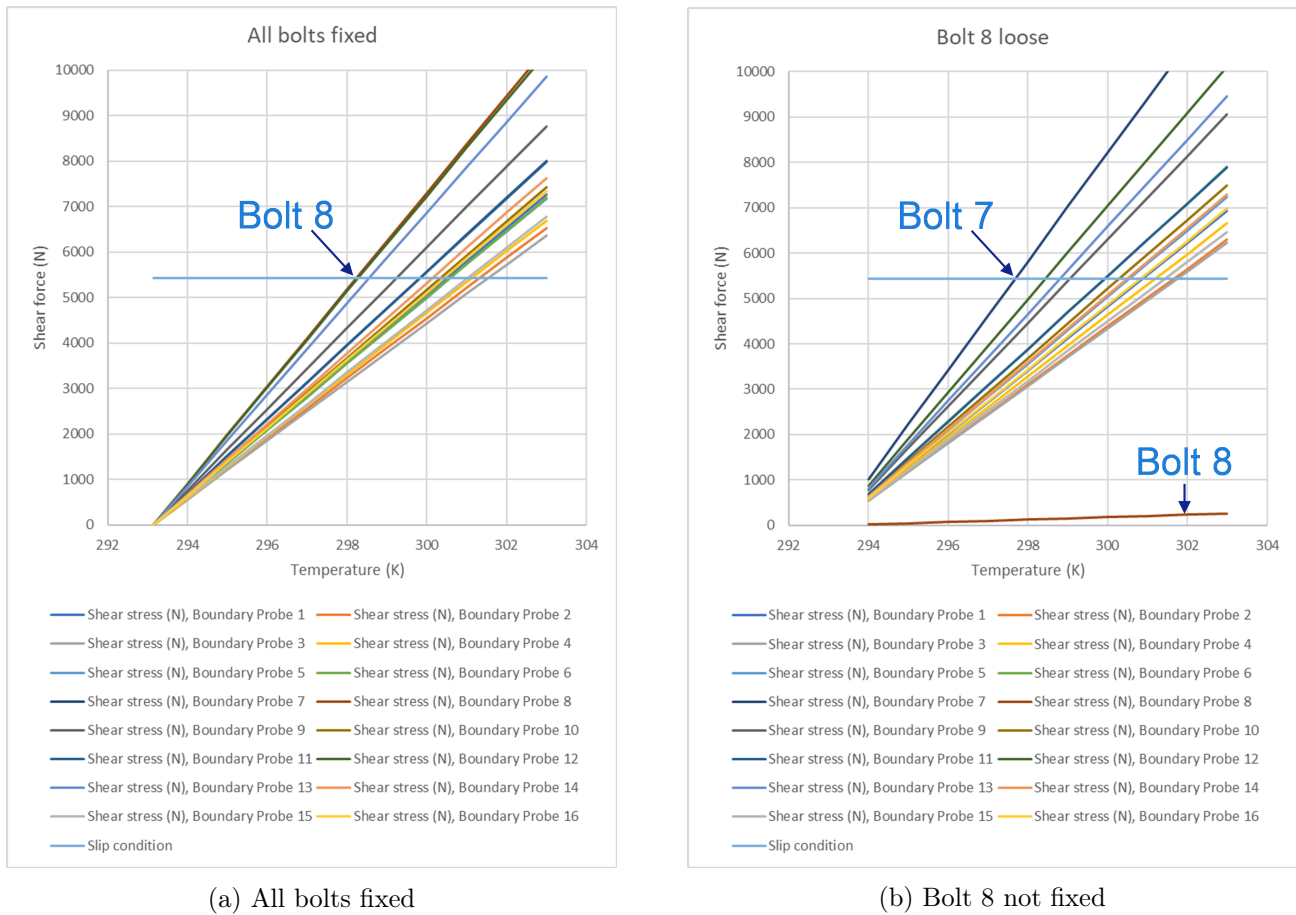


Figure 4.9: Temperature VS force per bolt part 1

By doing this bolt 7 has to take more force to compensate, this can be seen in fig. 4.9b. This means that when bolt 8 slips bolt 7 will follow and thus also slip. Thereafter bolt 6 will take more force and as can be seen in fig. 4.10a bolt 6 will slip as well.

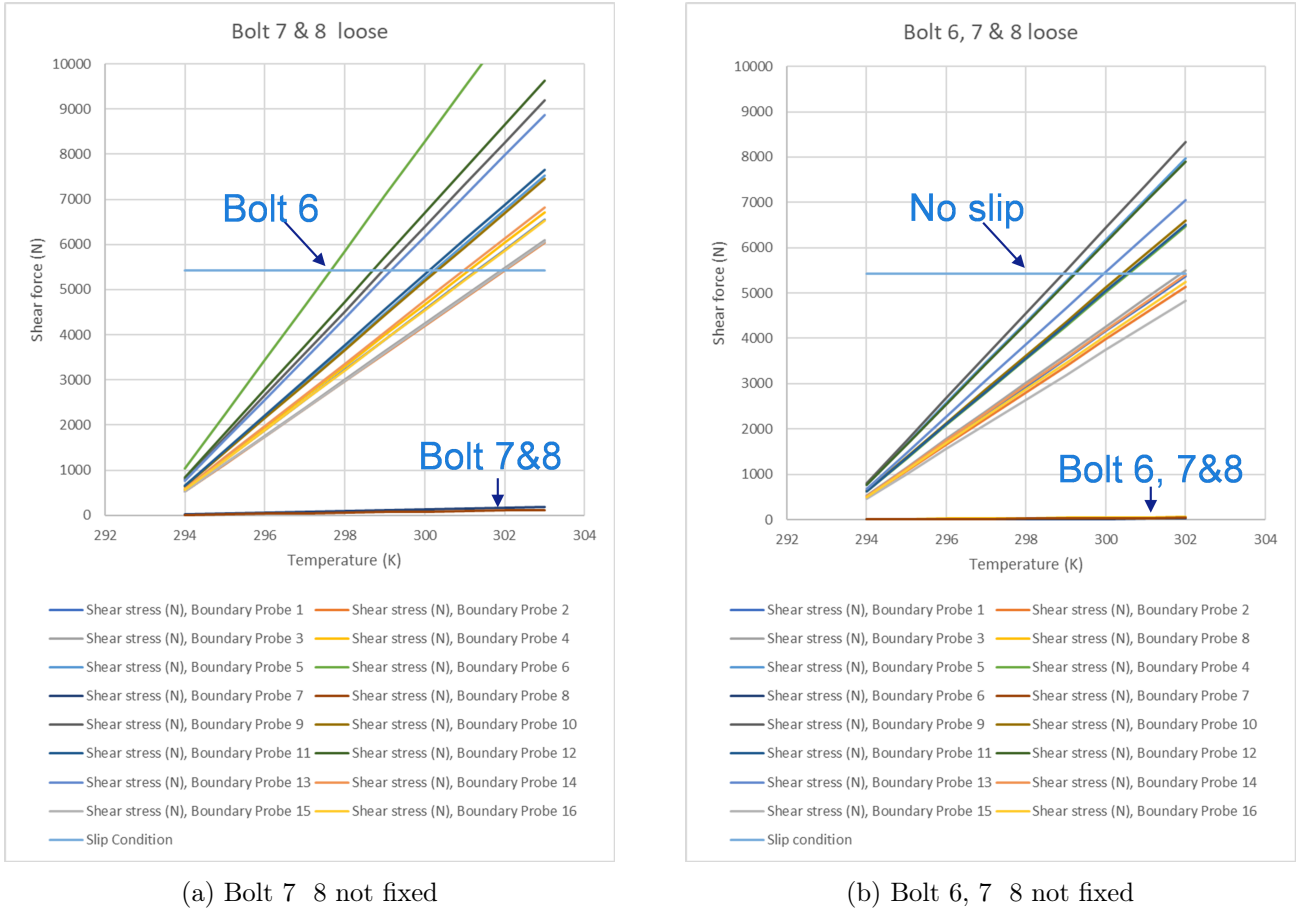


Figure 4.10: Temperature VS force per bolt part 2

The last simulation is done where bolt 6, 7 and 8 are not fixed and here again it can be seen that bolt 9 and 5 will take more force but lower than the slip boundary of 5430 N. This means that at 298 Kelvin bolts 6,7 8 will slip to the new position which is further outwards. If hysteresis is neglected for a moment and we simulate bolt 6, 7 and 8 are slipped to the new position and the model is cooled down the optical surface will look like fig. 4.11. Here the bolts are pushed further inwards due to the shrinking of the material. The Y-axis is parallel to the normal of the optical surface.

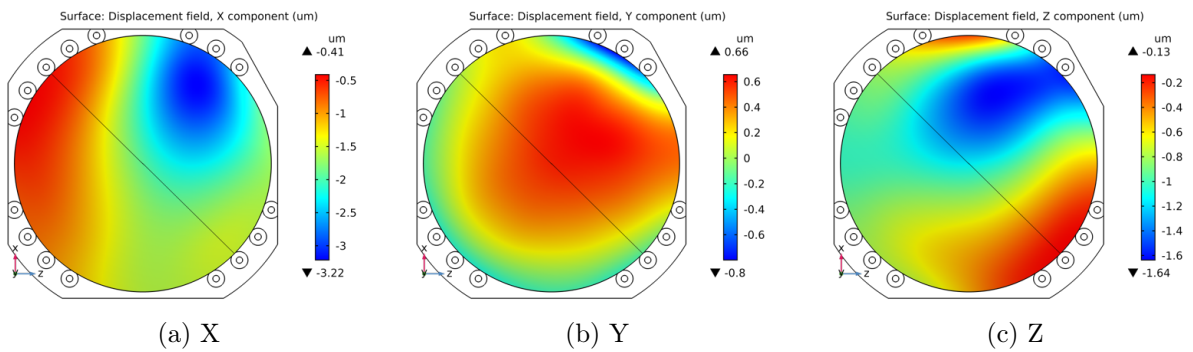


Figure 4.11: Surface deformation in x, y and z direction

It can be questioned if only looking at the Y displacement of the surface is sufficient to specify the deformation, because the actual displacement will happening not directly at that point but slightly shifted. To check this the difference in the Y surface divided by the diameter of the mirror can be calculated and used as a ratio to determine the error. Diagonal is the most deformed so t_{max} is calculated as follows.

$$t_{max} = \sqrt{x_{max}^2 + z_{max}^2} = 3.19\mu m. \quad (4.6)$$

where

t_{max} = Maximal in plane deformation [μm]

x_{max} = Maximal deformation in x direction [μm]

z_{max} = Maximal deformation in z direction [μm]

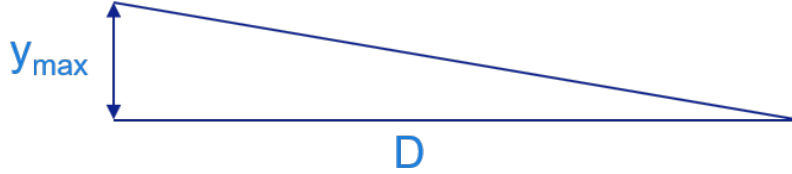


Figure 4.12: Y_{max} Vs Diameter

The maximum displacement in Y_{max} is $1.46 \mu m$ and the diameter of the mirror is given as 240 mm . Thus the ratio can be calculated as follow and is shown in fig. 4.12.

$$\frac{y_{max}}{D} = \frac{1.46e - 6}{240e - 3} = 6.0833e - 6 \quad (4.7)$$

where

y_{max} = Maximal deformation in y direction [m]

D = Total Diameter [m]

This ratio can be multiplied with the maximum displacement t_{max} as $19e-12 \text{ m}$. So by looking just at the Y displacement gives an error of just 19 picometers and can be neglected. From now on will only the Y plot be shown.

Discussion of optical surface

By comparing at the optical surface given in fig. 4.11b and plot the Zernike Polynomial's as shown in fig. 4.13 as V007 it can be seen that the first three Zernike polynomials are large compared to the measurement. This can be explained by the way of measuring and because it is possible to correct for those three Zernikes during a measurement. A large change in defocus is notable but if the first four Zernikes are ignored and the higher-order Zernikes are compared. It can be noticed that Z5 Z6 are increased but not more than the measured values. An increase of coma is also notable compared with the measurement. Z10, Z11, Z12, and Z13 are higher-order Astigmatism and has more like a triangle shape instead of the saddle. This can be seen back in the surfaces and in the Zernike overview. In the requirements is just $0.18\mu m$ astigmatism allowed as the budget for the mounting but in this case, is the mirror only heated until 298 K . And a conclusion can not yet be made it this will meet the spec. By heating further it becomes less predictable which bolt will slip next. However, a possible process that could be reasonable will be described.

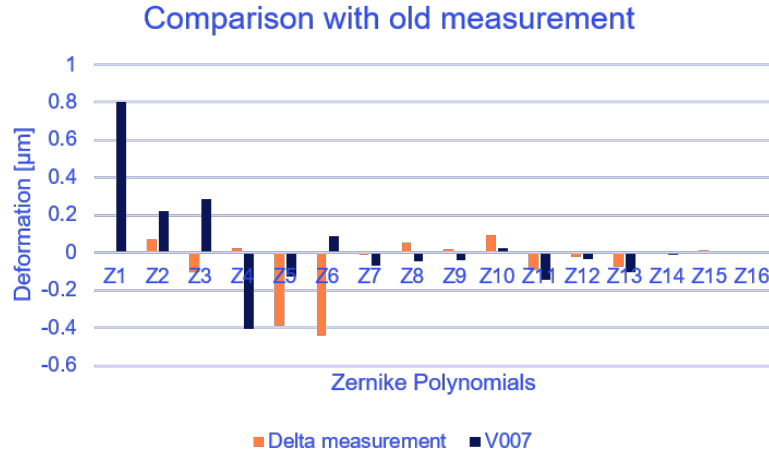


Figure 4.13: Zernike Polynomials simulation Vs measurement

By zooming in on the last graph fig. 4.10b that the order of slipping will be bolt 9, 5, 12, 13, 10, 11, 4. Bolt 9 & 5 do make sense because in this plot are 678 loose thus 9 and 5 have to take all those forces. Also, are the four bolts 9 till 12 weaker than the 5 bolts 1 to 5 simply because they are with less. However, after bolt 6 to 8 are slipped they can take force again which will lower the force in 9 & 5. This means that bolt 13 will get the most force and is most likely to slip. When this is happening the same thing will happen as before with the sequence of bolt 8 to 6 i.e. the whole set of bolt 13 till 16 will slip. Again this is a big assumption since a lot of things are not predictable and can be due to the change in friction force which can be due to the roughness below the bolts or the change in bolt force. In the simulation, it is assumed that all bolts have the same pretension and in real life, the bolt force is adjusted to tune the mirror surface.

4.3.2 Model Operation state

For the operation state, the same previous model is used to check for distortions. Again here in fig. 4.14 the blue part is copper and the gray part is Stainless steel. The pads are again fixed and will move with a CTE of Aluminium. A Gaussian laser beam with a $D4\sigma$ of 130 mm is applied to the surface at an incident angle of 15 degrees.

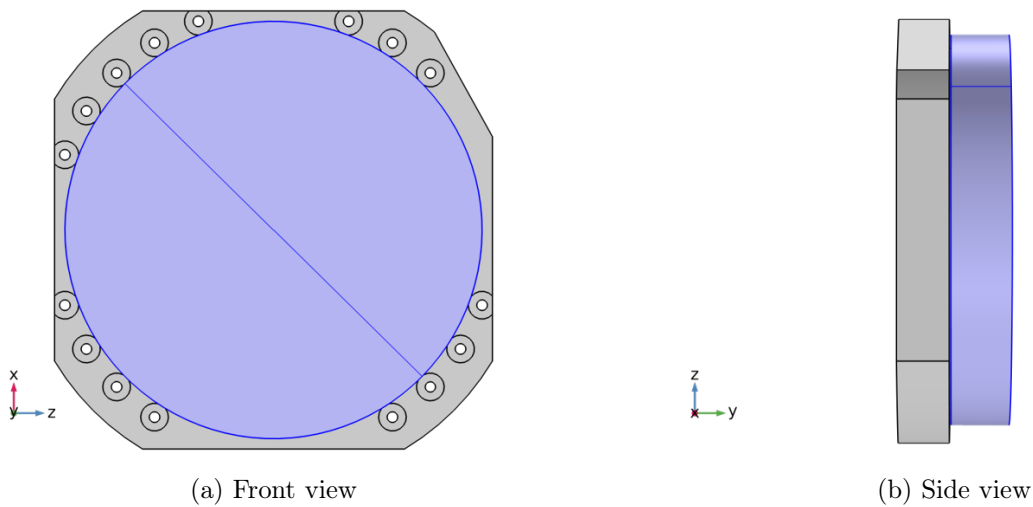
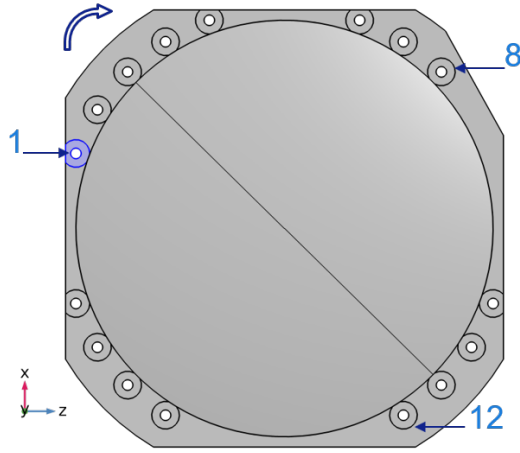


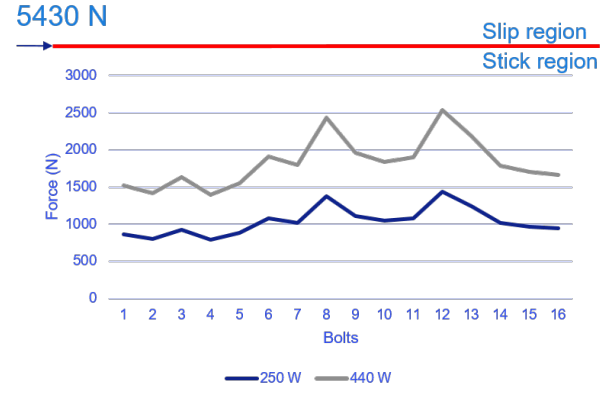
Figure 4.14: Operation model M2

This simulation is done with two different powers, 250 and 440 watts absorbed. Again here investigated is the force below the bolts, again what can be seen in fig. 4.15b is that bolt 8 and 12 do take the most stress but the force is still 2 times smaller compared to the friction force which means that stick-slip will not occur

during operation. Assumed is a thoroughly cooled mirror block as it is in real life as well. What also can be concluded from this is that if during transportation bolts have slipped, the stress will never be so high again to slip back.



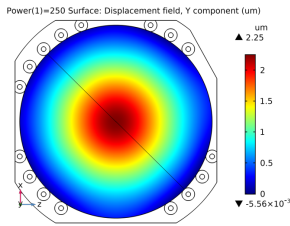
(a) Pad numbers



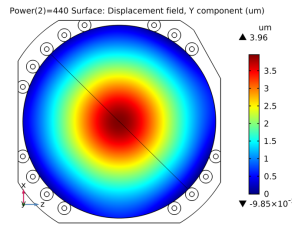
(b) Graph bolt forces due to laser

Figure 4.15: Forces at bolts

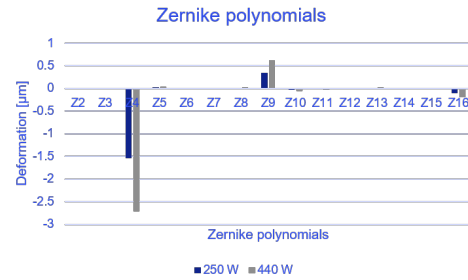
In Chapter chapter 6 multiple materials are investigated and sets out the deformations of the mirror surface due to the laser power. The different mirror surfaces of both 250 and 440 absorbed watts are given in fig. 4.16a and fig. 4.16b. From both solutions, the wavefront is compared and given in fig. 4.16c.



(a) Deformation 250 W



(b) Deformation 440 W



(c) Zernike polynomials

Figure 4.16: Mirror surface deformation due to laser power

Note that in fig. 4.16a and fig. 4.16b the mirror surface is shown and in fig. 4.16c are the Zernikes of the wavefront given. Those are determined on the $D4\sigma$ diameter and seen from a 0 Angle Of Incident (AOI).

4.4 Conclusion

As a conclusion, it can be said that the worst problem arises during transportation because there the force of the thermal expansion is bigger than the specified friction force. With a raise of 7 °C, the surface below the bolt will exceed the friction force delivered by the bolt. On the other hand, it can be concluded that during operation with proper cooling like it is today the bolts will not slip.

Part II

Literature Survey Mounting concepts

Chapter 5

Literature survey

This literature study contains two chapters, first, different mirror mounts are investigated and advantages and disadvantages are given. A distinction is made whether or not the mount is for a self-supporting mirror. The second chapter will dive into an A-thermal design strategy, where different solutions will be given to ensure an undisturbed light path.

5.1 Mirrormounts

The purpose of a mirror is to reflect the light and thereby introduce as little as possible aberrations to the wavefront. A mirror mount takes care of holding the mirror in place during operation and transportation where different disturbances will take place. As previously described in the requirements chapter, heat variations will provide expansion of the mirror and transportation will introduce shocks and vibrations. The mount should be able to keep the mirror in place without transferring those external influences into the mirror. An important distinction is whether the mirror is self-supporting or not. A Self-supporting mirror can survive without outside assistance, for example, support in the middle. The aspect ratio is leading here if a mirror is large and thin it can be imagined that self deflection is much more likely as by having a small thick mirror. To predict the behavior of the mirror it is desired to use a kinematic mount.

A rigid body is called static determined when all six degrees of freedom (DOF) are constrained ones. Figure 5.1 shows a kinematic mount where it easily can be seen that each DOF is constrained just ones. Benefits of a static determined structure are that calculations can be done quite easily, it's predictable and easy to imagine what will happen to the structure by applying force.[12] For example expansion of a strut has a one to one relation to the trajectory of the same strut and will not affect the others. Different from the flexure hinges used in actuator mechanism, a mirror mount flexure should minimizes optical surface distortions and maintains optical alignment under operation or transport and allow for local deformation as a result of thermal expansion.[13] Thus a flexure should minimize the deformation of the mirror if possible, otherwise, by its predictability, the behavior can be adopted to still satisfy the requirements. Different possibilities will be discussed and the advantages and disadvantages will be pointed out and at the end summarised in a table.

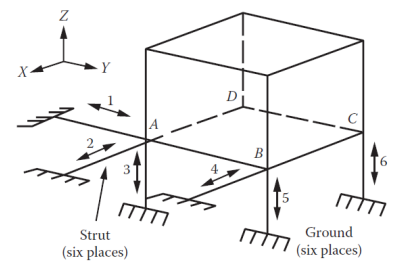


Figure 5.1: Kinematic mount

5.1.1 Whiffle tree

When larger mirrors are supported by kinematic supports, six points can be not enough to counteract for self deflection of the mirror. For those larger mirrors, it is desired to have more support points without overconstraining the mirror. So freedom is added elsewhere by adding a pivot point at a lower level. Those points are connected Y-shape shell with a wire rope in tension. These wire ropes and connected hexapod provide positioning of just six degrees of freedom [14]. In fig. 5.2 a whiffle three also for vertical mirrors can be used, by making sure that the contact point is connected to one pivot point [15]. A whiffle tree seems the ideal solution to a big thin mirror where the mirror can be supported by a lot of points without over constraining the design.

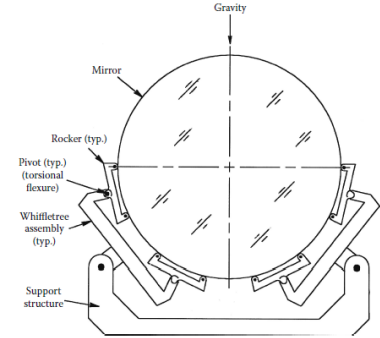


Figure 5.2: Whiffle tree

5.1.2 Hoop strap

A Hoop strap mount also, found in literature, just named as a strap mount is a cable that supports the mirror in a distributed way to divide the weight of the mirror over the whole surface. The strap mount was first described by Draper(1864) as a means of reducing the astigmatism of a mirror supported on an edge. This mount design offers the dual advantage of high performance and simplicity. Dual commercial roller chains have been used successfully instead of continuous straps to support several large horizontal-axis mirrors. A chain instead of a cable offers the advantage of rotating the mirror about its axis [15]. When having a non-axis symmetric mirror the rotation takes not place in one axis but it will move in a plane. The advantage of a hoop strap is the full support of the mirror. It works when the mirror is self-supporting and supports the radial stiffness needed. The tangential stiffness will be taken care of by the strap. A disadvantage is that it only works in gravitational direction and that by a temperature change friction will occur between the mirror and the strap.

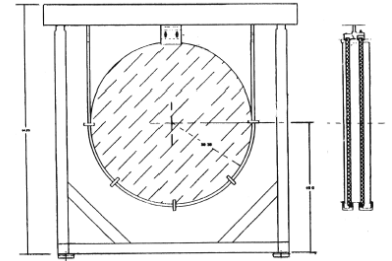


Figure 5.3: Hoop strap

5.1.3 Topology optimization

State of the art design approach of optomechanical instruments is characterized by the optical discipline creating a performance error budget. This defines deformation and limits for each optical component of the structural discipline [16]. Instead of controlling each tolerance for each mirror individual its preferred to control it at ones. This paper shows that the topology optimization used on two mirrors at the same time showed an improvement of 95.6% compared to the uncoupled optimization. However, this optimization technique is state of the art and studied in 2D, for a steady-state application with a defined load case. It also can be thought of by applying it to one mirror that this mirror can be optimized. In Topology optimization of coupled heat problems[17] this optimization is done for one mirror which includes cooling using a liquid. The advantage is that it optimizes the mechanics, fluids and optical performance. A disadvantage can occur for example during start-up where the transient behavior of the mirror comes into play or by increasing the total amount of power. By optimizing two mirrors at the same time, where the amount of power is taken into account, it can be imagined that deformation in mirror A will be countered by mirror B.

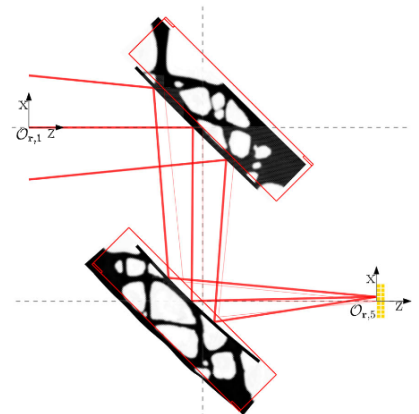


Figure 5.4: Topology

5.1.4 Nest of springs

A nest of springs fig. 5.5 is mostly used when repositioning is needed. Due to the fact of the combined stiffness of the springs, a certain location of the substrate will always be re-positioned, in that certain location.[18] Even if the shape of the object is not perfectly circular. By creating a hard reference point this will be the point where the object will be come back to after restoring the object. A property of a nest of springs is that it is easy to optimize the stiffness. By varying the number of flexures, thickness or/ and length the stiffness can be increased. In principle, the flexures should not be fixed to the optic to ensure no stress and prevent over constrains to the design. A disadvantage of a spring nest is that it is sensitive to axial when experiencing loads. The optic is fixed based on friction, and as previously discussed in the problem of the art is designing based on friction a questionable design strategy. The re-positioning effect of a spring nest can have a helpful outcome during the thermal cycle where a certain location would be at the focal point.

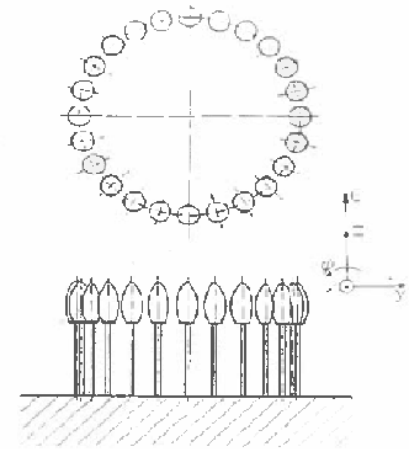


Figure 5.5: Nest of springs

5.1.5 Hexapod

A frequently seen mount for mirrors is the hexapod, in fig. 5.6. A hexapod consist of three bipods and a bipod is made out of two rods or two sets of flexures that behave in the same way as rods. A bipod has 2 DOF, one rotation at the point where the flexures cross and a translation in the perpendicular direction of the flexures [19]. A mirror supported with a hexapod with its optical axis placed vertically the paper shows a significant larger tilt into the flexures then when the optical axis is placed horizontal [20]. The hexapod mounting is a structure of six reinforced struts like the kinematic mount where the flexures are placed in an optimized orientation. For example, the bi-pod angle does not much influence the mechanical performance but the optical performance is affected because of the change in point of instant rotation center.

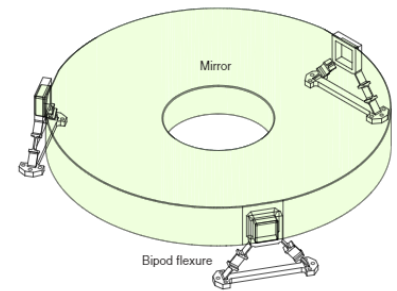


Figure 5.6: Hexapod

5.1.6 Blade flexure design

The typical blade flexure configuration fig. 5.7 consists of the bond-pad region a thin section of material and an attachment region. Three of these blade flexures are arranged uniformly around the optic which allows the mirror to remain centered on the axis by temperature variations. A study in Design and analysis of flexure mounts for precision optics is done to investigate the impact of where to bond the flexures and an optimum is found. The lower the flexures are bonded to the mirror, the less mirror surface deformation is found. But by placing the flexures further from the surface more tilt is observed [20]. This mount can be made as kinematic by making notches in the flexures but will bring undesired less stiffness into the mount.

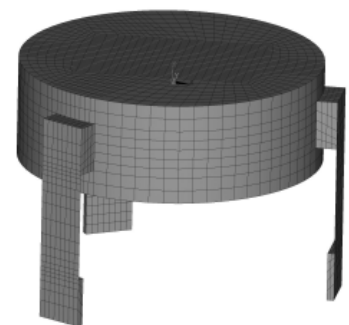


Figure 5.7: Blade flexure

5.1.7 Summary mirror mounts

	Advantage	Disadvantage	Self supporting mirror
Whiffle tree	Multiple support points	Complex	No
Hoop strap	Full support	Works in one direction	Yes
Topology optimization	Optimal in all fields	High complex	Yes
Nest of springs	Tunable	Friction based	Yes
Hexapod	Tunable	Complex	Yes
Blade flexure design	Simple	Low stiffness	Yes

Table 5.1: Mirror mounts

To already classify some mounts a table is built with pluses and minuses. With this table, a zoom-in can be made. Classifying is done in an early stage to have fewer options later on. As can be seen, some other mounts are added which will be investigated later on.

	Stiffness in plane (+ high stiff)	Stiffness out of plane	Complexity (- high complex)	Volume (- big volume)	Fit in old model	Long term drift	Thermal center at same place x y	Isostatic
Two sided leaf spring	++	-	+	+	+	+	yes	no
One sided leaf spring	+	--	+	+	+	+	no (rot)	no
Hexapod	+	+	-	-	+	++	yes	yes
Hoop-strap	--	--	+	--	--	-	no	yes
Whiffle tree	-	++	-	-	-	+	yes	yes
Topology optimazation	+	+	--	--	--	-	yes	no
Nest of springs	++	+	+	+	+	+	no (rot)	no
Current situation	++	++	+	--	+	--	no	no
six folded flexures	++	++	-	+	+	+	yes	yes
Three foldeld flexures and three rods	+	++	-	+	+	+	yes	yes

Table 5.2: All mounts

A zoom-in is made based on whether or not the mount is isostatic. Leftovers are five different mounts where two of them have more minuses then the other three. Thus in chapter 7 continued will be with those three types of mounting.

	Stiffness in plane (+ high stiff)	stiffness out of plane	Complexity (- high complex)	Volume (- big volume)	Fit in old model	Long term drift	Thermal center at same place x y	Isostatic
Hexapod	+	+	-	-	+	++	yes	yes
six folded flexures	++	++	-	+	+	+	yes	yes
Three foldeld flexures and three rods	+	++	-	+	+	+	yes	yes

Table 5.3: Selected mounts

Finally from here, a zoom-in is made in the isostatic mirror mounts, the hoop strap is excluded because of the orientation of the mirror. Also, the whiffle tree is excluded later on since the mirror will be self-supporting. Leftover is the Hexapod which is discussed in the literature study, what is notable is that the different Hexapods are tailored to the concerned mirrors. Therefor in chapter 7 continued will be with investigating the three leftover concepts that are the 6 folded flexures, 3 folded flexures + 3 rods and the Hexapod.

5.2 A-thermal design

A system where the optical light path that is limited affected by temperature is called an A-thermal design. Design guidelines are given in paper [21] and describe four ways to accomplish this. It should be noticed that these techniques are used for homogeneous heating and not due to laser power.

- Design in such a way that deformations of the system do not disturb the path.
- Use a combination of materials that compensate for the thermal expansion.
- Use materials with a low thermal expansion
- Use the fact that the optical path is insensitive to scaling effects.

5.2.1 Insensitive for deformations & scaling effects

All materials will change in size when the temperature is varying. However, a position in the material can be defined which will not move. This is called the center of thermal expansion[21]. It is possible to design in such a way that the thermal center of multiple components will end up at the same point. Then the whole system expands from this point, but complexity increases for increasing the amount of optics. By creating the entire structure from the same material the effect of temperature on the optical system can be minimized. The curvature of the mirrors and the mounting will scale as one.

5.2.2 Materials to compensate

By combining materials that have a different coefficient of thermal expansion (CTE) and varying the length points in a system can be designed to be fixed with respect to each other while the rest is deforming around it. In fig. 5.8 can be seen that by choosing the materials and lengths the focal point of M1 is always at point M2. With eq. (5.1) it can easily be calculated to have a stable length. In this case, the mirror is made from a low expansion material thus the mirror will not radially expand. But in principle, this also can be used for the radial expansion

$$L_0 = L_1\alpha_1 - L_2\alpha_2 \quad (5.1)$$

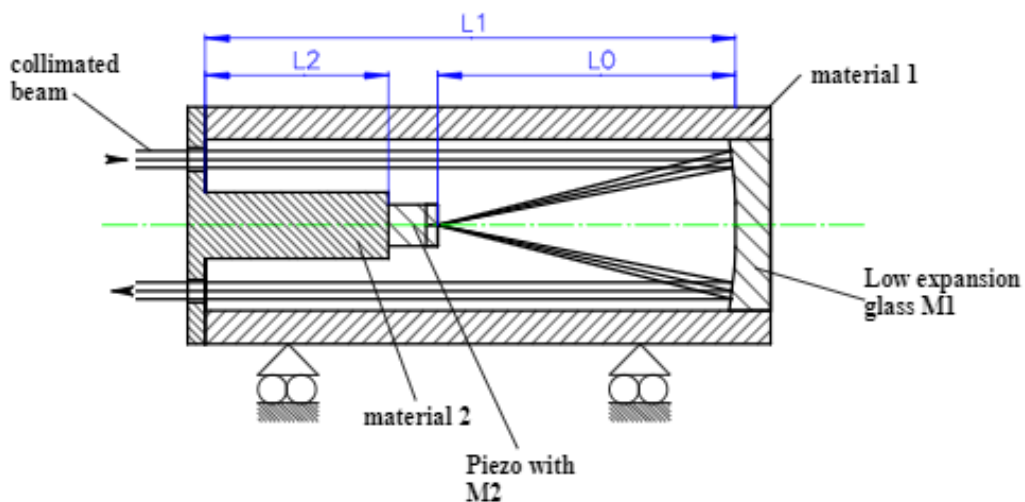


Figure 5.8: A-thermal design

5.2.3 Material properties

It seems perfect to have a low thermal expansion material and therefore can neglect the deformation, but the other properties should also fit the specifications. Therefore this section will set out some different materials that can be used in an A-thermal design and will be used during the design phase. A material to build a complete system should perform well in all aspects. A mirror needs to reflect light and therefore the material needs a high reflectivity. Also, high stiffness is desired for the structure part to create a high eigenfrequency.

Optical

One of the most important properties of a material for a mirror is of course that it will reflect the light. Reflectivity (R) is based on the material but also on the surface roughness, here the assumption will be made that the quality of the surface roughness is perfect. This means that the only factor is the material property. Also, it should be noticed that in this project the reflectivity should be maximized at the wavelength of the laser of approximately 10.6 μm . Another very important reason to increase the reflectivity is to decrease the absorbed energy of the light.

Mechanical

Properties of the mechanical structure are stiffness what is desired to be high to create a system with a high eigenfrequency. Mass or density is the second property to decrease to benefit the eigenfrequency. A high yield strength makes a material flexible without plastic deforming and that can be useful to make flexures from. A low yield strength makes a material brittle and can easily break, this is usually not desired. Young's modulus (E) is the mechanical stiffness of a solid material.

Thermal

From a thermal perspective a material, should preferably not deform therefore a low coefficient of thermal expansion (CTE) is the wish for. But since every material deforms it could better expand homogeneously. Therefore a high thermal conductivity (k) is to aim for. This ensures a quick spread out of the induced heat. A way to specify those two properties it is commonly used to combine those two as thermal stability ($\frac{k}{CTE}$).

Summary materials

Table 5.4 sets out some investigated materials with the above-mentioned properties.

Material	$R_{10.6\mu\text{m}}$ [%]	$\rho[\frac{\text{kg}}{\text{m}^3}]$	E [GPa]	σ_y [MPa]	CTE $[\frac{1}{\text{K}}]10^{-6}$	k $[\frac{\text{W}}{\text{m}\cdot\text{K}}]$	$\frac{k}{CTE}$ $[\frac{\text{W}}{\text{m}}10^6]$
Copper	99	8960	117	33.3	16 - 17	400	≈ 25
RSA-443	95	2540	102	150	13.6	135	≈ 10
Aluminum 6061	95	2700	69	276	23	180	≈ 7.8
RSA Aluminum 6061	95	2700	70	300	22.6	165	≈ 7.3
Stainless Steel 304		8000	193	215	15 - 17	16.2	≈ 1
Stainless Steel 301		8000	193	965	16.6	16.3	≈ 1
RSA-462 T6	95	2630	90	420	16.8	130	≈ 7.7
Diamond		3500	1050	HIGH	1.1	1000	≈ 1000
Titanium		4500	110	140	8	22	≈ 2.75
SiSic		3000	350	150 - 300	2.9	170	≈ 58.6

Table 5.4: Material properties

Part III

Design

Chapter 6

High-level Design

As previously discussed in the literature study a way to make a design that is not sensitive to thermal effects, is to make the entire system of the same material or use materials to compensate. Thereby use the fact that the optical path is insensitive to scaling and that there will be no stress between two of the same materials. Therefore, will this chapter present an investigation of multiple materials. Those materials can be interesting as a reflective surface during operation and at the same time provide predictable behavior during transportation. Next to this, will this chapter elaborate on the new design of a mirror in terms of size and cooling.

6.1 Material comparison

This section will discuss the difference between different deformations on mirrors due to the laser. Deformations due to the laser will depend on multiple parameters whereas the most important one will be the material of the mirror. An interesting material group that will be compared with the traditional copper is the Rapid Solidification Alloys (RSA). This relative new material made by a Rapid Solidification Process (RSP) has impressive properties and some variants have the same CTE as normal Aluminum or others as Stainless Steel which can take away the stress at the bolt interface. This section will evaluate multiple materials and conclude on the best, taking into account all areas where it should perform well.

6.1.1 Thermal stability

Materials, as discussed in the literature study, are investigated and the thermal stability is plotted in fig. 6.1. Furthermore, three fake materials are added to show the extremes. The fourth extreme material was close as diamond so the decision is made to use diamond as fourth outer edge material. The thermal stability is given by eq. (6.1).

$$Thermalstability = \frac{k}{CTE} [\frac{w}{m} 10^6] \quad (6.1)$$

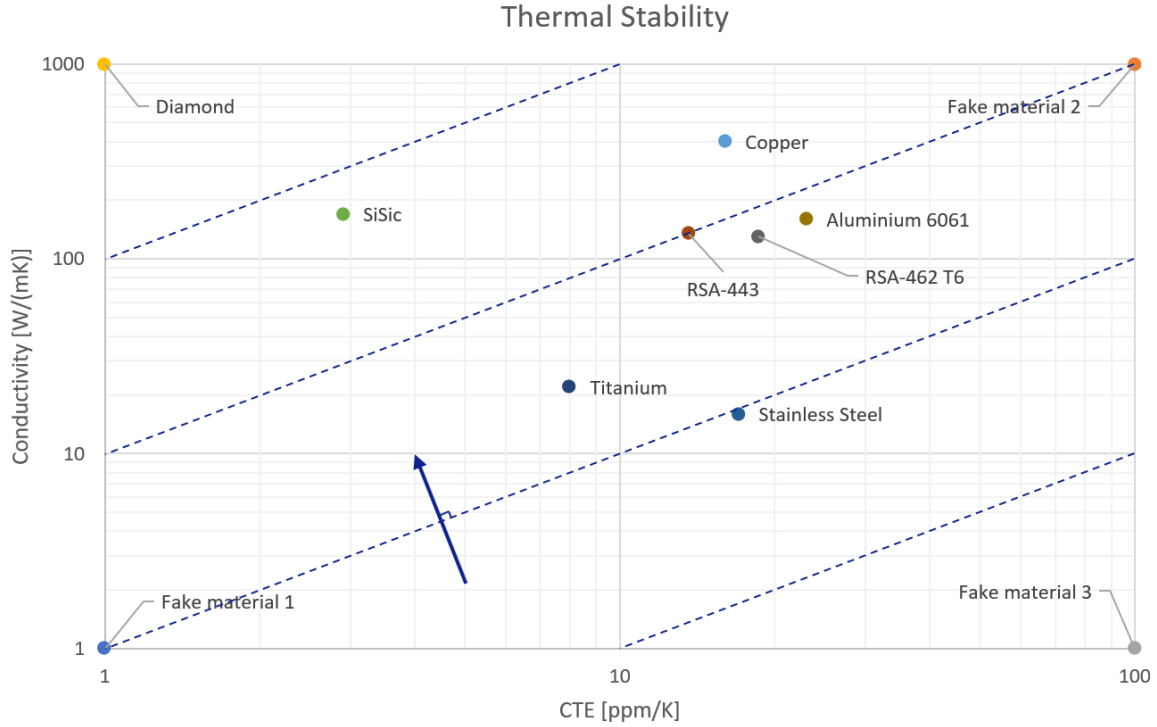


Figure 6.1: Thermal stability

Fake material 1 has a low conductivity and a low CTE, this will result in a low deformation but a high temperature. Fake material 2 is the opposite of fake material 1 and has a high CTE and high conductivity and thus will result in a higher deformation but a lower temperature. Fake material 3 has a high CTE and low conductivity. This means a high deformation and also a higher temperature. This is the complete opposite of what is desired in a mirror. Considering that deformation is also a result of a higher temperature, independent iso-lines are drawn to indicate where the thermal stability is constant and thus the deformation should be equal. Diamond has a low CTE and high conductivity. Therefore, is this the desired corner of the graph in fig. 6.1 where an ideal material could be found. From this graph, a choice for the mirror should be in the best case diamond and as second place SiSic. The fake materials will be left out from now because they were just to give insight and used to indicate an ideal corner. Chosen is to focus on five materials that can be seen in the plot in the upper part of the graph. The rest is left out because they will perform worse and the RSA alloys will be grouped. The question here is what will happen when that coating fails and thereby the absorption of the material will dominate the absorption of the coating.

6.1.2 Thermal stability Vs Absorption

If a coating fails the laser beam will end up on the material below this coating. Thus, to check the behavior of this bare material the coating is left out in this section. So first the Thermal stability is plotted against the absorption of the material in percentage. The absorption coefficient of Copper and the Aluminum types were calculated by knowing the amount of reflection. SiSic and diamond are both transparent and thus is the absorption depended on the thickness. For SiSic the absorption is found as a total of 70%, and for Diamond 9.5% per cm. Thus the amount of absorption for 3 cm is around 26% [22]. Another point here to make is the fact that since both materials are transparent thus if the coating fails the light will be transmitted. This itself shall be mitigated by handling the transmitted light by other means.

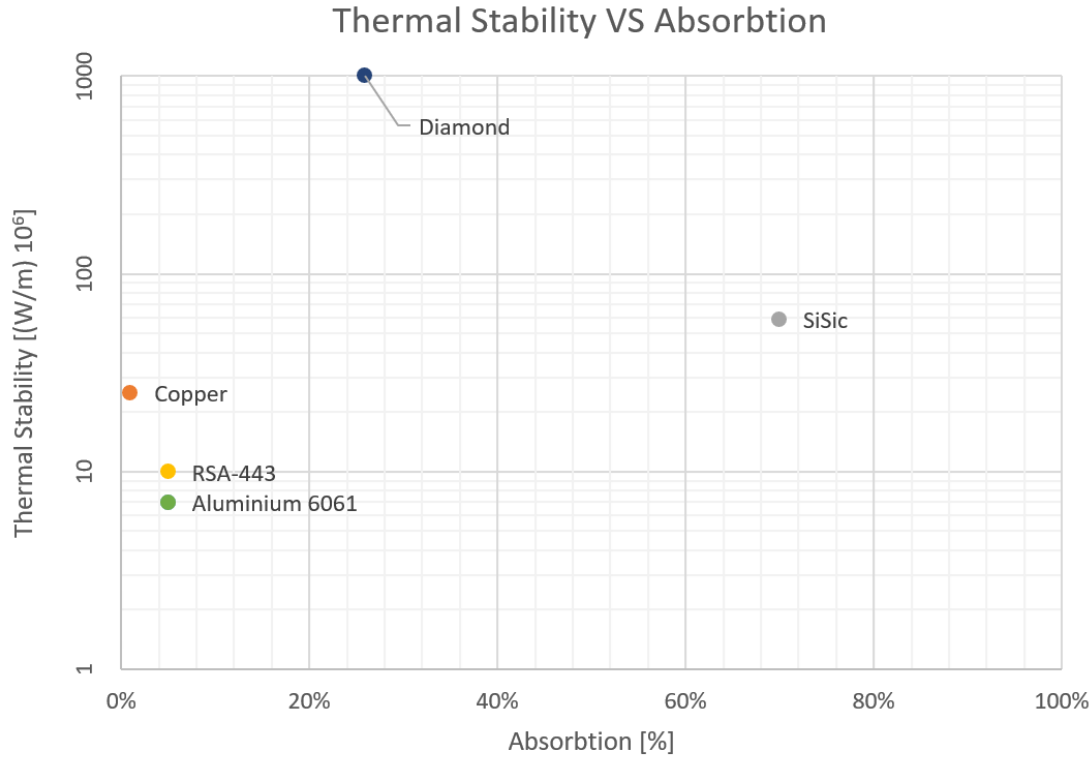


Figure 6.2: Thermal stability Vs Absorption

It can be seen in fig. A.15 that the thermal stability is again the highest of diamond and as second SiSic. What also can be noticed is the high absorption of SiSic, this is not desired because, high absorption means a higher temperature, and that means more deformation, and thus more displacement in the material. This will result in more stress and that will result in damage. In appendix A a simulation is done with the materials and their absorption and it can be seen that SiSic has a PV of more then 20 μ m. This amount of deformation is not allowed since it is 2x of the wavelength and will exceed the specified thermal budget. Therefore, to investigate how to reduce deformation, the next section will dive into the specific stiffness of the material.

6.1.3 Specific stiffness Vs (Thermal stability/Watt absorbed)

The specific stiffness of a material can give a value of how much the material can withstand deformation due to external forces. So by plotting the Specific stiffness against the Thermal stability over the amount of absorbed power, a feeling for how much the material can withstand the thermal forces can be obtained. Again here the same 5 materials are investigated and plotted in fig. 6.3. Placed on the vertical axis is the Specific stiffness which is specified as the E-modules over the density. On the horizontal axis is the Thermal stability over the power absorbed given per watt. This is calculated with eq. (6.2). As an example is the formula filled as it is calculated for diamond.

$$\frac{\text{Thermal stability}}{\text{Watt absorbed/w}} = \frac{k}{CTE} * \frac{1}{\%} = \frac{1000}{0.26} \quad (6.2)$$

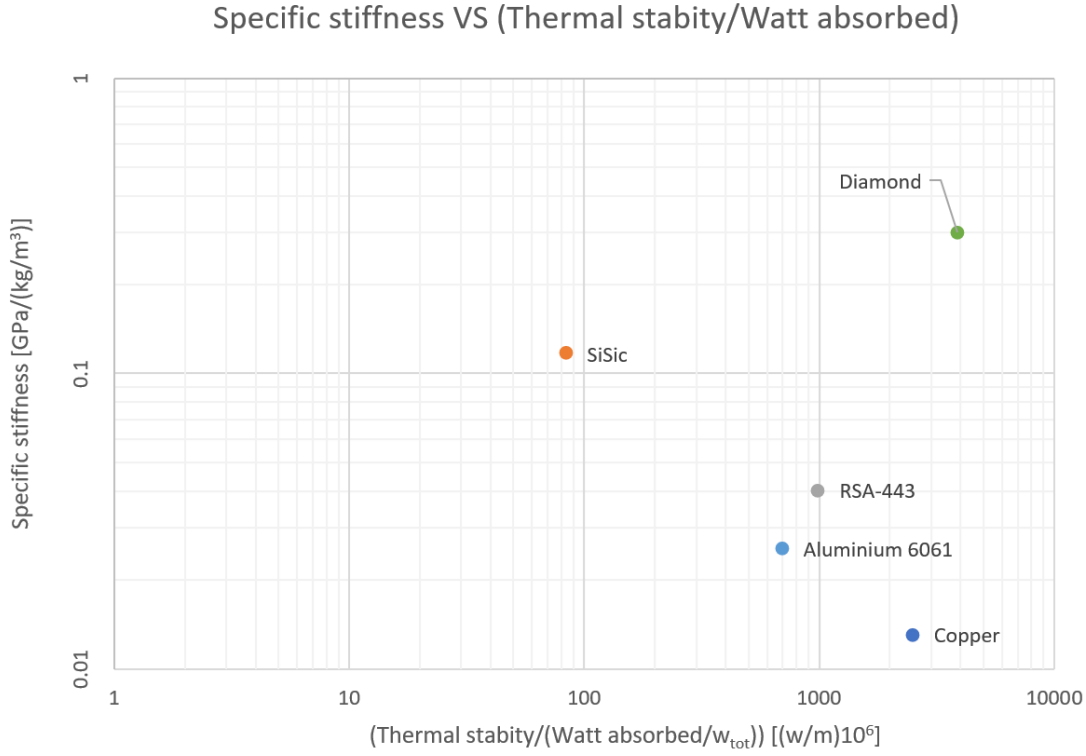


Figure 6.3: Specific stiffness Vs (Thermal stability/Watt absorbed)

That being said, by choosing a material with a high enough Specific stiffness it should be possible to withstand the thermal forces. On the other hand, choosing a material with a low specific stiffness is thus not able to withstand the thermal forces from outside. In this case, deformation should be taken care of by the mounting and make sure that during thermal cycling, not the mirror deforms but the mount instead. By choosing high thermal stability over the absorbed power it is guaranteed that even if the coating fails no damage will happen. Because stiffness can be created in the design, it is in this plot the horizontal axis more important. The remaining materials are diamond and copper but since the risk of the diamond being transparent after a coating fail is consequently, as can be seen in fig. 6.3 that copper is the way to go.

6.2 Cooling channels

To dissipate the absorbed energy cooling channels should be implemented into the mirror, assumed is the same size of channels as in the current model. The channels have a height of 1.1 to 1.3 mm by 2.0 mm and are 1.9 mm from the optical surface. The mirror with cooling channels can be seen in fig. 6.4.

A simple check is done to evaluate the size of the cooling channels and the heat transfer coefficient which will be used later on during simulations as well. Assumed for now is an absorbed laser power of 250W.

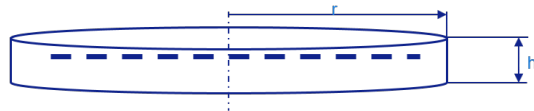


Figure 6.4: Minimal thickness with cooling channels

The velocity of the cooling water is specified at a maximum of 2 m/s and with this, the Reynolds number can be calculated with eq. (6.3) as 3135. Prandtl number of water is given as 6.99 so with these values Gnielinski correlation is valid.

$$Re_D = \frac{u * D_h * \rho}{\mu} \quad (6.3)$$

where

Re_D = Reynolds number [-]
 μ = Dynamic viscosity of water [Pa s]
 u = Velocity of the water [m/s]
 ρ = Density of the water [kg/m³]
 D_h = Hydraulic diameter [m]

The Gnielinski correlation is used to determine the Nusselt number, this correlation is valid within the ranges as specified in eq. (6.4).

$$\begin{aligned} 0.5 &\leq Pr \leq 2000 \\ 3000 &\leq Re_D \leq 5 * 10^6 \end{aligned} \quad (6.4)$$

The Gnielinski equation is a correlation that is valid for tubes with a large Reynolds number.[23] The correlation is given in eq. (6.5).

$$Nu_D = \frac{(f/8)(Re_D - 1000)Pr}{1 + 12.7(f/8)^{1/2}(Pr^{2/3} - 1)} \quad (6.5)$$

Where

$$f = (0.79 \ln(Re_D) - 1.64) - 2$$

where

Nu_D = Nusselt number [-]
 f = Darcy friction factor [-]
 Re_D = Reynolds number [-]
 Pr = Prandtl number [-]

The Nusselt number is calculated as 23.75

$$Nu_D = \frac{HTC}{k/L} \quad (6.6)$$

Here k is the conductivity of the fluid which is, in this case, is the water. And L is the characteristic length scale and the hydraulic diameter of the square channels is used. With these values, formulas and the Nusselt number the HTC can be calculated and is determined as 10000. This will later on used in the simulations as well.

$$\dot{Q} = hA(T_2 - T_1) \quad (6.7)$$

Assumed is a ΔT of 1 °C between the surface and the cooling channels. With eq. (6.7) a minimum area of the cooling channels is determined as 27500mm². A smaller ΔT means a bigger surface is needed to take out the heat, in this way an equilibrium will be reached. A disk with a diameter of 230 mm has an area of 40000mm². If half of the mirror will be used for the channels, and a channel has four sides this area for the cooling channels can be met. However, the heat distribution depends also on the size and shape of the beam. Since the beam is shaped as a Gaussian more heat will end up in the middle. Also, it can be questioned how effective the bottom and sides are for the cooling. The last point about the cooling channels is power variation. This calculation is done with 250 W but as specified it can go up to 500 W absorbed power.

Cooling water will flow through those cooling channels, which will induce forces and also vibrations. Nevertheless, those forces are so small compared to the size of the mirror and due to the trajectory of the channels, these forces can be neglected. A table can be found in the appendix C with the forces induced due to the cooling water and hoses. However, to verify this assumption, eq. (6.8) is done to check the amount of force.

$$F = \rho * A * u^2 \quad (6.8)$$

where

F = Force [F]

A = Area cooling channel [m²]

u = Velocity of the water [m/s]

ρ = Density of the water [kg/m³]

To choose a suitable area, the following is done. Known is that cooling is done with 6 liters per minute and a maximum velocity of 2 m/s. By calculating back the 6 l/s to 0.001 m³/s and divide this with the area velocity is determined and kept lower than 2 m/s. Chosen is to make a diameter of 26 mm which will result in a force of 2.12 N.

6.3 Mirror size

The mirror used now has a diameter of 242 mm and a thickness of around 40 mm which corresponds to the 6:1 ratio for mirrors as specified in Yoder vol 2 [15]. It can be questioned whether or not this thickness is needed. This part will determine the minimal mirror size to meet the mechanical specifications. The following formulas are used to determine the thickness based on the eigenfrequency, from the requirement chapter the eigenfrequency shall be ≥ 150 Hz.



Figure 6.5: Minimal mirror thickness

If a mirror is suspended at the edge then the maximum deflection of the mirror will be in the middle. Thus this will also be the deflection to use in the calculation for the eigenfrequency. The calculations are done with the values as if the mirror is now, so by use of the material copper and making use of a diameter of 242 mm. For simplicity and first-order calculations, this calculation will be done with a flat disk as shown in fig. 6.5.

$$f_n = \frac{1}{2\pi} \sqrt{\frac{g}{\delta_A}} \quad (6.9a)$$

$$\delta_A = C_A \frac{\rho(1 - \nu^2)}{E} g \frac{V_0}{I_0} r^4 \quad (6.9b)$$

$$\frac{V_0}{I_0} = \frac{12}{h^2} \quad (6.9c)$$

where

f_n = Natural frequency [Hz]

g = gravitational force [m/s²]

δ_A = displacement [m]

C_A = parameter dependent on the support geometry [-]

ρ = Density [kg/m³]

ν = Poisson's Ratio [-]

E = Young's modulus [Pa]

V_0 = Volume mirror [m³]

I_0 = cross-sectional moment of inertia [m⁴]

r = Radius of mirror [m]

h = Height of mirror [m]

For a solid mirror, the assumption of eq. (6.9c) can be made.

Support Parameter C_A for Various Mirror Mounting Geometries	
Geometry	C_A
Continuous ring at 68% of diameter	2.32×10^{-3}
Six points equally spaced at 68% of diameter	2.59×10^{-3}
Edge clamped	15.6×10^{-3}
Three points equally spaced at 64.5% of diameter	26.3×10^{-3}
Three points equally spaced at 66.7% of diameter	26.9×10^{-3}
Three points equally spaced at 70.7% of diameter	29.9×10^{-3}
Edge simply supported	65.8×10^{-3}
Continuous support along a diameter (scanning mirror)	78.6×10^{-3}
Central support (stalk or mushroom mount)	97.2×10^{-3}
Three points equally spaced at edge	113×10^{-3}

Figure 6.6: Support paramater C_A

From Yoder vol 2[15] C_A is a coefficient that specifies different mountings of the mirror, fig. 6.6 is from this source and from here the worst case as **three points equally spaced at the edge** is used to calculate the deflection. By plugging in the eigenfrequency $f_n = 150$ Hz, the critical thickness can be calculated as 4.3 mm. However, it is given that it assumes a mirror with an aspect ratio of at least 6:1. It is shown by having an aspect ratio of at least 6:1 the shear deflection can be neglected. In this case has a disk with a diameter of 240 mm and a thickness of 4.3 mm has an aspect ratio of 56:1. Therefore, should here the shear deflection of this thinner mirror be taken into account. This is also proven by using COMSOL, to check this thickness it seems that the 2D model is based on piston mode which is close to 150 Hz and shown in fig. 6.7b. The first eigenmode is around 50 Hz as shown in fig. 6.7a. A disk of 242 mm with a thickness of 15 mm will have a higher eigenmode than 150 Hz as can be seen in fig. 6.7c. Based on the dynamics of the mirror the thickness is determined as 15 mm thick.

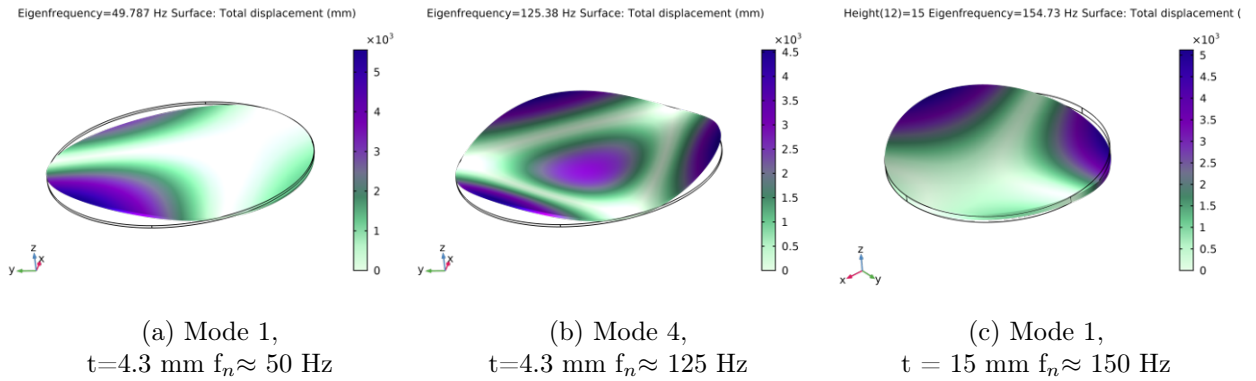


Figure 6.7: Eigenfrequency Vs Thickness

So as verified with COMSOL the thickness shall minimally be 15 mm, by adding the 1.3 mm of the cooling channels to the thickness of the calculated mirror thickness the final thickness shall be 16.3 mm for a copper mirror with a diameter of 242 mm.

6.4 Manufacturing

The calculated thickness of the mirror is much smaller compared to the original mirror, a reason for that is the manufacturability of the mirror. The optical surface is made by the use of diamond turning. This is done on a special lathe and turned with a diamond tip. This tip removes just a little material from the surface until the desired shape and roughness is reached. Being told is that the thickness of 35 mm is needed for this process. Thus the design will be continued with a mirror of 35 mm thick to ensure manufacturability at the supplier. With this thickness and radius, the mass of the mirror can be calculated and used in the next chapter 7 to specify flexures. In reality, is the mirror curved, but as a first-order calculation the mass is calculated as eq. (6.10).

$$Mass = \frac{\pi}{4} * D^2 * t * \rho \approx 14.5kg \quad (6.10)$$

6.5 Model

A model in COMSOL as can be seen in fig. 6.8a is build to simulate the deformations caused by the laser, and thereby verify the conclusions made in previous sectors about the material. The model is fixed in a weak spring foundation to isolate the deformations that are created by the laser and exclude side effects of the structure. A Gaussian laser beam with an incident angle of 15 degrees is applied and absorption of 250 W at the optical surface is applied. The cooling channels are modeled as circular rings with the comparable area and HTC of 10000 as calculated in section 6.2 and are shown in fig. 6.8b.

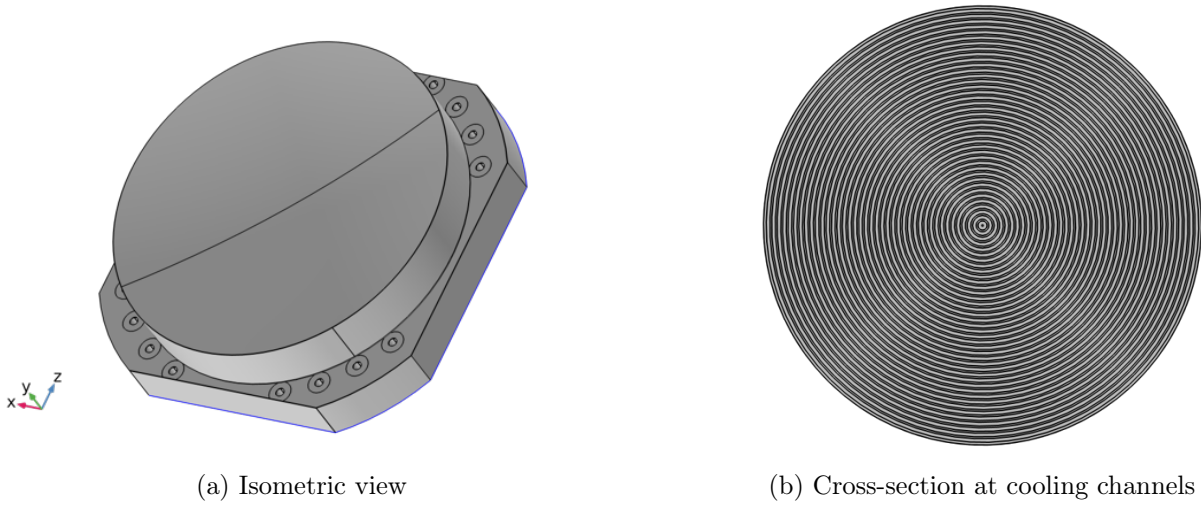


Figure 6.8: Material model

In section 6.1.1 multiple materials were investigated and here is the first fake material applied to the model and the result of this can be seen in fig. 6.9. shown is that the PV value is 0.78 μm and that the highest temperature is 370 Kelvin. As expected is this the result of a low CTE and low conductivity.

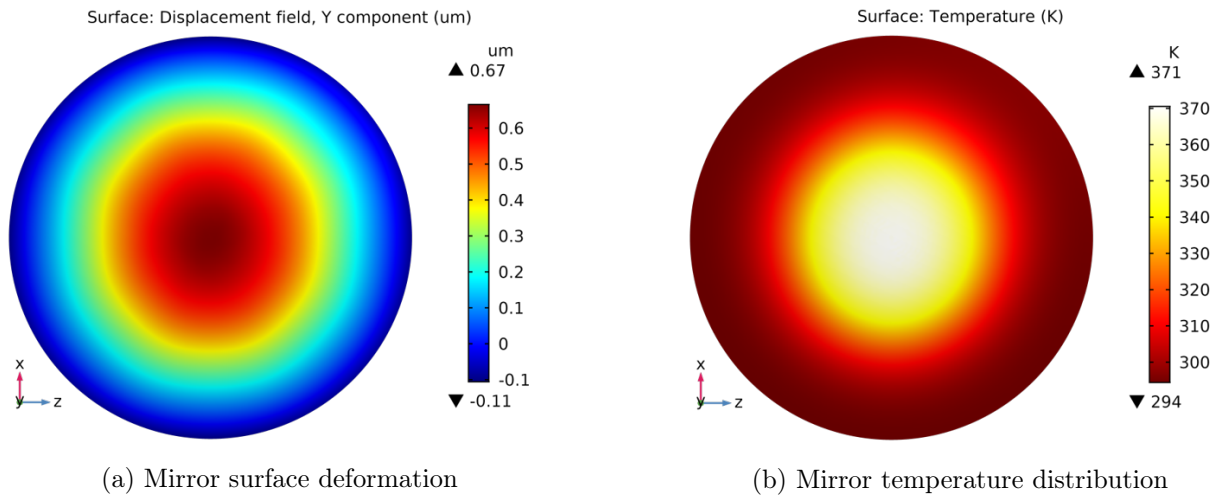


Figure 6.9: Effect of varying CTE and Conductivity

These plots are made for every material and are put in appendix A, here summarized as PV and temperature value in table 6.1. fig. 6.10 gives the Zernike polynomials of the mirror deformation. The biggest

Zernike polynomials are plotted here, the full graph with all polynomials are given in appendix A.

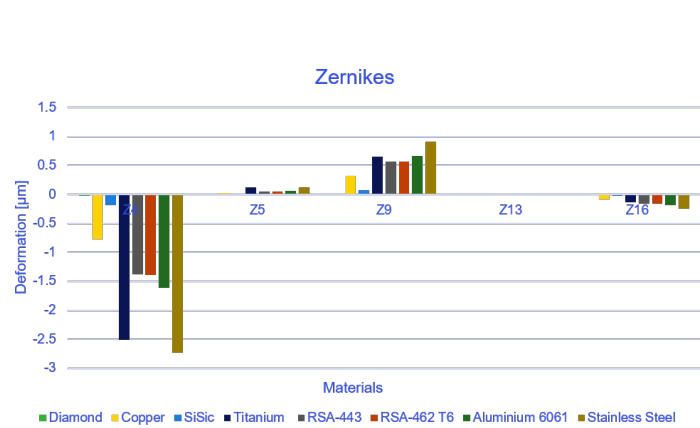


Figure 6.10: Zernike of different materials

	PV [μm]	Temp [K]
Fake material 1	0.78	370
Fake material 2	5.64	295
Fake material 3	77.2	370
Diamond	0.05	295
Copper	0.95	296
SiSic	0.21	297
Titanium	3.18	308
RSA-443	1.34	297
RSA-462 T6	1.69	297
Aluminium 6061	1.95	297
Stainless Steel	3.43	303

Table 6.1: PV and max temperature

And another point here that can be seen in fig. 6.10 is that the dominant aberration is Z4 or in other words defocus. This can be explained by the fact that the incident angle of the laser is just 15 degrees so the Gaussian beam is almost circular. This analyze is done and can be seen in appendix B.2

6.6 Conclusion mirror

Determined in this chapter is that the material of the mirror should not be changed, in terms of thermal stability copper scores well, and in terms of absorption is copper the one that absorbs the least of heat. The Specific stiffness of copper scores the least but this is a trade-off with Thermal stability over the absorbed power. Since the Specific stiffness is lower the mirror mount should be taking care of the deformations of the surrounding. The thickness is calculated as thicker than 16.3 mm. But since the manufacturer has specified that 35 mm is the minimum thickness that they can manufacture, this is the thickness where will be continued with. Furthermore, will the cooling channels be the same as they were before and the dimensions will be 1.3 mm x 2 mm. Also, the dominant aberrations when free-free suspended due to the laser are Z4, defocus and Z9, primary spherical. This is because the incident angle of the laser beam is relatively small.

Chapter 7

Mirror mount

An ideal mirror mount should be able to keep the optic within the boundaries in terms of position and orientation during operation mode. Due to thermal changes materials and thus also optics will expand and thus deform. Therefore a mirror mount should be as stiff as possible in the directions of optical performance and allow deformation in the direction of thermal expansion. This chapter will step by step dive into the development of a mirror mount that can withstand the circumstance mentioned in the requirements. It kicks off with determining the stiffness that will arise by heating the mirror in both radial as tangential direction. Different concept will be compared and the best one is chosen.

7.1 Expansion freedom

A predictable mirror mount is desired to ensure the foreseeable behavior of the position of the mirror. The stiffness of the mirror should be higher than the stiffness of the mount in the direction of expansion. This ensures that while expanding, the mount deforms in radial direction, but not the mirror see fig. 7.1 where the arrows are representing the flexures.

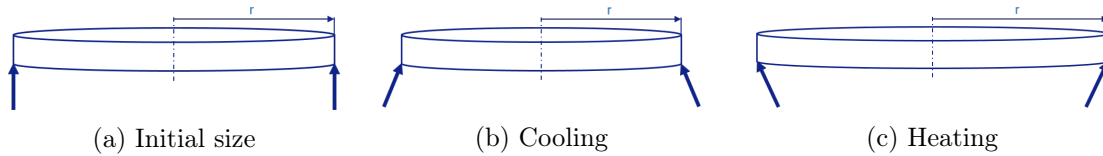


Figure 7.1: Deformation due to change in temperature

The length of expansion from the center of the mirror shall be the radius and is given as 121 mm. The initial temperature is given as 22°C and was specified in the requirements section. Also, the maximal temperature will be 45°C during transportation. Therefore, is the maximal ΔT chosen as 23°C. In fig. 7.1a the initial shape of the flexures is given at 22°C. Figure 7.1c illustrates the expansion of the mirror, this amount of expansion is calculated with eq. (7.1). The state where the mirror is cooled is shown in fig. 7.1b.

$$\Delta R = CTE_{Cu} * R * \Delta T \approx 47\mu m \quad (7.1)$$

The thermal expansion of the mirror is determined as 47 μm . Besides radial expansion will the mirror also deform in the axial direction. This problem will be sold by fixing the mirror at a single height. This ensures a free expansion in the axial direction.

To calculate the corresponding stiffness that arises with this expansion, a calculation is done in eq. (7.2) for the thermal expansion. The area chosen in this formula is chosen to be the same area given in chapter 4 since this has shown to be close to reality. Therefore, this area will be used again and with that, the maximal radial stiffness will be determined in eq. (7.2).

$$\left. \begin{aligned} F &= k * \Delta R \\ F &= \frac{EA}{R} * \Delta R \end{aligned} \right\} k = \frac{EA}{R} \quad (7.2)$$

The radial stiffness calculated in this way will be used as an upper boundary limit of stiffness delivered by the mirror mount. This stiffness is determined as 2.44E9 N/m.

The tangential and axial stiffness to keep the mirror in position can be determined by the eigenfrequency and also by the position tolerance. The stiffness concerning the position tolerance can then be determined by mass times acceleration over deflection. And the stiffness regarding the eigenfrequency is determined with the natural frequency formula, both shown in eq. (7.3).

$$\left. \begin{aligned} k_1 &= \frac{m * g}{\delta} \\ f_n &= \frac{1}{2\pi} \sqrt{\frac{k_2}{m}} \end{aligned} \right\} k_{min} = k_1 + k_2 \quad (7.3)$$

The minimal stiffness needed to meet both of the above-given specs is taken as the worst-case scenario and thus are added up. Taken for the maximal deflection due to gravity will be half of the spec of 50µm to keep some margin for alignment. The minimal stiffness is given as 1.92E7 N/m. In table 7.1 the stiffness range where the mount should be fit in is given.

Stiffness	
Tangential & Axial	Radial
1.92E+07 N/m	2.44E+09 N/m

Table 7.1: Stiffness

This table indicates the stiffness of the total mount. This means that the mirror mount should in both the X, Y, and Z direction end up having the stiffness in the tangential and axial direction as specified. A single flexure could be ending up having less stiffness in a certain direction, however, another flexure will take care of delivering this stiffness. Thus in the direction where the first flexure is compliant.

7.2 Boundaries of a flexure

This section will lay out the basics of a simple single flexure. This is done to create a feeling for the calculated values as shown in the previous section. And thus will show how this flexure can handle the stiffness. A single flexure is illustrated in fig. 7.2, ΔL_1 is the strong direction and ΔL_2 the flexible direction that can, for example, be used to compensate for the radial thermal expansion of the mirror.

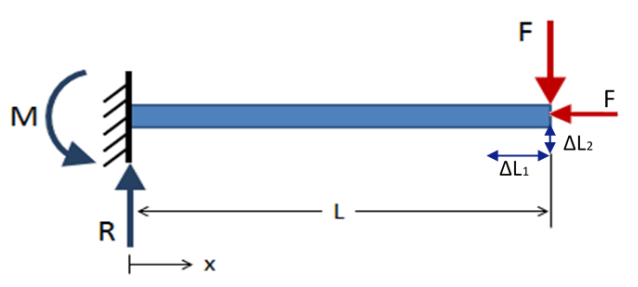


Figure 7.2: Single flexure

Corresponding formulas for the compression, ΔL_1 , and the deflection, ΔL_2 are shown in eq. (7.4).

$$\left. \begin{aligned} \Delta L_1 &= \frac{FL}{whE} \\ \Delta L_2 &= \frac{FL^3}{\frac{1}{12}wh^3E} \end{aligned} \right\} k_{tan} = \frac{EA}{L} \quad k_{rad} = \frac{wh^3E}{12L^3} \quad (7.4)$$

From eq. (7.4) will follow that both k_{tan} and k_{rad} has to fit in the specified stiffness as given before if the solution was done with one flexure. Following from this is that the variables to change will be, w,h, and L. E is material dependent and will give thus less freedom in options to vary.

To ensure the sustainability of the flexure the deformation may not go beyond the Yield stress. The Yield stress point is the moment where plastic deformation will occur, and this is also related to unpredictable behavior or possible failure. Another point is the fatigue of the material. During transport and operation, the flexures have to take an expansion but also a vibration. To satisfy this requirement is chosen to have the fatigue boundary as the Yield stress over 3 [24]. Thus $\sigma_{max} \leq \frac{Yield_{max}}{3}$. The stress that arises can be calculated with eq. (7.5).

$$\sigma_{max} = \frac{F * L * h * 12}{2wh^3} = \frac{6 * F * L}{wh^2} = \frac{h * E * \Delta L}{L^2} \quad (7.5)$$

Comparing k_2 from eq. (7.4) and σ_{max} from eq. (7.5) it can be noticed that by making L longer the stiffness will go down and also the stress goes down up, this means that an optimal could be found in the length and thickness. However, with increasing the length of a flexure also makes it more easy to buckle. The critical buckling load is given with eq. (7.6).

$$F_{buckling} = \frac{\pi^2 EI}{L^2} \quad (7.6)$$

This means a optimum can be found. But before optimizing the flexures, the orientation and layout of the different flexures will be elaborate.

7.3 Combined Flexures

By combining multiple flexures it is possible to create an isostatic mount. As explained in the literature study, an isostatic mount is a mount where every degree of freedom is constrained ones. From the literature study, some mounts were already rejected because they were only working in 2D, not isostatic or will not work in certain orientations. Three isostatic mounts are further investigated. Those three are the hexapod fig. 7.3b, the six folded flexure design fig. 7.3a and three folded flexures with three rods fig. 7.3c.

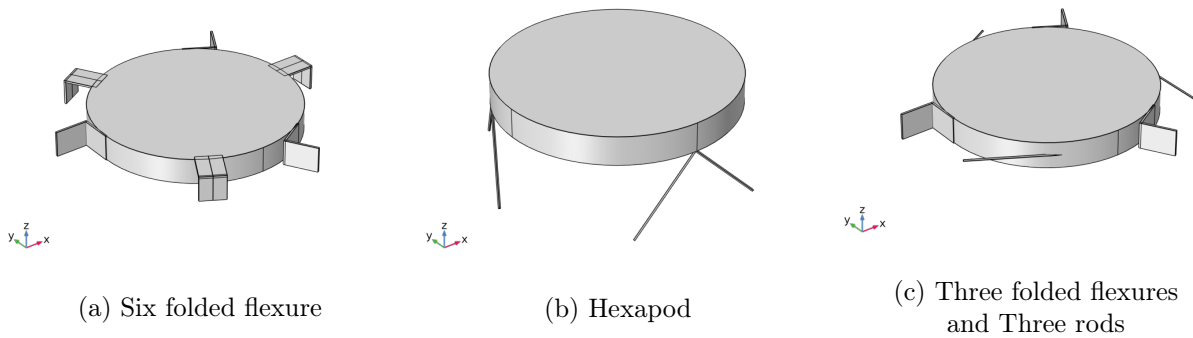


Figure 7.3: Combined flexures

To understand the different concepts all three designs are drawn in COMSOL and for all designs, the same material is used. By applying the same force to all three designs the displacement is determined and from that, the stiffness is resolved. This is done in the directions x,y and z to get a complete overview this

can be found in appendix D. First all three concepts are not reinforced, so just thin flexures in the orientations as shown in fig. 7.3. Then for each concept, the stiffness and eigenfrequency are determined. After that, the concepts are reinforced and checked again for stiffness and eigenfrequency all possibilities are kept in an Excel file. Since Stiffness is not the only design condition, also volume and stress in the flexure itself it is worth it to dive into a single flexure. The following section will dive into those designs and will be verified with the COMSOL models.

7.3.1 Design options

To get a fair comparison between the three concepts, some parameters are kept the same and some are varied. The material in all setups is the same and the material for both the flexures and the disk are equal. The eigenfrequency is determined by fixing the end of the flexures and then calculated in COMSOL. The stiffness of the designs is tested by applying a known load separate in all three directions. The displacement is then measured in all three separate directions. The stiffness and eigenfrequency are used to classify the three designs. Varied in all designs are the thickness and length of the flexures and in case of the rods, the reinforcement part is adjusted.

7.3.2 Hexapod

The hexapod is built from six rods, in this case, six reinforced rods. The parameters that can be played with are the length, the thickness, and the angle of each leg. Every rod will constrain the DOF in the length direction of the flexure and because there are 6 in all different directions all six degrees are constrained.

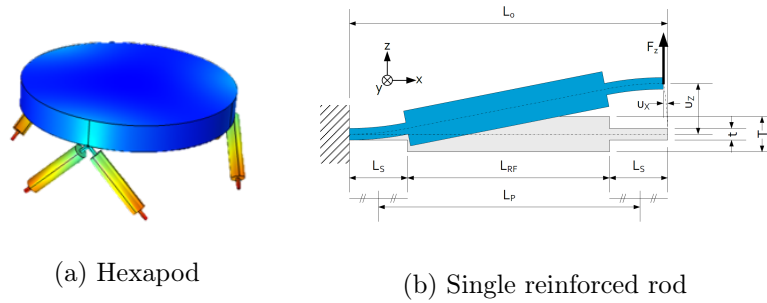


Figure 7.4: Hexapod

The calculation of one flexure is relatively easy and since every flexure will add mainly stiffness in the known direction the total stiffness can be calculated by adding those stiffnesses with some geometry. Parameters used can be found in table 7.2

Parameters		Comparison
Variables	[mm]	Stiffness [N/m]
d	4	COMSOL
D	16	C_x 9.21E+07
l	12.5	C_y 9.21E+07
L	75	C_z 1.75E+08
L_p	87.5	
L_0	100	

Table 7.2: Parameters and comparison Hexapod

As said before, the stiffness is determined by applying a known force and look at the displacement in COMSOL. Table 7.2 shows the stiffness values for x, y, and z-direction.

7.3.3 Six folded flexures

This setup is done with six of the same folded leaf springs, what should be noticed is the fact that the flexures are not reinforced. Therefore the total stiffness, in this case, is lower than other designs. Again, the overview can be found in appendix D.

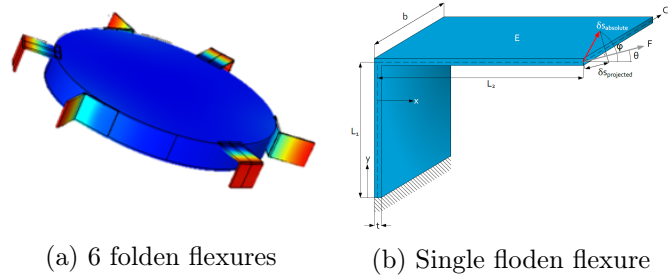


Figure 7.5: Six folden flexures

Figure 7.5a shows the design of six folded leaf springs and fig. 7.5b illustrates the variables of the individual flexure. For simplicity, both thicknesses and length are chosen to be equal.

Parameters		Comparison	
Variables	[mm]	Stiffness [N/m]	
		COMSOL	
Thickness	2	C_x	3.91E+07
Length	40	C_y	3.86E+07
Height	40	C_z	6.63E+07

Table 7.3: Parameters and comparison of sixfolded leafsprings

As can be seen in table 7.3 the stiffness values in x, y, and z-directions are given.

7.3.4 Three folded flexures and three rods

This design is a combination of the two designs as before, fig. 7.6a shows the model in COMSOL. Both flexure types can be seen in fig. 7.6b and fig. 7.6c. Used formulas are also the same as in previous sections above and because every flexure again constrains one DOF the total stiffness can be determined.

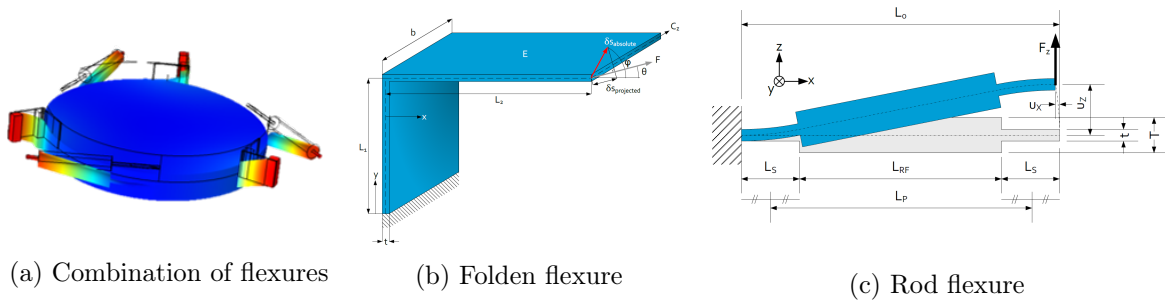


Figure 7.6: Three folded flexures and three rods

For simplicity the parameters used are the same as in the design as before, table 7.4 shows all parameters used.

Parameters		Comparison	
variables	[mm]	Stiffness [N/m]	
d	4		
D	16		
l	12.5	COMSOL	
L	75	C_x	9.27E+07
L_p	87.5	C_y	9.27E+07
L_0	100	C_z	8.20E+07
Thickness	2		
Length	40		
Heigth	40		

Table 7.4: Stiffness three folded leafsprings and three rods

Also here in table 7.4 is the stiffness shown in x, y, and z-direction.

7.3.5 Conclusion design choice

Three different flexure setups where discussed, parameters and a relative stiffness are given. All models has shown to have stiffness in the same order of magnitude. However, the six folded leaf spring design has the highest stiffening potential. And, as a result, ends up having the highest eigenfrequency. Also from a manufacture, volume, and cost perspective, the six folded leaf spring concept is the cheapest and most easy to machine compared to the other designs. Also, is it be possible to manufacture that design out of one piece which should increase the precision.

7.4 Concept detailed design

This section will dive into the different specific design chooses for the chosen design concept the 6 folded leaf spring design. It will focus on the flexure position and thickness to optimize the design to fulfill the requirements. Also, a section about the manner of fixation of the flexures will be presented.

7.4.1 Backplate & location flexures

To manufacture the flexures, mirror support and cooling channels a material has to be selected which can do all of this. By reminding the material table of the literature study there is no doubt that Stainless Steel is the way to go. Because, there is a CTE match with the copper mirrors and a relative high yield strength to make the flexures of. This section will elaborate on the place to support the mirror. A few considerations can be made here, a lower mass means a higher eigenfrequency. Therefore by placing mass on the right place stiffness can be added while keeping the weight low. Placing the flexures far from the center of the mirror will make the mirror more stable since the rotation points are further outwards. On the other hand, by placing the flexures more inwards, shall reduce the amount of expansion. Because the Thermal expansion depends on a length that then is smaller will also the expansion be less. A model is made in COMSOL to compare deformation due to gravity in two directions and the eigenfrequency is also compared.

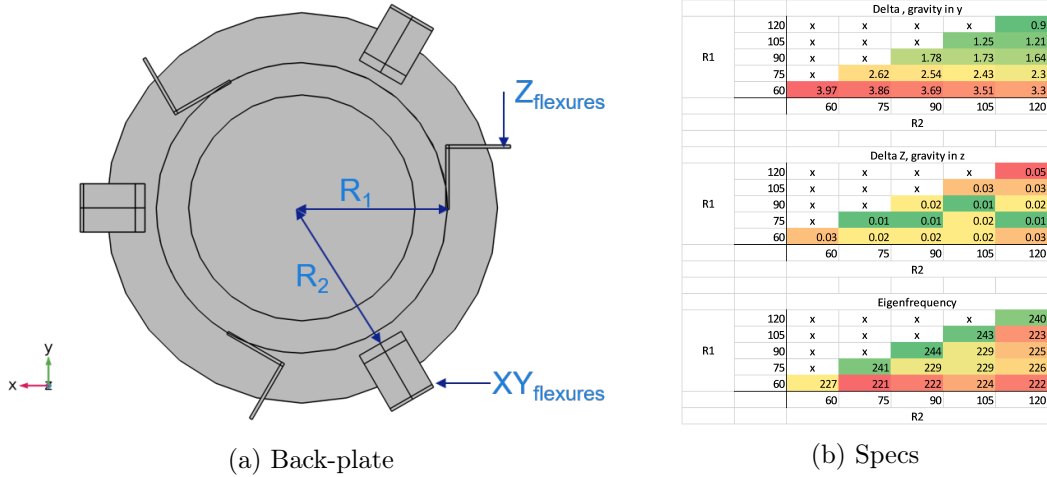


Figure 7.7: Back-plate design

In fig. 7.7a it can be seen that R_1 is the distance to the Z constrain flexure and R_2 is the distance to the XY constrain flexure. In fig. 7.7b the results can be found, and a bigger version is presented in appendix D.1. In the first two tables, gravity is applied and the mirror surface deformation is observed in the optical direction. The aim is of course to minimize those values. Last table in fig. 7.7 the eigenfrequency is given as a result of the positions of the flexures. It should be noticed that this is done with random flexures of the same size and that this will be optimized later on. For now, the choice is to go with R_1 at 90 mm and R_2 at 105 and thus place the flexures here. It can be questioned by putting the flexures all on 105 mm will be better. However as said before the thermal expansion is excluded here and will have more influence on the Z flexures. Also, the ring can, later on, be used to route the cooling channels in which is a nice side effect.

7.4.2 Folded leafspring design

The thickness and dimensions of the flexure are optimized in COMSOL, first a single flexure is drawn with parameters and calculated is the stress in the flexure. As said before will the flexure be designed within its yield range. And a margin will be taken into account to ensure some uncertainties, for example, the shocks during transport. The material used is Stainless Steel 301 and is given with a yield strength of ≈ 965 MPa. As a safety factor the fatigue stress limit will be used to design the flexure. The design of the flexure will be designed for ≈ 67 MPa.

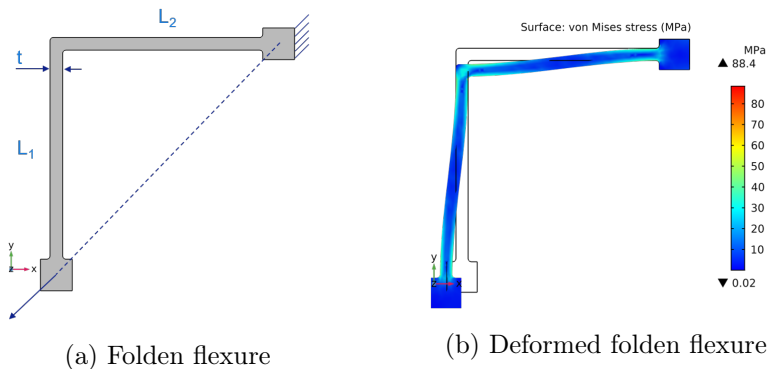


Figure 7.8: Folded leafspring

Shown in fig. 7.8 is the folden flexure that is used. In the right upper corner is the flexure fixed and a pre-described displacement in the left lower corner. The amount of this displacement is the amount of the thermal expansion of the outer radius and for the CTE is the difference used between the CTE of Aluminum

and the CTE of Stainless steel. Thus a diagonal displacement of about 25 μm . Variations of L_1 , L_2 and t are investigated and analyzed for stress. Small radii of 0.5 mm are used. This is not optimized but ensures the mesh in COMSOL to go smaller in the corners and thus give a more reliable solution. Figure 7.9 shows the result of this calculation and plotted in green are the allowed options.

T = 1 [mm] Mpa						
mm	50	325	38.6	14.7	8.29	6.31
	40	349	40.6	16.1	10.6	8.13
	30	379	45.9	21.4	14.9	13.2
	20	426	65.5	38.8	33.5	30.6
	10	788	268	232	215	201
	mm	10	20	30	40	50
L2						

T = 2 [mm] Mpa						
mm	50	257	80.5	33.5	21.6	16.6
	40	277	84.7	39.1	27.5	21.4
	30	303	95.2	55.2	39.1	32.4
	20	404	161	93.3	79.6	72.5
	10	1080	461	382	339	311
	mm	10	20	30	40	50
L2						

T = 3 [mm] Mpa						
mm	50	197	102	52.7	38.2	29.8
	40	206	110	68.6	48.8	38.1
	30	294	157	94.9	69	55.9
	20	513	259	159	135	123
	10	1300	603	478	409	362
	mm	10	20	30	40	50
L2						

T = 4 [mm] Mpa						
mm	50	189	115	75.9	56.5	43.6
	40	251	150	98.3	72.2	56.2
	30	361	210	137	100	89.5
	20	654	352	239	207	190
	10	2330	734	574	487	421
	mm	10	20	30	40	50
L2						

Figure 7.9: Solutions within the allowed stress

A selection is given where to choose from. But the orientation and position still can add a positive effect. In section 7.4.2 a top view of the folded flexure is given. To optimize this flexure within the boundaries L_t is calculated as $\sqrt{2} * L_1 + R_1$, in fig. 7.9 is the green part the allowed sizes of the flexures. To optimize further is a length for both flexures chosen as 30 mm. Because this is in the middle for both expansion as for support. To determine the actual deformation of the flexure the CTE of Aluminum has to be subtracted with Stainless Steel since this also expands. In the case of section 7.4.2 the deformation will be parallel to the L_t . In the case of fig. 7.10b, which is a side view of the XY flexures, the deformation will be higher parallel to L_t then perpendicular to this. This is due to the aspect ratio of the mirror.

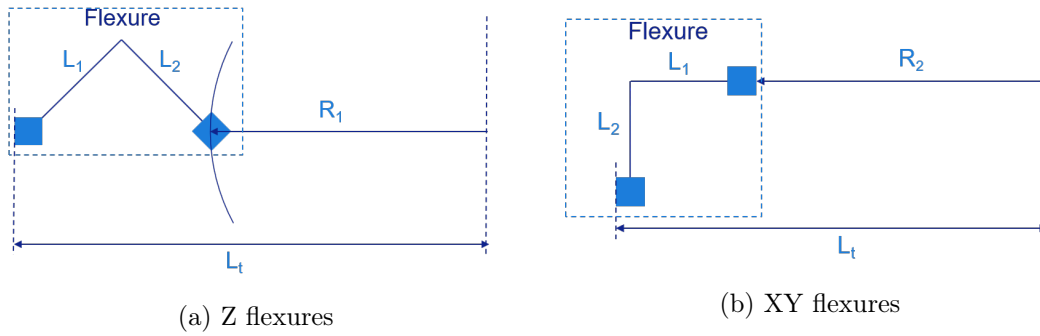


Figure 7.10: Flexure positions

Final dimensions of the folded flexures are shown in table 7.5, L_t for the Z flexures is calculated as 146.56 mm and L_t for the XY flexures is determined as 135 mm. With these lengths, the thicknesses are optimized to 2.2 mm for the Z flexure and 3.3 mm for the XY flexures.

	Z flexures	XY flexures
L_t	146.56 mm	135 mm
ΔL_t	21 μm	18.6 μm
ΔL_h	0 μm	4.83 μm
L1	30 mm	30 mm
L2	30 mm	30 mm
w	30 mm	30 mm
t	2.2 mm	3.3 mm
Stress	63.3 MPa	62.2 MPa

Table 7.5: Final dimensions of the folden flexures

The final flexures that will be implemented are shown in fig. 7.11 and it can be seen that both of the flexures are designed to have stress below 67 MPa. A thicker part is added at the base and at the end to ensure that by fixation no stress is induced in the flexible part.

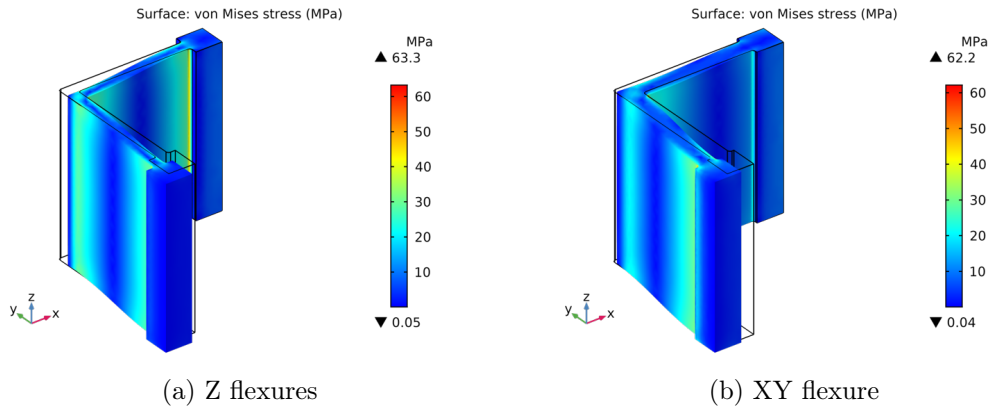


Figure 7.11: Final folden flexures

7.4.3 Flexure fixation

The folden flexures will be fixed to aluminum and because this is a different material the flexures should be fixed in a manner that the not change position during temperature variations. The way to fix this problem is making the area small enough to allow for shear. In fig. 7.12a the initial state is given where no heat is added and fig. 7.12b illustrates the flexure fixation while heat is added. Note here that there are two different materials and thus that there will be a different expansion length.

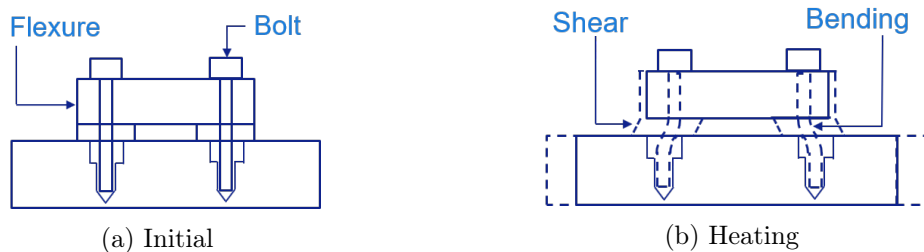


Figure 7.12: Flexure fixation

As shown before, will this problem exists of two subproblems, namely shear, and bending. Basically should the friction force delivered by the bolts be higher than the shear plus bending force of the bolt. To calculate shear which can be seen in fig. 7.13a and calculate with eq. (7.7).

$$F_{shear} = \frac{GA\Delta x}{l} \quad (7.7)$$

where

F_{shear} = Shear force [N]
 G = Shear modulus [Pa]
 A = Area [m²]
 Δx = Thermal expansion [m]
 l = Height [m]

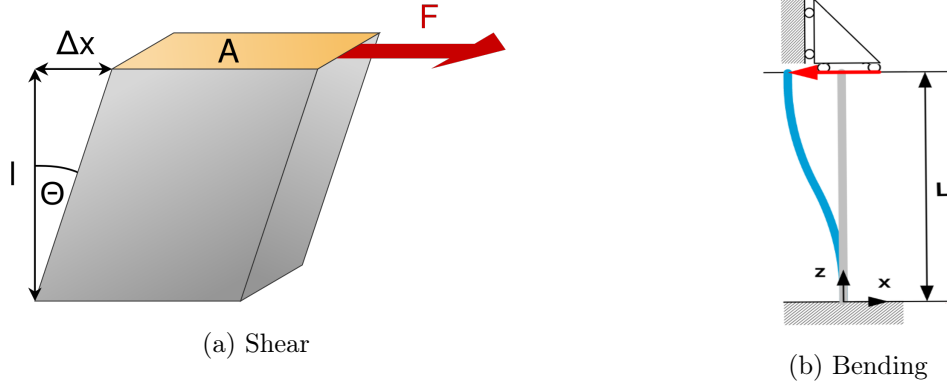


Figure 7.13: Shear and bending

To calculate the bending in the bolt which can be seen in fig. 7.13b and calculate with eq. (7.8). It can be seen that there is taken into account that the bolt head will not slip.

$$F_{bending} = \frac{12 * \Delta x EI_y}{l^3} \quad (7.8)$$

where

$F_{Bending}$ = bending force [N]
 Δx = [m]
 E = Young's Modules [Pa]
 I_y = [m⁴]
 Δx = Thermal expansion [m]
 l = Height [m]

Final values used to ensure no slip at the fixation of the flexures can be found in section 7.4.3. It can be seen that the shear of the pad plus bending of the bolt is lower than the friction force.

	Shear				Bending				Bolt M5		
Height	1.5	mm		Height	11.5	mm		Diameter	5	mm	
width	9.5	mm		width	5	mm		μ	0.3	-	
G	26	GPa		E	193	GPa		F_N	11350	N	
F_{Shear}	3240	N		$F_{Bending}$	97	N		$F_{Friction}$	3405	N	

Table 7.6: Fixation pads

7.4.4 Conclusion Conceptual design

Conclude can be that a concept is chosen based on manufacturing and the highest amount of stiffness with the design chooses. The folded flexures are optimized in individual directions in terms of length and thicknesses. Also, the back-plate is optimized in terms of weight and where to support the mirror. The back-plate

will also have the function to route the cooling channels through.

This final proposed design will consist of basically three parts, the mirror fig. 7.14a, the back-plate fig. 7.14c with flexures, and the housing fig. 7.14b . The housing here is modeled as an Aluminium plate, this plate can either be used and bolted to a bigger assembly or the fixation points can directly be integrated into another part.



Figure 7.14: Proposed design

Chapter 8

Evaluation of Detailed Design

This chapter will evaluate the final proposed Predictable Opto-mechanical Design for a Critical Reflective Surface and will evaluate if the design meets their specific spec.

8.1 Eigenfrequency & Stiffness

As described in the requirements should the design have a higher eigenfrequency of 150Hz. While this already was taken into account during the design phase by keeping the mass low, the first three eigenmodes are given. These eigenmodes are shown in fig. 8.1.

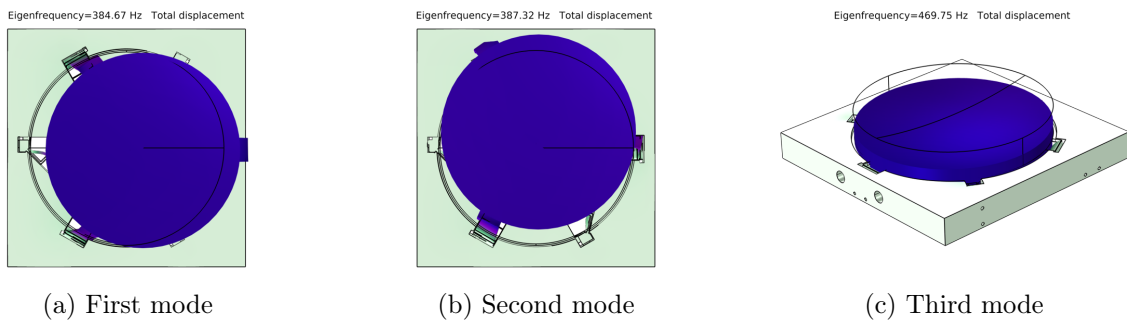


Figure 8.1: Eigenfrequency

What can be seen in fig. 8.1a is that the first eigenmode is already 2x higher than the requirement. Also, it is shown that this first mode is horizontal and second mode, and can be seen in fig. 8.1b is perpendicular to that. And then finally the third mode is in the direction of the optical axis and is shown in fig. 8.1c.

Related to those eigenfrequencies is the corresponding total stiffness. This stiffness is calculated with eq. (8.1). As mass for the mirror is used the 14.5 kg as in section 6.3 plus the Stainless steel part which is determined as 2.8 kg. Thus in total a mass of 17.3 kg.

$$k = (2 * \pi * f_n)^2 * m_{mirror} = 1.01E + 08 N/m \quad (8.1)$$

8.2 Stress

As previously discussed will the most stress rise during transportation, this stress will come from the difference in temperature and CTE of the materials. By heating the model the von Mises stresses can be plotted and the areas were most stress will be is indicated in red. As previously described will the most complicated part be the back-plate and will be made from Stainless Steel. This Stainless Steel has a Yield strength of 200 MPa. As previously described in chapter 7 will the Yield strength over 3 be used as a safety factor for the fatigue stress.

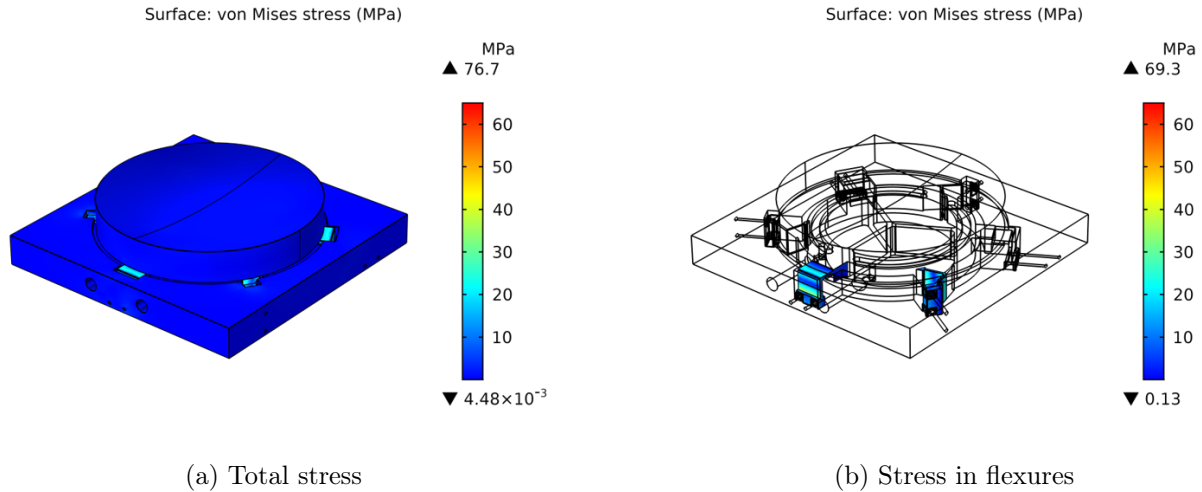


Figure 8.2: Von mises stress

In fig. 8.2 is the von Mises stress given in the complete assembly in fig. 8.2a and a zoom in to the flexures can be seen in fig. 8.2b. As can be seen, is the amount of stress lower than the allowed Yield stress and therefore will the design survive the temperature variation during transportation.

8.3 Shock Load

The shock load is also a requirement that should be met. Questioned can be, in what direction will the shock load do the most harm. However, as shown in the previous section was the direction of the first eigenmode shown to be in line with the flexures. In fig. 8.3 the shock load in the same direction as the first mode is shown.

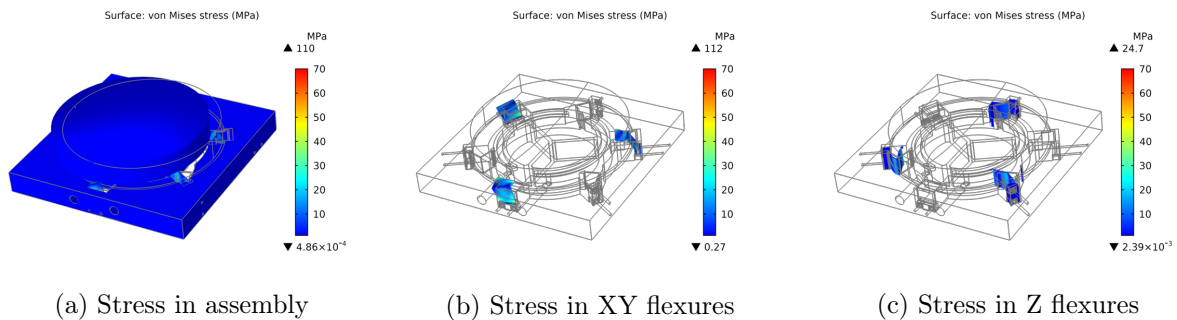


Figure 8.3: Shock load

The stress in the assembly is shown in fig. 8.3a and is shown to stay below the yield strength and fatigue strength of the Stainless Steel. The stress in the flexures is split into the XY flexures and the Z flexures. It can be seen that the XY flexures, in fig. 8.3b, take the most stress since in this movement only two flexures take the force. In fig. 8.3c the stress is rather low also because of the direction of the force. However, by placing the direction of the shock in the Z- direction, this is the third eigenmode, the stress is not as high as in the XY flexures. This is because there are three flexures to take this force and the flexures are a bit thinner.

8.4 Cooling forces

Forces will be introduced to the mirror since it has to be cooled with flowing water. As previously described, those forces not that high and are in the direction of the channels in such a way that most force is canceled

out. Nevertheless, it has to be shown that the design will not fail due to these forces.

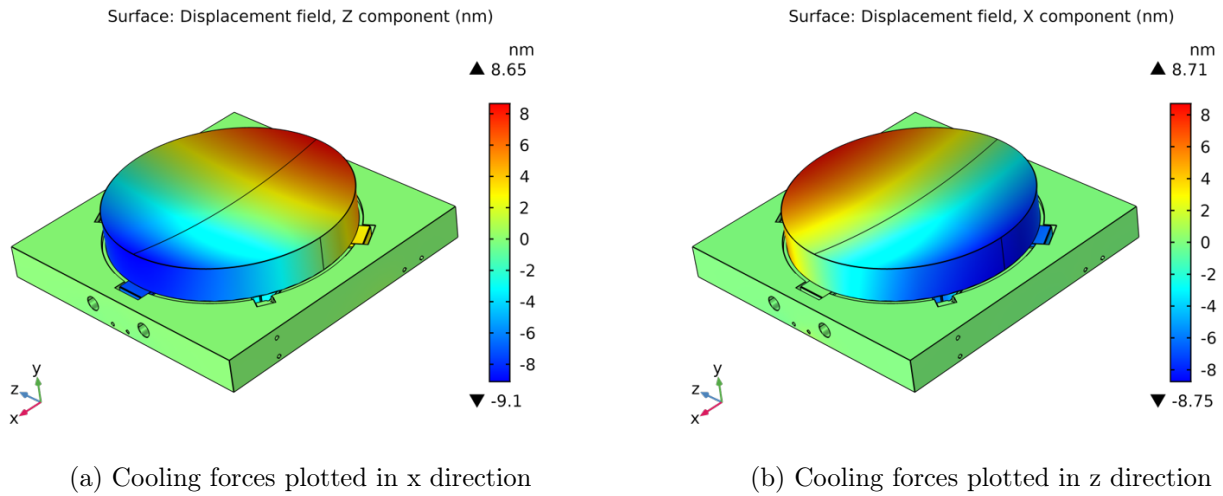


Figure 8.4: Cooling forces

As shown in fig. 8.4 is the displacement so small that this doesn't influence the properties of the design. It can be seen that due to the in and outlet of the cooling channels there is a small rotation around the y axis.

8.5 Tooling and placing

It can be questioned if the mirror can be positioned precise enough if the aluminum plate is used and bolted to another part. In theory, as shown in the requirements should astigmatism, create by a misaligned mirror on manufacture tolerances, stay with in the budget. However, less is better for the conversion efficiency thus improving this could be beneficial. There are multiple ways to ensure the precise position of this mirror. The first manner is to shim the whole Aluminium plate and then bolt it down to the Aluminium mirror house. Another possibility is to make a tool that can adjust the fixation of the flexures. For example in the Z flexures is some space to adjust in the bolt holes.

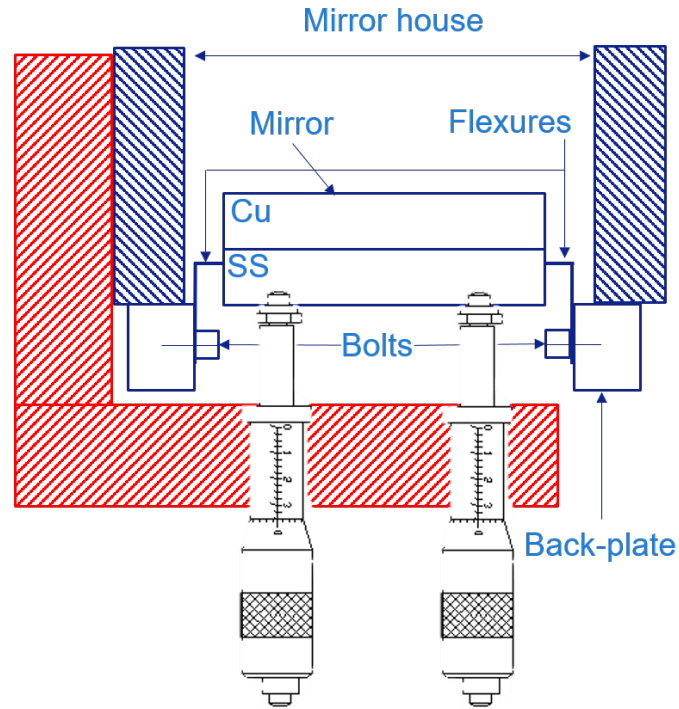


Figure 8.5: Tooling

In fig. 8.5 the red part is drawn as the tool where, in the figure, two micrometers are attached. However, in reality, will for each Z flexure one, thus 3 micrometers in total will be attached. With this tooling system, the tip, tilt, and piston be adjusted. The remaining degree of freedom, rotation over the optical axis and translation in its plane, can be done by moving the plate. This by themselves can be done with three other micrometers place in a plane with the plate or just with a micrometer hammer.

Another strategy to align the mirror is by place it with out alignment and align the other mirror to it. So for example blot this as an assembly to the mirror house and align the M1 to it.

Anti torque plates

If necessary, anti-torque plates could be used to ensure no torque will be transferred to the thick part of the flexure. This can just be a thin small plate and is easy to add if this is a problem.

8.6 Manufacturing

The most complicated part in this assembly will be the back-plate, this part needs to be made with a wire spark erosion technique. Before this, with a milling machine the cooling channels can already be milled and the holes to connect to this can be manufactured simultaneously. The spark erosion technique ensures a stress-free manufacture manner and to cut the flexures with high precision. As the Back-plate is done the Copper slab can be flattened on two sides, at one side the cooling channels as under the mirror surfaces can be milled. On the other side, the cooling channels can be milled in the same patterns in the back-plate. With some dowel pins, the slab of copper can be aligned with the back-plate. The two parts will be brazed upon each other and also the final mirror surface will be brazed as a final part. Now the back-plate and mirror are placed on a vacuum chuck and the final diamond turn process will be done. This will ensure the mirror surface to have the final shape and roughness. The star design which can be seen in fig. 7.14c is just there to support the last manufacturing process on the vacuum chuck.

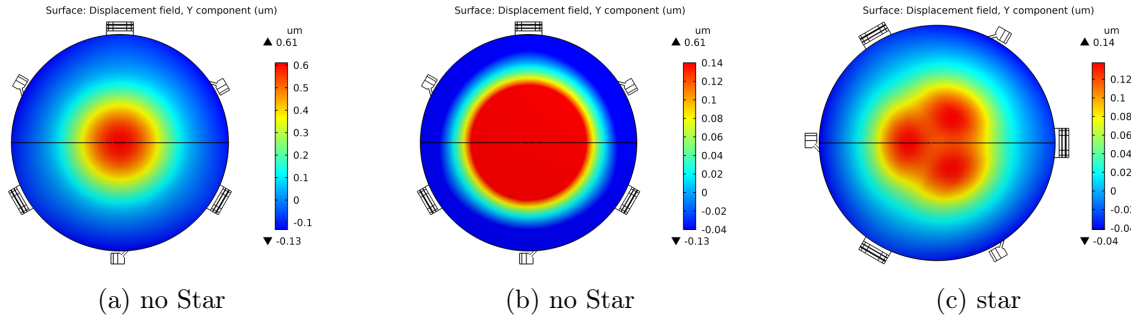


Figure 8.6: Vacuum effect

In the fig. 8.6 the deformation due to the final diamond turning on the vacuum-chuck can be seen. In fig. 8.6a the surface deformation is shown, the same deformation is illustrated in fig. 8.6b but the color range is adjusted to fig. 8.6c. This is done to compare the pictures and the difference in deformation is given PV in μm . However, by taking the Zernike polynomials of the two surfaces it becomes more clear why to choose the back-plate with star design.

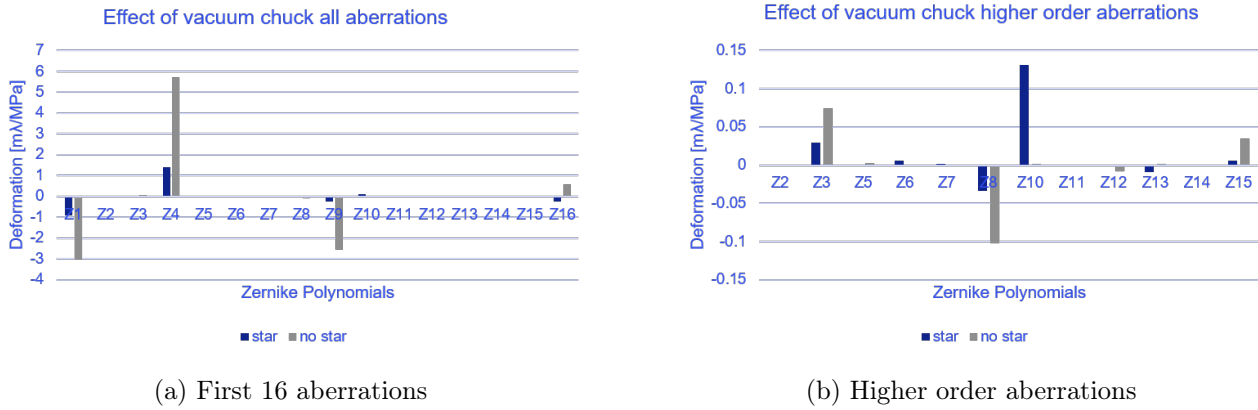


Figure 8.7: Zernike Polynomials vacuum deformation

Shown in fig. 8.7 are the Zernike polynomials of both surfaces. A zoom in is made in fig. 8.7b with the higher order aberrations. Used is a wavelength of $10.6 \mu\text{m}$ and as 0.1 MPa is used as vacuum. As usual, Z1 can be neglected as this is just piston. Defocus is three times higher without the back star. Some Z6 and Z7 can be noticed at the no star design. Some higher-order terms are visible in the star design but those are very small compared to the difference in lower order terms and therefore it's better to manufacture a small star in the back-plate.

8.7 Sensitivity

To show how the design will perform in the future, were the laser power can go up 2 times, it is shown in fig. 8.8 how the mirror surface responds to this power increase. It can be seen that the model is linear, the color scheme is different in both pictures but the range is given and shows a clear 2x increase.

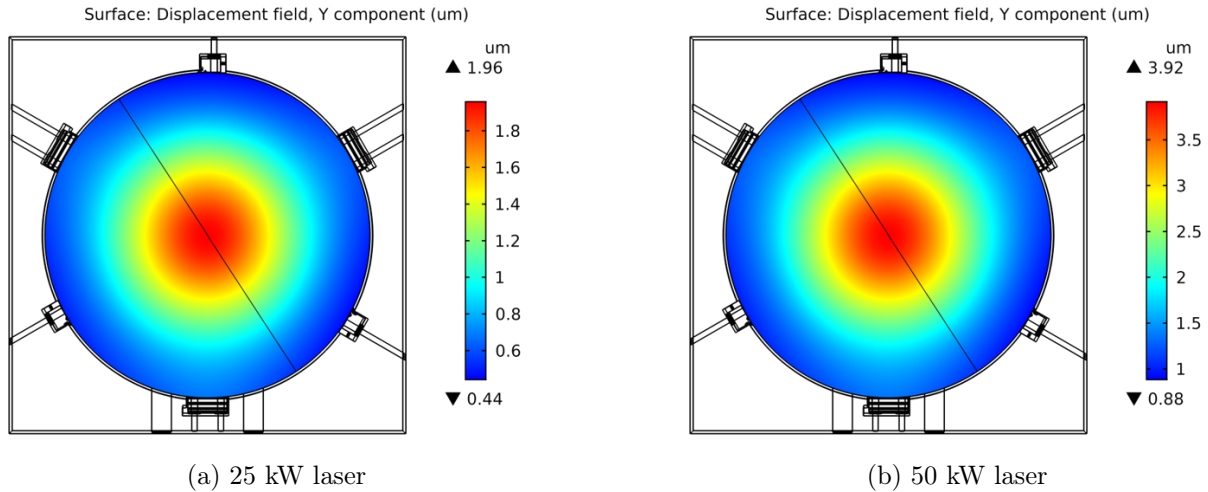


Figure 8.8: Laser power sensitivity

Same wise as other sections are the Zernike polynomials of the laser power sensitivity given in fig. 8.9. Also here the linearity of the problem is visible but gives a good indication of the aberrations due to power increase.

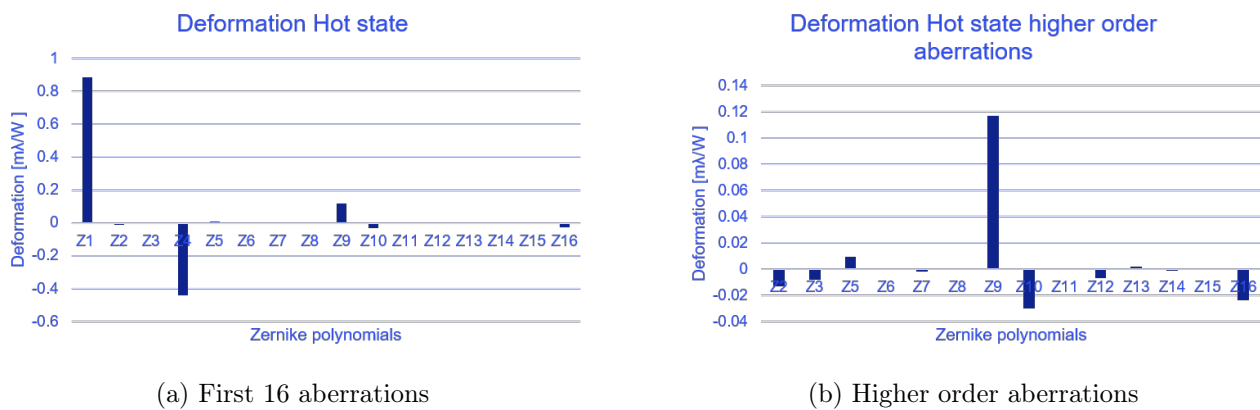


Figure 8.9: Zernike Polynomials laser sensitivity

It can be seen that the dominant aberration here again is Z4 and Z9, and for Z4 is compensation available so the increase in power in the future will not give a problem here. However, by looking to Z5 there is also an increase which means that probably by increasing the laser power, even more, this can give issues.

8.7.1 Astigmatism

The astigmatism is build-up from multiple aspects, every deformation or misalignment will result in an amount of astigmatism. In section 9.2 a table is given for both the Z5 and Z6 with all the potential errors combined.

Part IV

Comparison Proposed design

Chapter 9

Discussion

This chapter shall be used to examine the proposed design in terms of the requirements. As explained in the previous chapter the design met the requirements in terms of the stress limit, eigenfrequency and the shock-load that arises during transport stays below the fatigue stress. A summary will be given in the form of a table to provide a overview and, onto which a discussion will follow.

9.1 Mechanical performance

In table 9.1, a summary about the mechanical requirements is shown. What can be seen is that all the models have a higher eigenfrequency then the specified 150 Hz. The current mirror has a higher eigenfrequency since this one is bolted down. The position accuracy is based on chapter 3 were the error in position of the mirror is based on the arising astigmatism. It is shown with check-marks whether or not the design is approved for the matching requirement.

Mechanical validation			
	Requirement	Current	Proposed 1
Eigenfrequency	150 Hz	» 150 Hz	384 Hz
Position accuracy	50µm	50 µm	50 µm
Shock load	7g	>7g	45g
Environment Vacuum	Material compatibility	✓	✓
Temperature variation	± 23 °C	± 7 °C	± 23 °C
Approve		✗	✓

Table 9.1: Mechanical validation

What can be noticed in the table is that the shock-load is shown as 45g, this is based on the fatigue value given for the AISI 301 stainless steel. As can be seen is the eigenfrequency higher then specified, questioned can if the flexures can be optimized by lowering the eigenfrequency and thereby lowering the stress from the shock-load or increasing the range of the temperature. However, with thinner flexures and with the same shock-load, more deformation will arise and this results in a higher stress value and thus requires careful evaluation. By comparing the temperature variations it can be seen that the current design does not meet the specification, and hence affect performance as demonstrated in section 4.3. And the new proposed design will reach the requirement of ± 23 ° C.

The position precision of the mirror is in this case based on manufacturable tolerances, which can be improved using proper tooling see section 8.5. As this is related to the AST, this will be discussed in next section.

9.2 Optical validation

The optical validation is mostly based on the astigmatism requirements and budget. In order to compare, all values are shown in μm , and for the laser power a representative value is used being in line with the earlier mentioned range.

- The manufacturing precision is based on the vacuum effect as shown in previous chapter.
- The gravity gives a small deformation in the surface what also results in a part of the astigmatism, and thus is this used in the gravity part.
- Position accuracy is based on worst case misalignment as shown in section 3.1.2.
- The Hot state Operation is the amount of AST created due to the heat of the laser.

The current model is the one which was also used in chapters before to get a fair comparison. However, for the transportation are the Zernike of the figures used as in chapter 4 where also the Zernike plot was made. This comparison is split up into Z5 and Z6 since there was some difference between the two. The budget was specified for Z5 and Z6 making it easy to compare. First the tables will be discussed separate and after that the both will be compared.

Optical validation Z5			
	Requirement [μm]	Current	Proposed 1
Transportation	0	0.385	0
Manufacturing	} 0.3	} 0.424	9E-5
Gravity			0.039
Position accuracy			0.18
Misaligned external	0.18		
Hot state Operation	0.8	0.0253	0.0249
Total	1.28	0.8343	0.2440
Approve		✓	✓

Table 9.2: Optical validation Z5

As can be seen in table 9.2 is that the biggest improvement is reached in the transport AST. The reason for this is the iso-static mount which is optimized for the temperature range during transportation. Thus the AST is reduced to zero there. For manufacturing the vacuum values are used that arise due to the star design. During the hot state in operation mode it can be seen that there is no real improvement and as shown before and has two main reasons. First, AST originates from the incoming angle being the same for both. Secondly, given the cooling channel layout, most heat is transported away from the surface directly, hence the effect of the suspension is limited. In the end a improvement up to 3.4x of Z5, vertical astigmatism is reached.

Optical validation Z6			
	Requirement [μm]	Current	Proposed 1
Transportation	0	0.437	0
Manufacturing	} 0.3	} 0.424	6E-4
Gravity			0.039
Position accuracy			0.18
Misaligned external	0.18		
Hot state Operation	0.8	0.0067	0.0093
Total	1.28	0.8677	0.2289
Approve		✓	✓

Table 9.3: Optical validation Z6

What can be seen in table 9.3 are comparable values as in table 9.2. However, there are some differences that needed to be explained. The manufacturing in Z6 has a higher contribution then in Z5, the reason for this is the orientation of the back-star in the back-plate. Anyway, this is still in the order of nanometers, and thus also a small number in the table. Again in this table is the hot-state comparable with the current design. The largest improvement in current en the new proposed design is made in the transport. Overall an improvement of 3.8x is realized.

What can be seen in both of the tables is that both in the Z5 and Z6 the amount of AST is equal for the gravity, this is because the gravity is determined by placing the design in all directions and have than check the optical surface. After this the highest value is used to get the worst case AST value. Since Z5 and Z6 are perpendicular to each-other is in one orientation Z5 dominant and in the other Z6. As previously said, is the position accuracy based on the AST created by the misaligned mirror. The $0.18\text{ }\mu\text{m}$ was specified as a budget and with that tolerances are made which are manufacturable on machine tolerances. Thus used is the worst case so max budget of the position precision of the mirror. However, by using the tooling which was shown this amount of AST can be lowered and a better end result can be reached. As shown in section 3.1.2 is the amount of AST linear decreasing with the position accuracy. The exact amount will depend on the precision of the tooling.

In the Hot state, it is shown that there is no direct improvement since this is coming from the angle of the incoming laser beam. However, literature [25] describes thermal path optimization and the optical surface can be shaped in such a way that there can be compensated for this error.

To summarize the discussion the total amount of AST is given in table 9.4. The total is calculated with the sum of squares and then normalised. It can be seen that the proposed design has an improvement up to 3.6x.

Total AST comparison			
	Requirement [μm]	Current	Proposed 1
Total Z5	1.28	0.8343	0.2440
Total Z6	1.28	0.8677	0.2289
Sum of squares AST	1.8102	1.2037	0.3346
Ratio of specification	1	0.6650	0.1848

Table 9.4: Total AST comparison

Both might be in spec, but future throughput increase will require higher power in order to increase the conversion efficiency. This will reduce the specification and hence the design space. As such, the proposed design is more road-map robust and frees up design space elsewhere in the system.

Chapter 10

Conclusion & Recommendations

The throughput of the latest ASML machines is limited by the EUV source. This source can provide more power but, more power also results in more problems in the form of mirror deformations. This research aims to examine the largest curved mirror to see what problems arise. First, the existing system is explored and the requirements are discussed. Subsequently, simulations have been done with these requirements that indicated that problems mainly arise during transport.

The most important thing is that it has been demonstrated that a temperature variation of 7 Kelvin can result in a permanent deformation. This distortion, coming from slipping bolt interfaces, has been simulated and compared with existing measurements. An iso-static mount is introduced to overcome this problem of deformation during transportation. This mirror mount is in the form of six folded flexures, each constraining 1 DOF. The flexures are optimized to survive the thermal fluctuation during transportation and are designed to have a higher eigenfrequency than 150 Hz.

The proposed design has the largest improvement on transportation AST and the positioning AST for which a design has been developed. This results in an optical improvement up to 4x.

10.1 Recommendations

In this thesis the Zernike used are obtained with matlab, the program which is available within ASML, namely, Main_text2zernike.m. Throughout this document all Zernike's are created with this file to get fair comparisons. All Zernike's are obtained by looking from the normal of the mirror surface, even as the beam was entering at an angle. By speaking with optical professionals, it was pointed out that it could be done in a more proper way in Zemax. However, for the purpose of this thesis and by doing all the measurements in the same way the comparisons are valid and conclusions are not changed.

The main focus of this thesis is the mounting of the M2; however, some work is done on a higher level. Material choice is another strategy that can be utilized in order to reduce stresses at interfaces and within the design. This can take the form of either matching the CTE's of the materials used or simply using one material throughout the housing, the mounting, and the mirror. One difficulty is that the thermal capacity can vary across the design and thus stresses can still arise in transient behavior. A promising material for CTE matching is RSA-462 T6, the downsides of this material are the lead time and cost. More research is needed to check the possibilities.

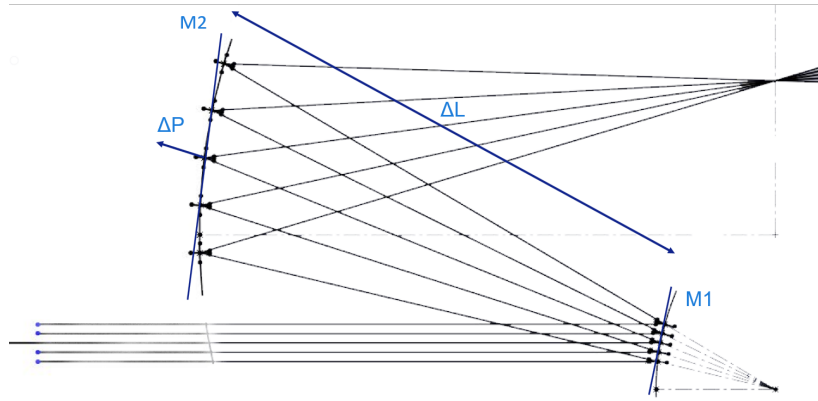


Figure 10.1: Sensitivity system level

The sensitivity analysis in section 3.1.2 can be used to increase the systems boundary from the M2 suspension to the frame. This analysis gives the amount of AST as a result of the accuracy of the position. What can be seen in fig. 10.1 is that the ΔL has the same influence as ΔP has. So the stiffness and accuracy of this housing can be obtained from this analyse.

The tooling shown in section 8.5 is a schematic drawing. However, as shown in the discussion, the biggest improvement after the iso-static mount, is AST based on the position of the mirror. Thus, a proper tooling mechanism to place the mirror in the optimal position can reduce the amount of AST even more and thereby improve the throughput of the machine. That being said, that the position of the mirror is this AST sensitive means that the mirror housing is also very important to be stable, by deforming this, the mirror will change position. More investigation is needed to say something about the tooling, for example it should be investigated whether the tooling will be used in the factory and that the assembly will be shipped. Or that the tooling will be also delivered at the costumer and that the service engineer can use this tooling. Another strategy could be to not align this mirror but align the other mirror to this on, this can be seen in fig. 10.1.

Another recommendation is a relative simple one but could have a major benefit. When designing the mirror in a manner that it can be reached easily in the machine, it should be possible to transport this mirror separate from the rest of the machine. This means that the temperature variation during transport will have no influence on the assembly, because they will be bolted together at a later time. The question that arises is, can this not be done for the current design?

Well, since the bolts nowadays are used in the current design to adjust the optical surface this is not possible. Because in the first place is the measurement device nowadays not available at the costumer, and secondly since there are 16 bolts to tune, this is a very difficult action. In the proposed design doesn't need this adjustment since the optical surface is decoupled due to the flexures.

Part V

Appendices

Appendix A

Material deformation

A.1 Fake material 1

First fake material 1 that is investigated has a CTE of $1\text{e-}6$ $1/\text{K}$ and a conductivity k of 1 $\text{W}/(\text{mK})$ aswell. What can be seen in fig. A.1 is that the PV value is 0.78 μm and that the highest temperature is 370 Kelvin. Conclusion would be low CTE is low deformation and low conductivity is high temperature.

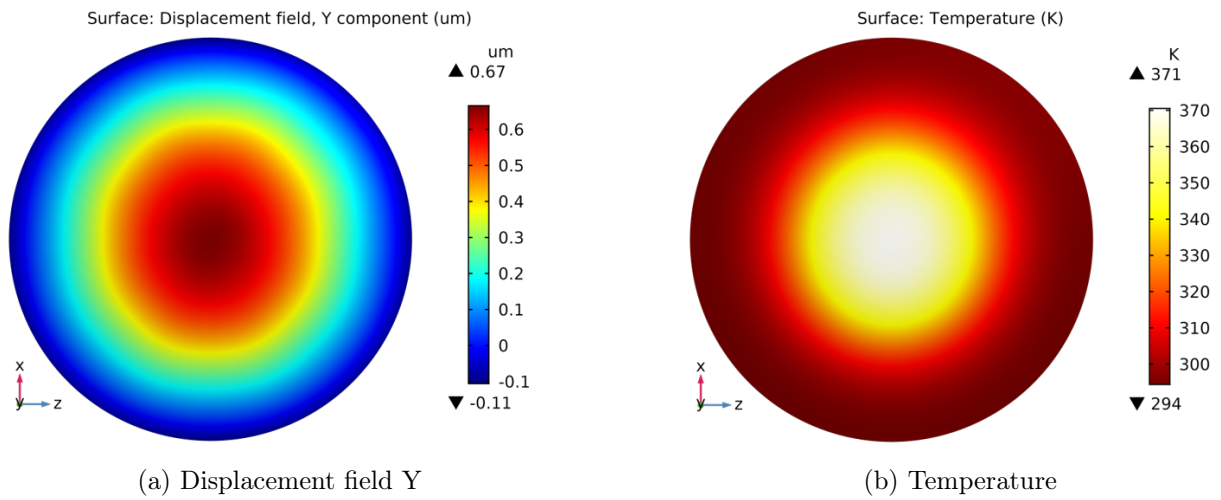


Figure A.1: Fake material 1

A.2 Fake material 2

Fake material 2 is opposite of fake material 1 and has a high CTE of $100\text{e-}6$ $1/\text{K}$ and a high conductivity k of 1000 $\text{W}/(\text{mK})$. Figure A.2 illustrates the PV value of 5.64 μm and a final temperature of 295 K.

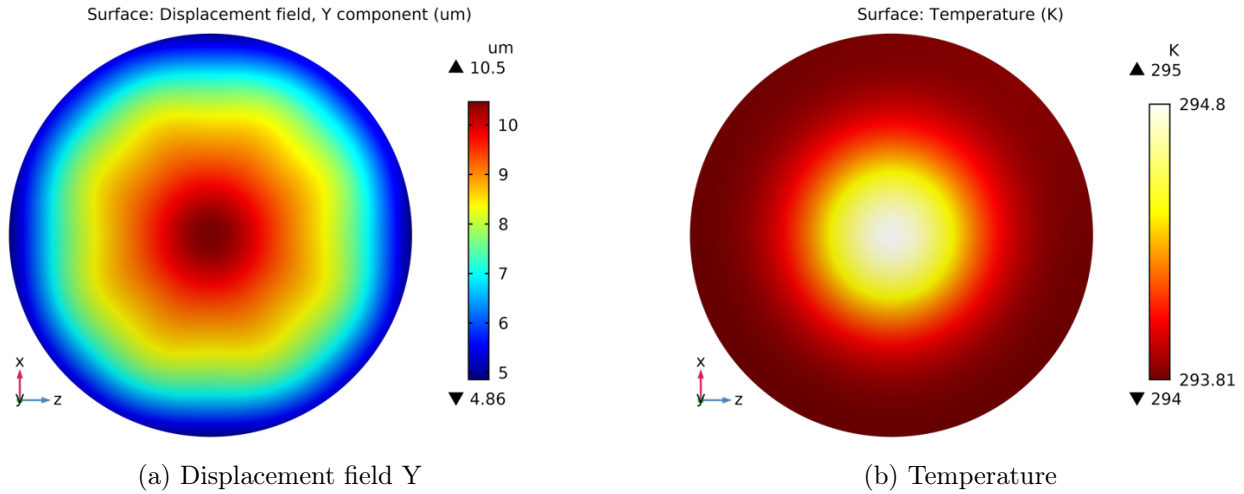


Figure A.2: Fake material 2

A.3 Fake material 3

Fake material 3 has a high CTE of $100 \times 10^{-6} \text{ 1/K}$ and a low conductivity k of 1 W/(mK) . Figure A.3 illustrates the PV value of $77.2 \text{ }\mu\text{m}$ and a final temperature of 370 K . This is the complete opposite what is desired in a mirror.

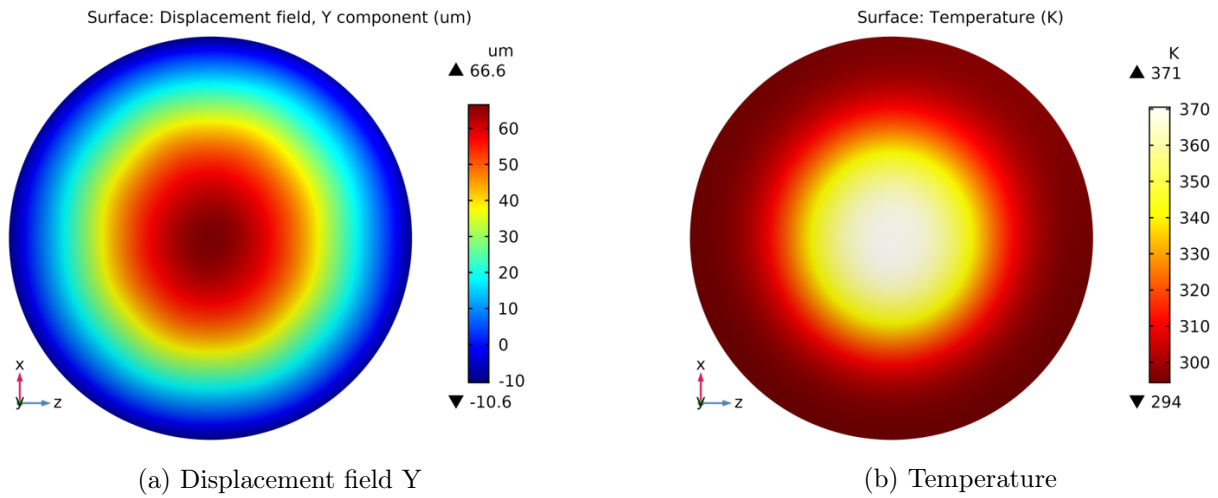


Figure A.3: Fake material 3

A.4 Fake material 4 / Diamond

Diamond has a low CTE of approximately $1 \times 10^{-6} \text{ 1/K}$ and a high conductivity k of approximately 1000 W/(mK) . Figure A.13 illustrates the PV value of $0.05 \text{ }\mu\text{m}$ and a final temperature of 295 K . This is what is desired in a mirror.

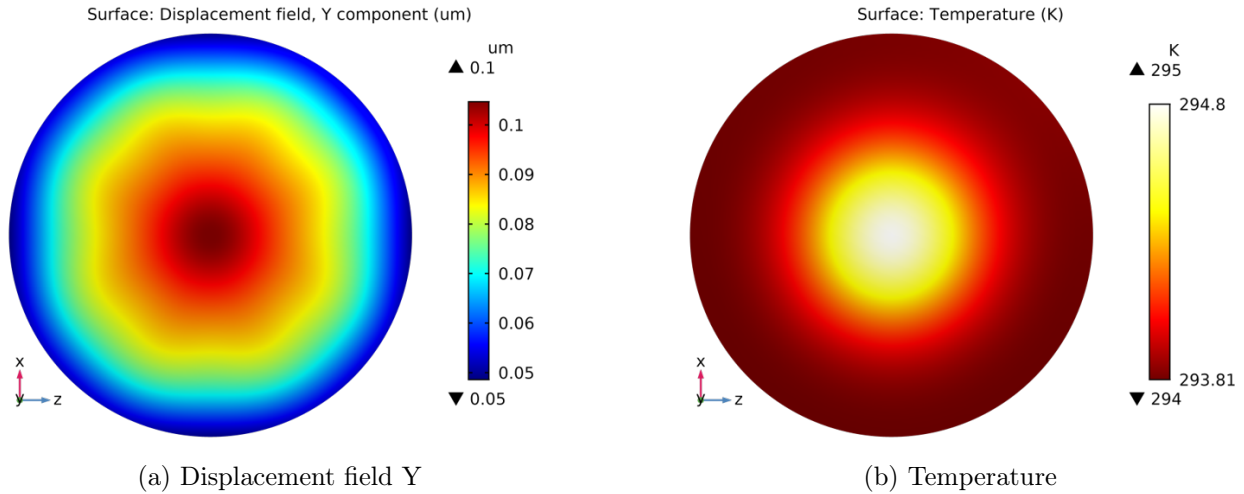


Figure A.4: Fake material 4

A.5 Copper

Copper as the mirror is now has a low CTE of $16 \times 10^{-6} \text{ 1/K}$ and a high conductivity k of 400 W/(mK) . Figure A.5 illustrates the PV value of $0.92 \text{ }\mu\text{m}$ and a final temperature of 296 K .

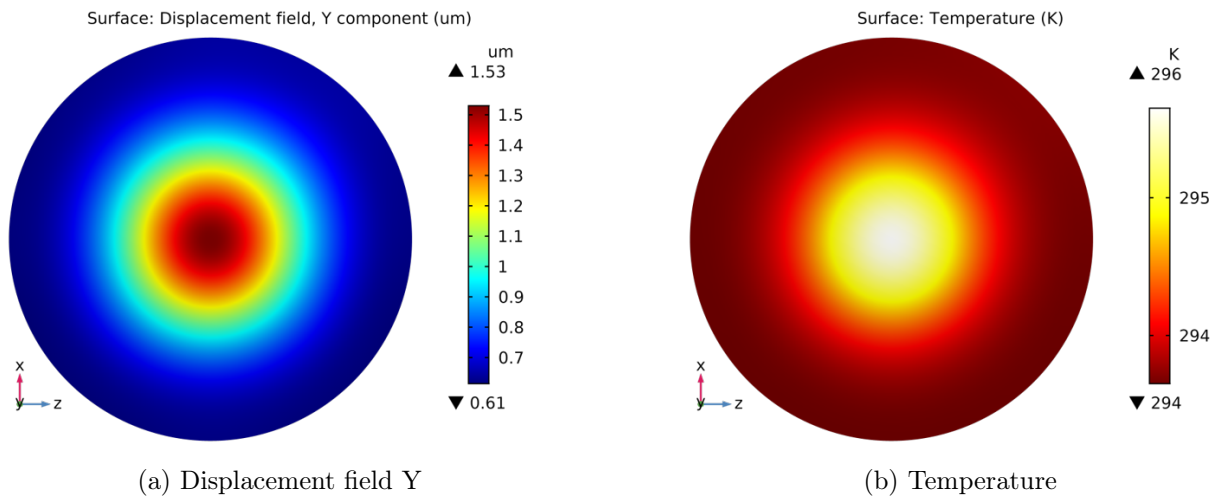


Figure A.5: Copper

A.6 SiSic

SiSic has a low CTE of $2.9 \times 10^{-6} \text{ 1/K}$ and a conductivity k of 170 W/(mK) . Figure A.6 illustrates the PV value of $0.21 \text{ }\mu\text{m}$ and a final temperature of 297 K .

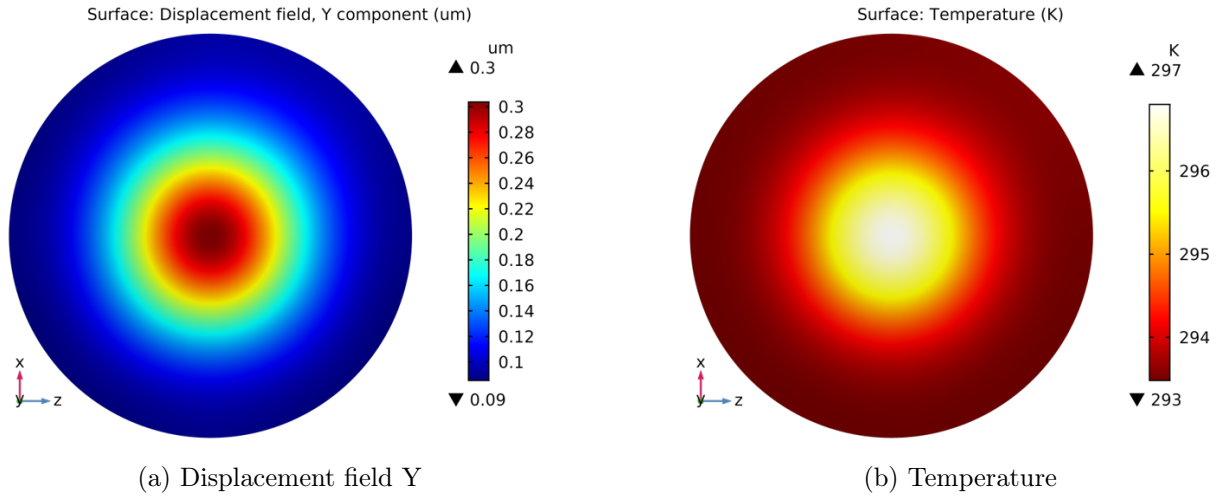


Figure A.6: SiSic

A.7 Titanium

Titanium has a low CTE of $8 \times 10^{-6} \text{ 1/K}$ and a conductivity k of 22 W/(mK) . Figure A.7 illustrates the PV value of $3.18 \text{ }\mu\text{m}$ and a final temperature of 308 K .

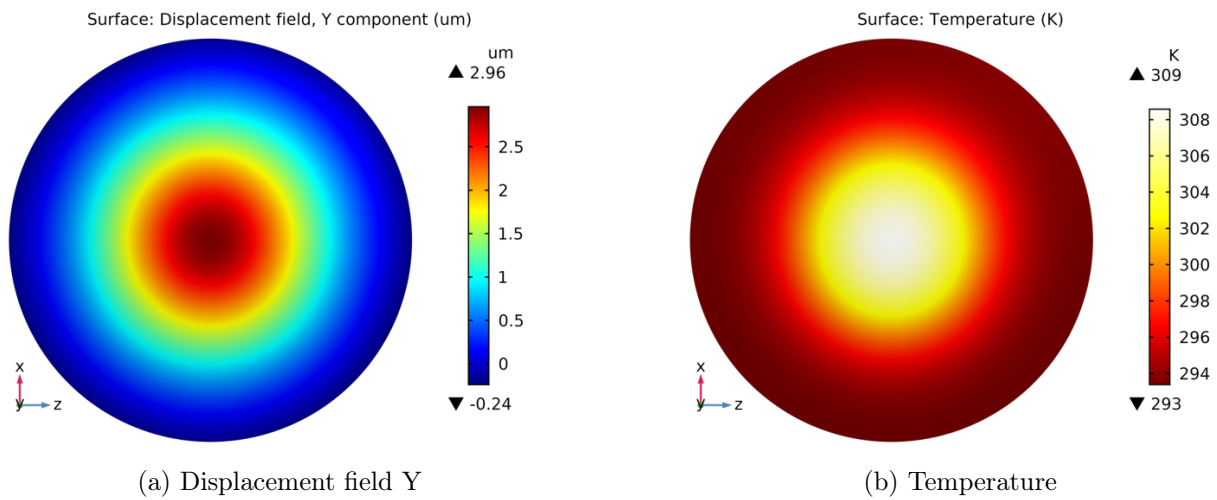


Figure A.7: Titanium

A.8 RSA-443

RSA-443 has a low CTE of $13.6 \times 10^{-6} \text{ 1/K}$ and a conductivity k of 135 W/(mK) . Figure A.8 illustrates the PV value of $1.34 \text{ }\mu\text{m}$ and a final temperature of 297 K .

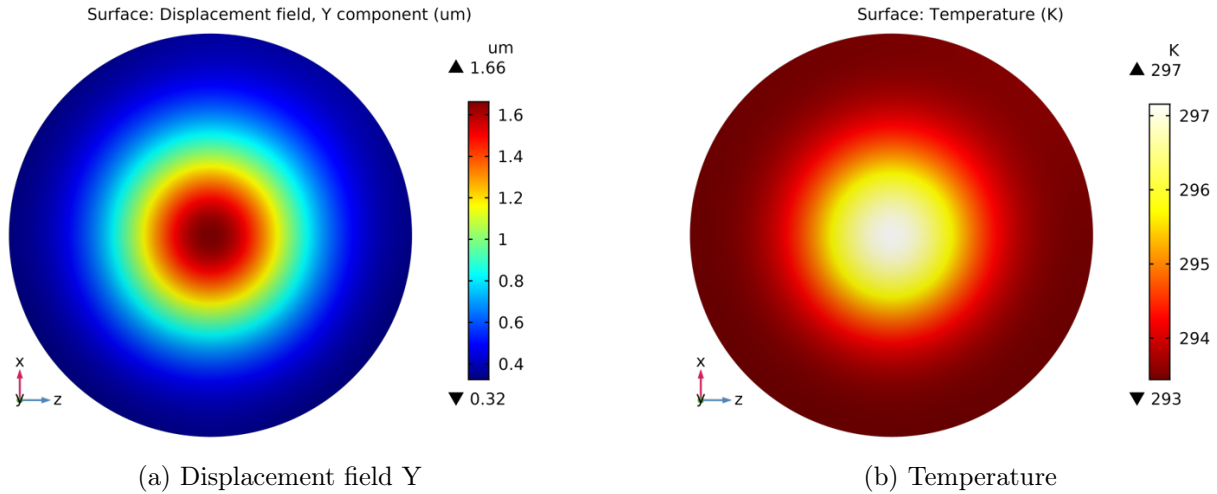


Figure A.8: RSA-443

A.9 RSA-462 T6

RSA-462 T6 has a CTE of $16.8 \times 10^{-6} \text{ 1/K}$ and a conductivity k of 130 W/(mK) . Figure A.8 illustrates the PV value of $1.69 \text{ }\mu\text{m}$ and a final temperature of 297 K .

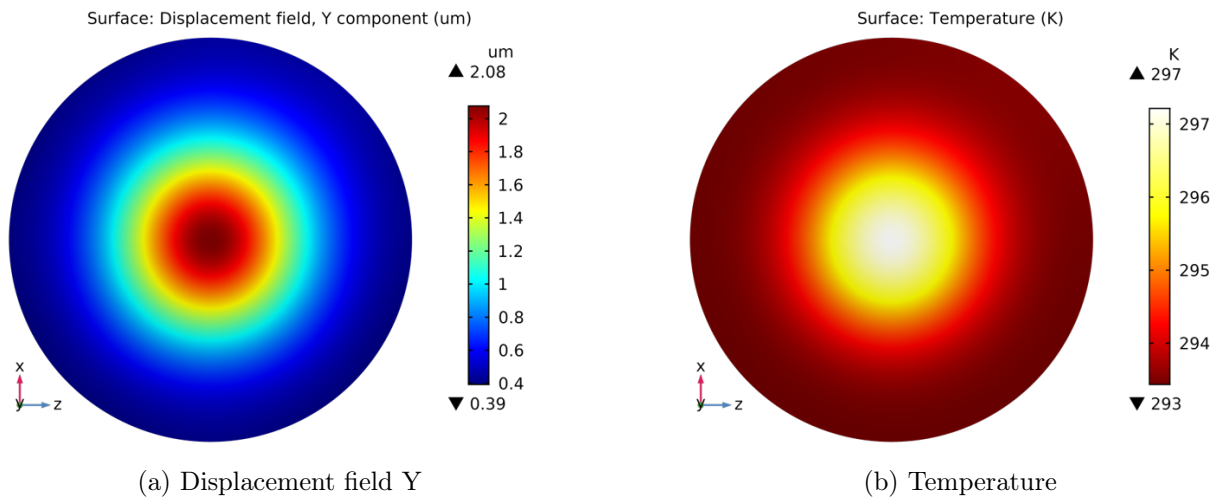


Figure A.9: RSA-462 T6

A.10 Aluminium (6061)

Aluminium 6061 has a CTE of $23 \times 10^{-6} \text{ 1/K}$ and a conductivity k of 160 W/(mK) . Figure A.8 illustrates the PV value of $1.95 \text{ }\mu\text{m}$ and a final temperature of 297 K .

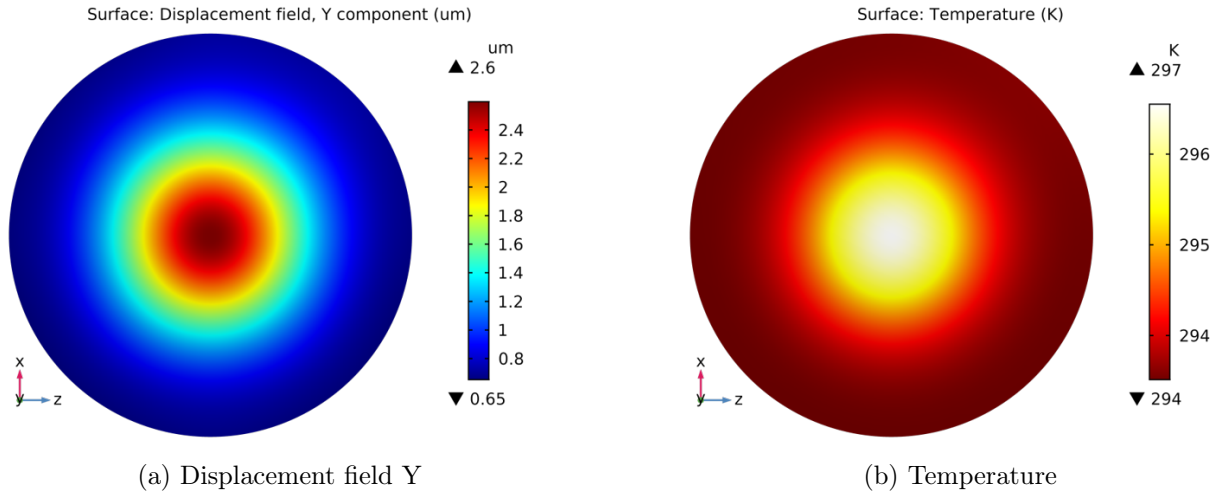


Figure A.10: Aluminium (6061)

A.11 Stainless Steel

Stainless Steel has a CTE of $17\text{e-}6$ 1/K and a low conductivity k of 16 W/(mK). Figure A.8 illustrates the PV value of 3.43 μm and a final temperature of 303 K.

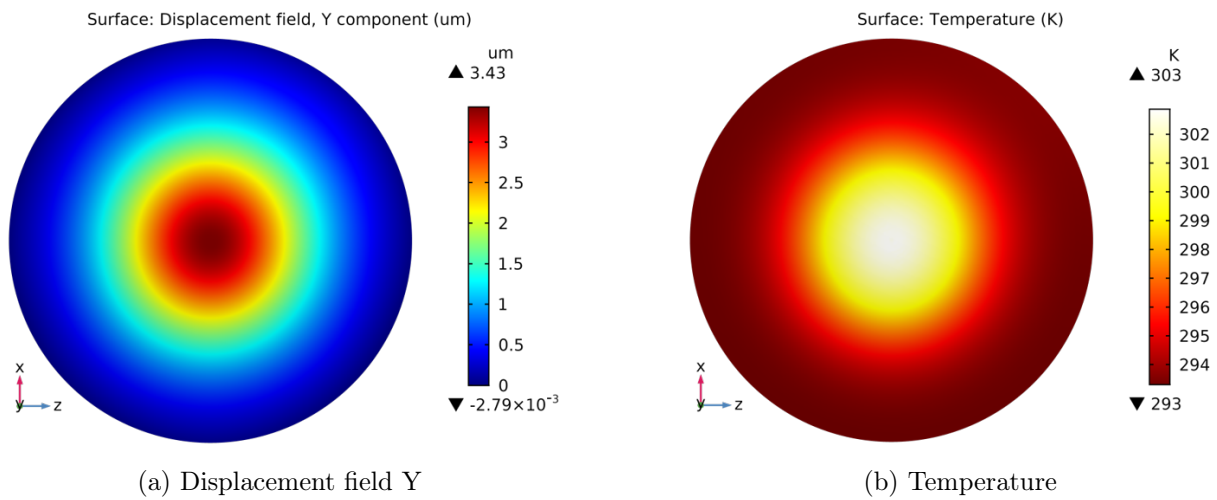


Figure A.11: Stainless Steel

A.12 SiSic 70% absorbed power

SiSic has a low CTE of $2.9\text{e-}6$ 1/K and a conductivity k of 170 W/(mK). Figure A.12 illustrates the PV value of 21.3 μm and a final temperature of 549 K.

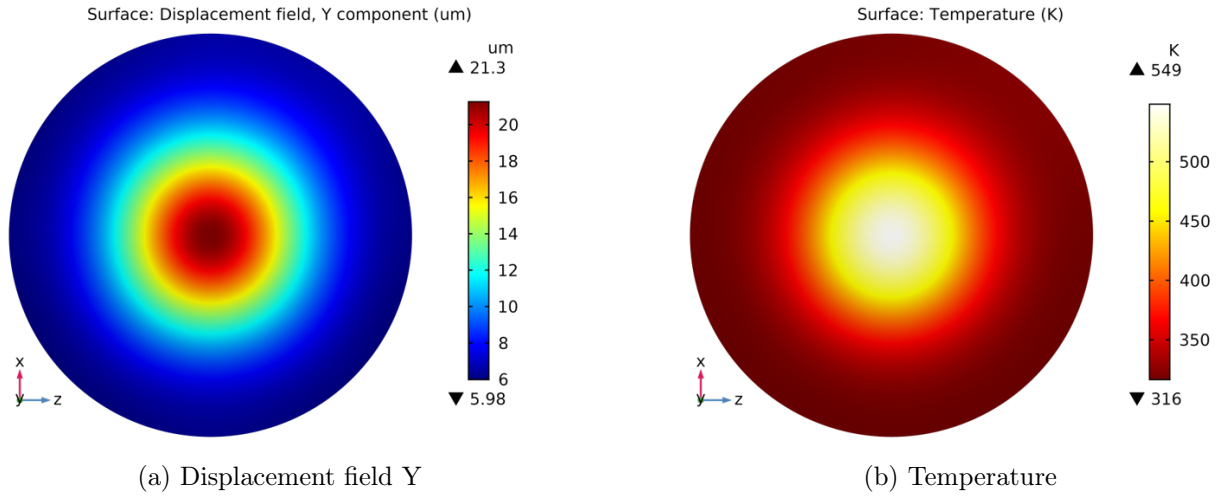


Figure A.12: SiSiC 70% absorbed power

A.13 Diamond 19% absorbed

Diamond has a low CTE of approximately $1\text{e-}6$ 1/K and a high conductivity k of approximately 1000 W/(mK). Figure A.13 illustrates the PV value of 1.07 μm and a final temperature of 325 K.

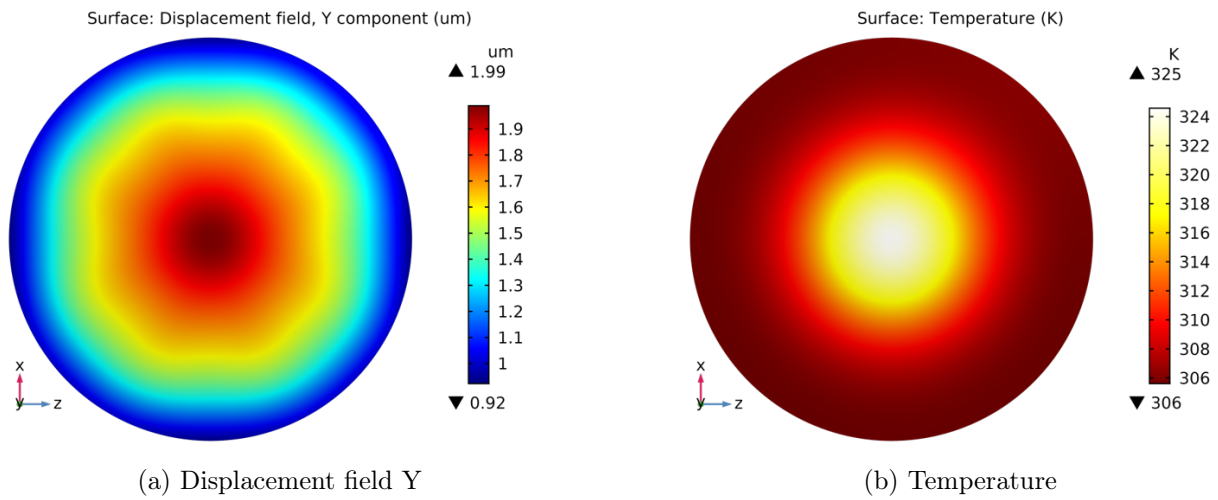


Figure A.13: Diamond 19% absorbed

Zernike Ploynomials of all the tested materials

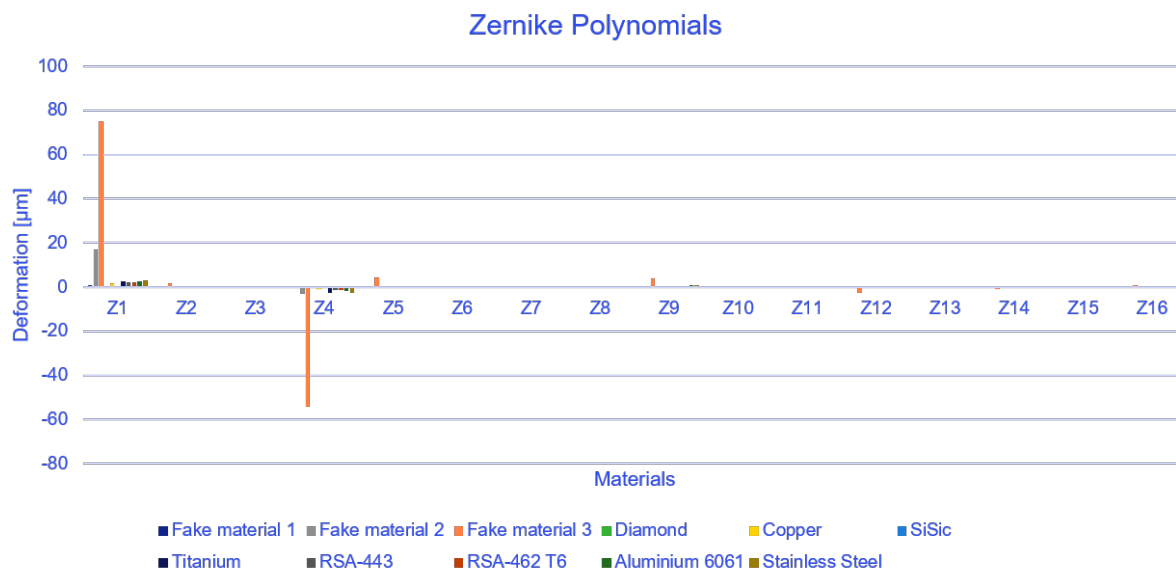


Figure A.14: Zernike Polynomials of all the tested materials

Zernike Polynomials of relevant tested materials, the fake materials are excluded with the big outliers.

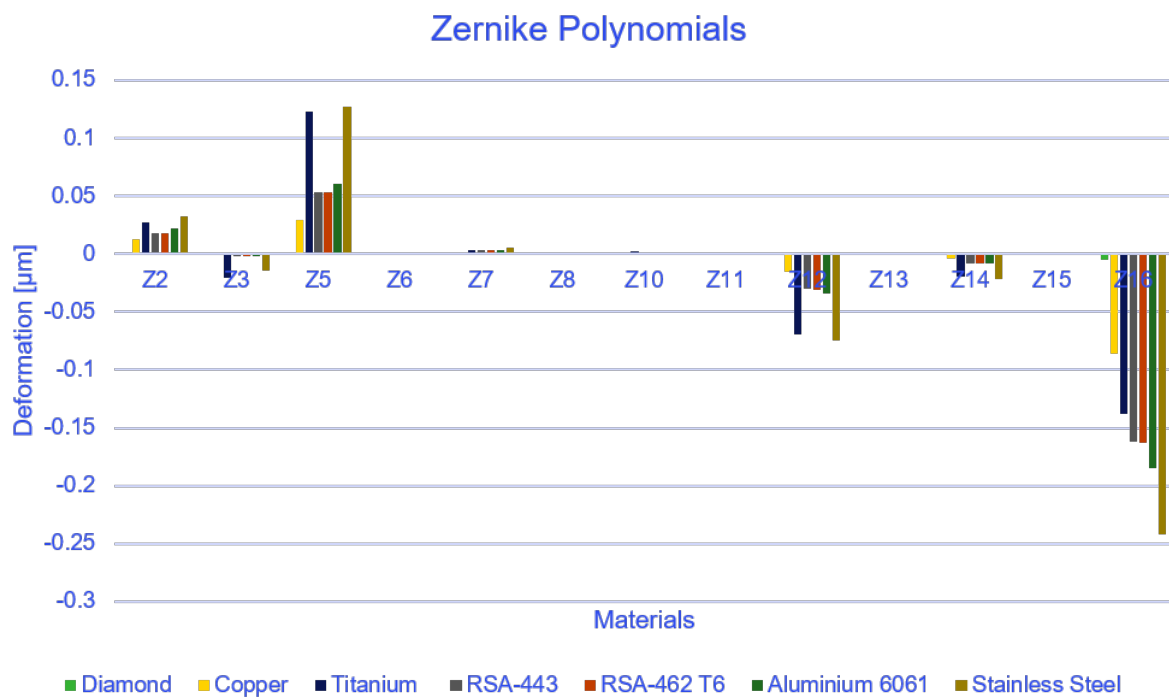


Figure A.15: Zernike Polynomials of relevant tested materials

Appendix B

Model check

B.1 Mirror surface measurement setup

The measurement setup use to measure the deformation after transport is shown in fig. B.2. Those pictures are used to indicate the problem of deformation of the optical surface during transportation of the assembly.

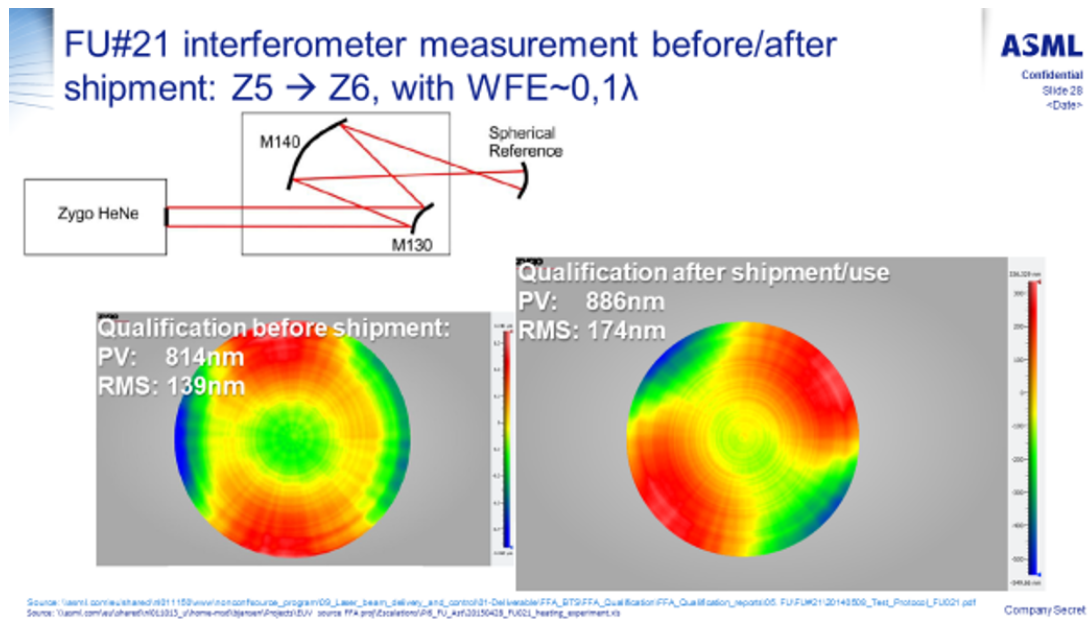
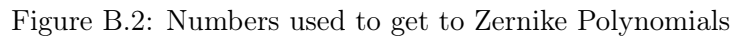
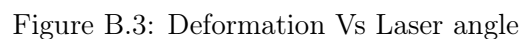


Figure B.1: Measurement setup

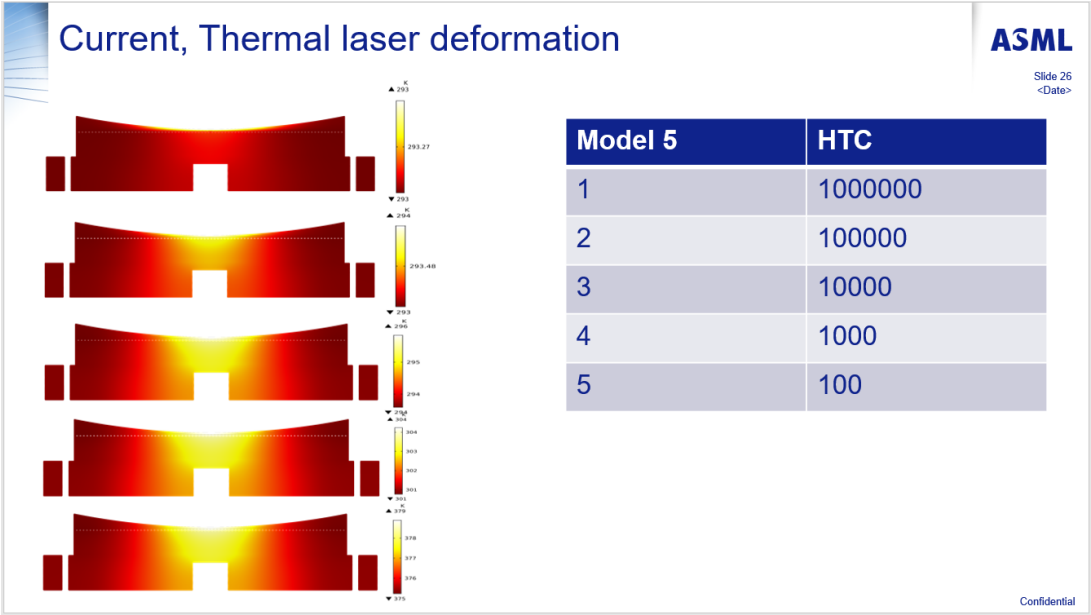
As explained in the main thesis are in both figures numbers added to find the deformation in Zernike terms. The figures with the corresponding numbers can be seen in fig. B.2.



To show that a laser beam with an increasing angle of incidence has an impact on AST, an analyse is done where the angle is varied. By enlarging the angle it can be seen that Z5 is also increasing. If however, the elliptical shape was vertical, Z6 was introduced. But in this case, as can be seen in fig. B.3, Z5 is increasing with an increasing angle of incidence.



To show the influence of the cooling channels and by showing the increase of the HTC in this channels, it can be seen that with an increasing HTC both the model gets less warm and also the thermalgradient becomes less. This means less deformation. This is shown in fig. B.4



Appendix C

Forces of cooling water

3 Table 4: $3 \cdot \sqrt{\text{CumPSD}}$ of forces and moments for the situation with flow limiter 6.0 LPM

Flow [LPM]	P1 [Barg]	P2 [Barg]	Fz [N]	Rx [Nm]	Ry [Nm]
0	0.0	0.0	0.019	0.003	0.002
	0.0	0.0	0.016	0.002	0.002
3	0.2	0.6	0.071	0.005	0.004
	0.2	0.6	0.031	0.004	0.003
4	0.4	1.1	0.060	0.006	0.004
	0.4	1.1	0.058	0.006	0.004
5	0.6	1.6	0.100	0.011	0.008
	0.6	1.6	0.099	0.011	0.007
6	1.9	3.4	0.155	0.017	0.012
	1.9	3.4	0.153	0.017	0.012

Figure C.1: Forces of flow

RE: Cooling hoses

Tom,

Voor M150 hebben wij stijfheden van koper water slangen aan een spiegel afgeschat in onze krachtenbudget. Hiervoor hebben we twee posten gebruikt:

- Massa verplaatsing van water (omdat we een bewegende spiegel hebben moeten we een waterkolom verplaatsen over een afstand dus moet onze servo hiervoor kracht leveren)
- Verplaatsing van de waterslang wie aan een spiegel trekt (oftewel: stijfheid). Ik heb de stijfheid afgeschat op 0.45 N/mm uit mijn hoofd (dus: $F = k \cdot x$; $k = 0.45 \text{ N/mm}$, $x = 4.6 \text{ mm}$)

Betreffende metingen van dynamische performance vanuit locale turbulentie/acoustische effecten in watercircuits (lees: FIV) heb ik wel een rapport beschikbaar. Ik heb samen met MECAL en onze Systeem Dynamica collega's een TPS/TAR gemaakt om dit te bekijken, echter slaat dit niet op de stijfheden wie je verwacht.

TPS/SOW: <https://tc-eu.asml.com/getpdf.html?D000642964>

TAR: <https://tc-eu.asml.com/getpdf.html?D000664657>

PIR SysDyn (waar FIV een onderdeel van is): <https://tc-eu.asml.com/getpdf.html?D000672340>

Laat me even weten of je hier iets aan hebt en anders, mocht je toch gevonden hebben wat je nodig hebben (lees: testen op slang stijdheden) zou ik da took graag even willen weten.

Best regards,
Met vriendelijke groet,

Toni

Figure C.2: Cooling hoses stiffness

Appendix D

Isostatic mounts

During this thesis a lot of options for a mirror mount were available. However, in order to choose the best a lot of simple designs are made and compared against each other. The blue disk was kept constant and flexures were added and a force was applied to measure the distance and with that the stiffness is determined. An attempt is made to create a program as well in Excel as in Matlab to make it easy to compare and combine separate flexures. Unfortunately the model deviated too much from the model in COMSOL and therefore is COMSOL used to compare the different designs.

The following three types were compared first, a bi-pod and a reinforced bi-pod, secondly, the sixfolded leafspring design and third the three folded leafspring and three rods design. From the following figures, fig. D.1 till fig. D.4 it can be seen that the 6 folded leafspring design has the highest stiffness potential.

			Settings	unit	Stiffness in Z matlab	Stiffness Z in Comsol	eigenfreq		disp due to force in direction	
1.1	Hexapod		d l angle bi Material F	2 mm 100 mm 45 deg 305 N	x 1.82E+07 y 1.58E+07 z 2.73E+07	x 8.89E+06 y 8.89E+06 z 1.88E+07	mode 1 2 3 4	hz 147.3 147.31 210.21 292.9	x y z	3.43E-05 3.43E-05 1.62E-05
2.1	Reinforced Hexapod		d D	2 8	x y z	x 2.72E+07 y 2.72E+07 z 5.67E+07	mode 1 2 3 4	hz 257.66 257.72 366.6 506.82	x y z	1.12E-05 1.12E-05 5.38E-06
3.1	Six folded leaf		lfol thick	40 mm 2	x y z	x 3.91E+07 y 3.86E+07 z 6.63E+07	mode 1 2 3 4	hz 301.72 301.77 397.7 587.52	x y z	7.80E-06 7.90E-06 4.60E-06
4.1	3 folded leaf 3 rods		drot l lfol thick F	2 100 40 2 305	x y z	x 1.58E+07 y 1.58E+07 z 6.37E+07	mode 1 2 3 4	hz 193.73 193.76 339.43 389.33	x y z	1.93E-05 1.93E-05 4.79E-06

Figure D.1: Iso-static mounts part 1

			Settings	unit	Stiffness in Z matlab	Stiffness Z in Comsol	eigenfreq		disp due to force in direction	
1.2	Hexapod		d	4 mm	x 7.31E+07	x 3.42E+07	mode	hz	x	8.91E-06
			l	100 mm	y 6.33E+07	y 3.42E+07	1	289.69	y	8.91E-06
			angle bi	45 deg	z 1.09E+08	z 6.98E+07	2	289.69	z	4.37E-06
			Material	Steel			3	408.08		
			F	305 N			4	564.06		
2.2	Reinforced Hexapod		d	4	x	x 9.21E+07	mode	hz	x	3.31E-06
			D	16	y	y 9.21E+07	1	475.01	y	3.31E-06
					z	z 1.75E+08	2	475.05	z	1.74E-06
							3	654.82		
							4	883.59		
3.2	Six folded leaf		lfol	40 mm	x	x 7.08E+07	mode	hz	x	4.31E-06
			thick	3	y	y 7.04E+07	1	404.7	y	4.33E-06
					z	z 1.01E+08	2	404.8	z	3.02E-06
							3	493.73		
							4	770.29		
4.2	3 folded leaf 3 rots		drot	4	x	x 5.13E+07	mode	hz	x	5.94E-06
			l	100	y	y 5.13E+07	1	350.38	y	5.95E-06
			lfol	40	z	z 6.94E+07	2	350.41	z	4.78E-06
			thick	2			3	389.78		
			F	305			4	564		

Figure D.2: Iso-static mounts part 2

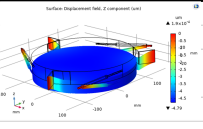
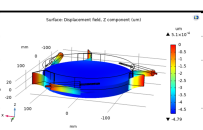
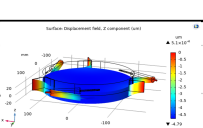
			Settings	unit	Stiffness in Z matlab	Stiffness Z in Comsol	eigenfreq		disp due to force in direction	
5.1	3 folded leaf 3 reinforced rots		d	4 mm	x	x 6.78E+07	mode	hz	x	4.50E-06
			D	8 mm	y	y 6.78E+07	1	389.08	y	4.50E-06
					z	z 6.37E+07	2	403.82	z	4.79E-06
							3	403.84		
							4	563.01		
5.2	3 folded leaf 3 reinforced rots		d	4 mm	x	x 8.43E+07	mode	hz	x	3.62E-06
			D	16 mm	y	y 8.43E+07	1	387.58	y	3.62E-06
					z	z 6.37E+07	2	450.68	z	4.79E-06
							3	450.72		
							4	557.2		
5.3	3Reinforced leaf and 3 reinforced rots		d	4 mm	x	x 9.27E+07	mode	hz	x	3.29E-06
			D	16 mm	y	y 9.27E+07	1	441	y	3.29E-06
			thick	2	z	z 8.20E+07	2	471	z	3.72E-06
							3	471		
							4	634		

Figure D.3: Iso-static mounts part 3

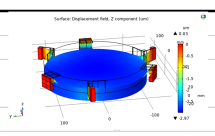
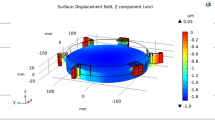
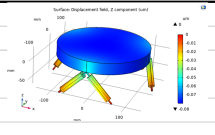
			Settings	unit	Stiffness in Z matlab	Stiffness Z in Comsol	eigenfreq		disp due to force in direction	
6.1	Six reinforced folded leaf		lfol thick	30 mm 2	x y z	x 9.00E+07 y 9.00E+07 z 1.03E+08	mode 1 2 3 4	hz 316.25 316.27 412.28 612.35	x y z	3.39E-06 3.39E-06 2.97E-06
6.2	Six reinforced folded leaf		lfol thick	30 mm 3	x y z	x 1.59E+08 y 1.58E+08 z 1.61E+08	mode 1 2 3 4	hz 584.99 585.14 631.43 1020.8	x y z	1.92E-06 1.93E-06 1.90E-06
6.3	Six reinforced folded leaf		lfol thick	30 mm 4	x y z	x 2.42E+08 y 2.42E+08 z 2.18E+08	mode 1 2 3 4	hz 722.95 723.22 744.38 1230.4	x y z	1.26E-06 1.26E-06 1.40E-06
2.3	Reinforced Hexapod		d D	4 12	x y z	x 8.54E+07 y 8.54E+07 z 1.64E+08	mode 1 2 3 4	hz 458.87 458.9 633.76 858.82	x y z	3.57E-06 3.57E-06 1.86E-06

Figure D.4: Iso-static mounts part 4

D.1 Backplate table

Here the bigger version of the table from section 7.4.1 is shown this table is used to determine the position of the folded flexures.

		Delta , gravity in y				
R1	120	x	x	x	x	0.9
	105	x	x	x	1.25	1.21
	90	x	x	1.78	1.73	1.64
	75	x	2.62	2.54	2.43	2.3
	60	3.97	3.86	3.69	3.51	3.3
		60	75	90	105	120
		R2				
		Delta Z, gravity in z				
R1	120	x	x	x	x	0.05
	105	x	x	x	0.03	0.03
	90	x	x	0.02	0.01	0.02
	75	x	0.01	0.01	0.02	0.01
	60	0.03	0.02	0.02	0.02	0.03
		60	75	90	105	120
		R2				
		Eigenfrequency				
R1	120	x	x	x	x	240
	105	x	x	x	243	223
	90	x	x	244	229	225
	75	x	241	229	229	226
	60	227	221	222	224	222
		60	75	90	105	120
		R2				

Figure D.5: Iso-static mounts part 5

References

- [1] wyant optics. psfMtfZernikes. <http://wyant.optics.arizona.edu/psfMtfZernikes/psfMtfZernikes.htm>, 2019. [Online; accessed 19-September-2019].
- [2] Wikipedia contributors. Astigmatism (optical systems) — Wikipedia, the free encyclopedia. [https://en.wikipedia.org/w/index.php?title=Astigmatism_\(optical_systems\)&oldid=915315707](https://en.wikipedia.org/w/index.php?title=Astigmatism_(optical_systems)&oldid=915315707), 2019. [Online; accessed 18-September-2019].
- [3] Juequan Chen. *EDS 3300 BTS/FFA Optical design-D000186420-04*. 2015.
- [4] Wikipedia contributors. Asml holding — Wikipedia, the free encyclopedia. https://en.wikipedia.org/w/index.php?title=ASML_Holding&oldid=902225693, 2019. [Online; accessed 4-July-2019].
- [5] Wikipedia contributors. Moore’s law — Wikipedia, the free encyclopedia. https://en.wikipedia.org/w/index.php?title=Moore%27s_law&oldid=904615533, 2019. [Online; accessed 4-July-2019].
- [6] Wikipedia contributors. Extreme ultraviolet lithography — Wikipedia, the free encyclopedia. https://en.wikipedia.org/w/index.php?title=Extreme_ultraviolet_lithography&oldid=904692763, 2019. [Online; accessed 4-July-2019].
- [7] van den Dungen Clemens. *EPS FFA FU mk11*. 2018.
- [8] Wikipedia contributors. Circle of confusion — Wikipedia, the free encyclopedia. https://en.wikipedia.org/w/index.php?title=Circle_of_confusion&oldid=897200762, 2019. [Online; accessed 4-July-2019].
- [9] Jonas Becker. D000565390-05 FC72 ast budget. ASML document, October 2018.
- [10] <http://tsftsh.com/files/catalogs/precargas>. [http://tsftsh.com/assets/files/catalogs/Precargas%\\$20Web.pdf](http://tsftsh.com/assets/files/catalogs/Precargas%$20Web.pdf), 2019. [Online; accessed 19-September-2019].
- [11] . friction-coefficients-in-atmosphere-and-vacuum. <http://www.tribonet.org/wiki/friction-coefficients-in-atmosphere-and-vacuum/>, 2019. [Online; accessed 19-September-2019].
- [12] Vukobratovich D Yoder PR. *Opto-Mechanical Systems Design volume 1*. CRC Press, 2015.
- [13] Hagyong Kihm, Ho Soon Yang, and Yun Woo Lee. Bipod flexure for 1-m primary mirror system. *Review of Scientific Instruments*, 2014.
- [14] Mirror Design For Optical Telescopes 2.1 Specifications for Optical Mirror Design 2.1.1 Fundamental Requirements for Optical Mirrors.
- [15] Vukobratovich D Yoder PR. *Opto-Mechanical Systems Design volume 2*. CRC Press, 2015.
- [16] S. Koppen, M. van der Kolk, F. C.M. van Kempen, J. de Vreugd, and M. Langelaar. Topology optimization of multicomponent optomechanical systems for improved optical performance. *Structural and Multidisciplinary Optimization*, 2018.

- [17] Hoogerbrugge A.J. *Topology optimization of coupled heat problems*. 2019.
- [18] Koster M.P. *Constructie principes M.P Koster*. 2008.
- [19] Hagyong Kihm and Ho-Soon Yang. Design optimization of a 1-m lightweight mirror for a space telescope. *Optical Engineering*, 2013.
- [20] Joeleff Fitzsimmons, Darren Erickson, Alexis Hill, Randall Bartos, and James K. Wallace. Design and analysis of flexure mounts for precision optics. In *Advanced Optical and Mechanical Technologies in Telescopes and Instrumentation*, volume 7018, page 70181K. SPIE, jun 2008.
- [21] Design guidelines for thermal stability in optomechanical instruments. In *Optomechanics 2003*, volume 5176, page 126. SPIE, dec 2003.
- [22] Advanced Diamond Technology. cvd diamond booklet. http://www.diamond-materials.com/downloads/cvd_diamond_booklet.pdf, 2019. [Online; accessed 19-September-2019].
- [23] -. Gnielinski equation, 2019.
- [24] Marcel Thomas. Flexures. <http://web.mit.edu/mact/www/Blog/Flexures/FlexureIndex.html>. [Online; accessed 15-November-2019].
- [25] Martin van Mierlo. Design of an astigmatically neutral mirror using thermal path optimization. <https://repository.tudelft.nl/islandora/object/uuid%3A3c1000eb-2fe9-450a-ad9b-a47b6e8053e9?collection=education>, 2019. [Online; accessed 19-November-2019].